WEAR BEHAVIOR OF MAGNESIUM BASED NANOCOMPOSITES

BY

SYED ZABIULLAH

A Thesis Presented to the

DEANSHIP OF GRADUATE STUDIES

KING FAHD UNIVERSITY OF PETROLEUM & MINERALS

DHAHRAN, SAUDI ARABIA

In Partial Fulfillment of the
Requirements for the Degree of

MASTER OF SCIENCE

In

MECHANICAL ENGINEERING

December 2012

KING FAHD UNIVERSITY OF PETROLEUM & MINERALS
DHAHRAN 31261, SAUDI ARABIA

DEANSHIP OF GRADUATE STUDIES

This thesis, written by **SYED ZABIULLAH** under the direction of his thesis advisor and approved by his thesis committee, has been presented to and accepted by the Dean of Graduate Studies, in partial fulfillment of the requirements for the degree of **MASTER OF SCIENCE IN MECHANICAL ENGINEERING.**

Thesis Committee

Dr. Syed Fida Hassan (Advisor)

Dr. Amro M. Al-Qutub (Member)

Dr. Tahar Laoui (Member)

Dr. Zuhair Mattoug Gasem
Department Chairman

Dr. Salam A. Zummo
Dean of Graduate Studies

19/5/13

Date

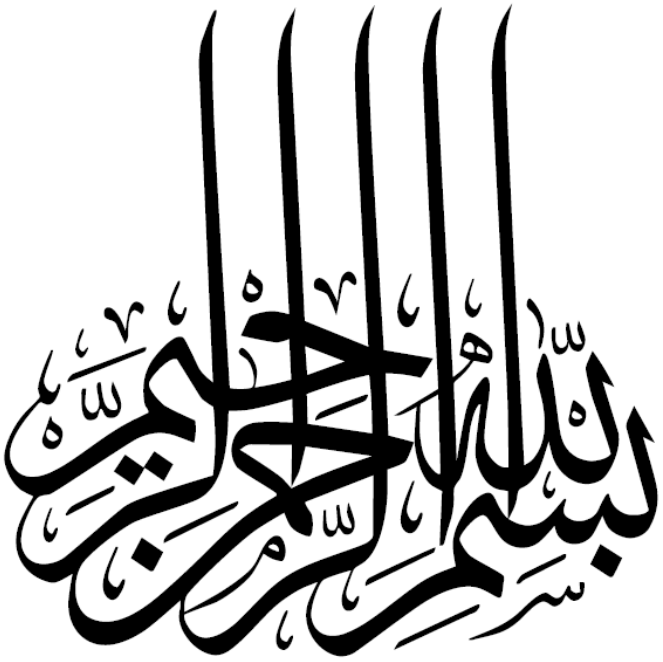

This Work is dedicated

to

My Family for their dua, constant support and encouragement throughout my life

ACKNOWLEDGEMENTS

All praise belongs to Almighty ALLAH (S.W.T.) for bestowing me with health, knowledge and patience to carry out this work and complete my M.S. successfully at King Fahd University of Petroleum and Minerals, Dhahran.

Acknowledgement is due to King Fahd University of Petroleum and Minerals for providing me financial support and good academic environment during the course of my study. Special thanks to the Deanship of Scientific Research (DSR) for funding this work.

My deep gratitude and appreciation goes to my thesis advisor Dr. Syed Fida Hassan for his constant help, guidance and motivation during the course of my study. His priceless suggestions made this work interesting and challenging for me. I also wish to express my deep appreciation to Dr. Amro Al-Qutub for his constant help, guidance and encouragement during my study. I am greatly indebted to Dr. Amro Al-Qutub for the valuable time he spent throughout my thesis work and also for always being supportive and helping me during difficult times. Sincere thanks to Dr. Tahar Laoui for his interest and cooperation. I would also like to acknowledge all the Mechanical Engineering faculty members with whom I took courses during my master's program. Special thanks to Mr. Murtuza, Lateef Hashmi for helping me carry out the experimental work.

I would like to thank all my family members and friends for their strong encouragement at times of difficulty and for their patience and moral support which made this work possible and made me achieve one of the important goals of my life.

TABLE OF CONTENTS

LIST OF TABLES ..... **x**

LIST OF FIGURES ..... **xi**

ABSTRACT (ENGLISH) ..... **xvi**

ABSTRACT (ARABIC) ..... **xviii**

CHAPTER 1 INTRODUCTION **1**

CHAPTER 2 LITERATURE REVIEW **4**

2.1 Metal Matrix Composites and Nanocomposites **5**

2.2 Tribology of particulate reinforced metal matrix composites **6**

2.3 Wear behavior of Mg based MMCs **8**

2.3.1 Mg – SiC MMCs 9

2.3.2 Mg – Al_2O_3 MMCs 10

2.3.3 Mg reinforced with other particulate reinforcements 11

2.4 Wear regimes **12**

2.5 Wear Mechanisms in MMCs **14**

2.6 Summary **18**

CHAPTER 3 EXPERIMENTAL PROCEDURE **20**

3.1 Materials **20**

3.2 Processing Technique **21**

3.2.1 Disintegrated Melt Deposition Technique for AZ31/Al_2O_3 and AZ31/CNT Nanocomposites 21

3.2.2 Powder Metallurgy Technique for Mg/(Y_2O_3+Cu) and Mg/(Y_2O_3+Ni) Hybrid Nanocomposites..... 24

3.3 Material Characterization 24

3.4 Experimental Apparatus 26

3.4.1 Pin-on-Disc tribometer..... 26

3.5 Wear Tests 29

3.5.1 Pin Specimen Preparation 29

3.5.2 Disc Preparation..... 29

3.5.3 Experimental Conditions 29

3.5.4 Experimental Procedure..... 30

3.5.5 Wear measurements 31

3.5.6 Scanning Electron Microscopic and Energy Dispersive X-ray Analysis 32

3.6 Uncertainty Analysis 32

CHAPTER 4 RESULTS..... 39

4.1 Magnesium alloy (AZ31) based Nanocomposites 39

4.1.1 Wear Rate of AZ31 and its AZ31/Al_2O_3 nanocomposite 39

4.1.2 Wear Mechanisms in AZ31 and its AZ31/Al_2O_3 nanocomposite 43

4.1.3 Wear Rate of AZ31 and its AZ31/CNT nanocomposite 55

4.1.4 Wear Mechanisms in AZ31 and its AZ31/CNT nanocomposite 58

4.1.5 Comparison between AZ31/Al_2O_3 and AZ31/CNT Nanocomposites 67

4.2 Magnesium/(yttria + nickel) Hybrid Nanocomposites 69

4.2.1 Wear Rate for Mg/(0.7Y_2O_3 + (0.3-1.0Ni) Nanocomposites 69

4.2.2 Wear Mechanisms in Mg/(0.7Y_2O_3 + (0.3-1.0Ni) Nanocomposites 71

4.3 Magnesium/(yttria + copper) Hybrid Nanocomposites 79

4.3.1 Wear Rate for Mg/(0.7Y_2O_3 + (0.3-1.0Cu) Nanocomposites 79

4.3.2 Wear Mechanisms in Mg/(0.7Y_2O_3 + (0.3-1.0Cu) Nanocomposites 81

4.4 Comparison between Mg/(0.7Y_2O_3 + (0.3-1.0Ni) and Mg/(0.7Y_2O_3 + (0.3-1.0Cu) Hybrid Nanocomposites 88

CHAPTER 5 DISCUSSION 90

5.1 Magnesium alloy (AZ31) based Nanocomposites 90

5.1.1 Wear Rate for AZ31 and its AZ31/Al_2O_3 Nanocomposite 90

5.1.2 Wear Mechanisms in AZ31 and its AZ31/Al_2O_3 Nanocomposite 92

5.1.3 Wear Rate for AZ31 and its AZ31/CNT Nanocomposite 95

5.1.4 Wear Mechanisms in AZ31 and its AZ31/CNT Nanocomposite 96

5.1.5 Comparison between AZ31/Al_2O_3 and AZ31/CNT Nanocomposites 99

5.2 Mg/(0.7Y_2O_3 + (0.3-1.0Ni) Nanocomposites 101

5.2.1 Wear Rate for Mg/(0.7Y_2O_3 + (0.3-1.0Ni) Nanocomposites 101

5.2.2 Wear Mechanisms in Mg/(0.7Y_2O_3 + (0.3-1.0Ni) Nanocomposites 101

5.3 Mg/(0.7Y_2O_3 + (0.3-1.0Cu) Nanocomposites 103

5.3.1 Wear Rate for Mg/(0.7Y_2O_3 + (0.3-1.0Cu) Hybrid Nanocomposites 103

5.3.2 Wear Rate for Mg/(0.7Y_2O_3 + (0.3-1.0Cu) Hybrid Nanocomposites 103

5.4 Comparison between Mg/(0.7Y_2O_3 + (0.3-1.0Ni) and Mg/(0.7Y_2O_3 + (0.3-1.0Cu) Hybrid Nanocomposites 105

CHAPTER 6 CONCLUSION AND RECOMMENDATIONS 107

6.1 Recommendations for Future Work 109

REFERENCES 110

VITAE 119

LIST OF TABLES

Table 2.1 Difference between mild and severe wear 13

Table 3.1 Some important properties of pin materials used in the present work..... 25

Table 3.2 Bias, Precision and Nominal values for different variables..... 38

LIST OF FIGURES

Figure 3.1 Schematic Diagram of DMD process 23

Figure 3.2 Pin-on-Disc tribometer at KFUPM 28

Figure 4.1 Variation of wear rate with applied load at different sliding speeds for AZ31 and its AZ31/Al_2O_3 nanocomposite. 41

Figure 4.2 Effect of sliding speed on the wear rate at various applied loads for AZ31 and its AZ31/Al_2O_3 nanocomposite. 42

Figure 4.3 Grooves and scratches on the pin surface indicating abrasive wear for the AZ31/Al_2O_3 nanocomposite at 2 m/ sliding speed and 5 N applied load. 44

Figure 4.4 Difference in extent of abrasion on the pin surfaces of (a) unreinforced alloy and (b) Al_2O_3 reinforced nanocomposite at 1 m/s sliding speed and 10 N applied load... 44

Figure 4.5 Magnesium ribbon shaped strips in the wear debris of AZ31/Al_2O_3 nanocomposite showing cutting action of an abrasive particle at 10 N and 2 m/s. 45

Figure 4.6 Steel strip in the wear debris of the AZ31/Al_2O_3 nanocomposite due to abrasive wear of tool-steel counterface at 2 m/s sliding velocity and 10 N applied load... 46

Figure 4.7 Long and small wear particles formed due to breaking of ridges showing ploughing action of AZ31 at 10 N and 5 m/s..... 47

Figure 4.8 Series of cracks perpendicular to the sliding direction indicating delamination in the AZ31/Al_2O_3 nanocomposite under a load of 15 N at 2 m/s sliding speed. 48

Figure 4.9 Large crater on the pin surface due to delamination for (a) AZ31/Al_2O_3 at a load of 10 N and 5 m/s sliding speed. (b) AZ31 magnesium alloy at a load of 15 N and 2 m/s sliding speed. 49

Figure 4.10 Wear debris of the AZ31/Al_2O_3 nanocomposite showing large sheet-like wear particles at 10 N and 5 m/s. 49

Figure 4.11 Rows of furrows indicating adhesive wear of AZ31/Al_2O_3 nanocomposite under a load of 10 N and 2 m/s sliding speed. 50

Figure 4.12 Optical microscopic examination of the wear track indicating transfer of material from the surface of AZ31/Al_2O_3 nanocomposite at a normal load of 20 N and 2 m/s sliding speed. 51

Figure 4.13 Material extrusion from the interface that have re-solidified around the periphery of AZ31/ Al_2O_3 nanocomposite under a load of 20 N and 2 m/s sliding speed. 52

Figure 4.14 Presence of oxide particles on the surface of AZ31 nanocomposite at a load of 10 N and 2 m/s sliding speed. 53

Figure 4.15 EDX analysis of oxide particles indicating presence of magnesium oxide on the surface of AZ31/AL_2O_3 nanocomposite at a load of 10 N and 5 m/s sliding speed. 54

Figure 4.16 Variation of wear rate with applied load at different sliding speeds for AZ31 and its AZ31/CNT nanocomposite. 56

Figure 4.17 Effect of sliding speed on the wear rate at various applied loads for AZ31 and its AZ31/CNT nanocomposite. 57

Figure 4.18 Grooves and scratches on the pin surface indicating abrasive wear for the AZ31/CNT nanocomposite at 1 m/ sliding speed and 5 N applied load. 59

Figure 4.19 Magnesium ribbon shaped strips in the wear debris of AZ31/CNT nanocomposite showing cutting action of an abrasive particle at 10 N and 5 m/s. 59

Figure 4.20 Series of cracks perpendicular to the sliding direction indicating delamination in the AZ31/CNT nanocomposite under a load of 10 N at 2 m/s sliding speed. 60

Figure 4.21 Large crater on the pin surface due to delamination for AZ31/CNT at a load of 10 N and 2 m/s sliding speed. 61

Figure 4.22 Rows of furrows indicating adhesive wear of AZ31/CNT nanocomposite under a load of 10 N and 5 m/s sliding speed. 62

Figure 4.23 Optical microscopic examination of the wear track indicating transfer of material from the surface of AZ31/CNT nanocomposite at a normal load of 15 N and 5 m/s sliding speed. 65

Figure 4.24 Material extrusion from the interface that have re-solidified around the periphery of AZ31/ CNT nanocomposite under a load of 20 N and 1 m/s sliding speed... 64

Figure 4.25 Presence of oxide particles on the surface of AZ31/CNT nanocomposite at a load of 10 N and 2 m/s sliding speed. 65

Figure 4.26 EDX analysis of oxide particles indicating presence of magnesium oxide on the surface of AZ31/CNT nanocomposite at a load of 10 N and 2 m/s sliding speed. 66

Figure 4.27 Variation of wear rate with applied load at different sliding speeds for AZ31/Al_2O_3 and its AZ31/CNT nanocomposite. 68

Figure 4.28 Variation of wear rate with applied loads at a constant sliding speed of 0.5 m/s for Mg/(Y_2O_3 + Ni) nanocomposites. 70

Figure 4.29 SEM image of Mg/(0.7Y_2O_3 + 0.6Ni) indicating abrasion at a load of 5 N. .. 73

Figure 4.30 EDX analysis of fine particles indicating oxidation of the pin surface at a load of 5 N. 73

Figure 4.31 Perpendicular cracks indicating delamination in Mg/(0.7Y_2O_3 + 0.3Ni) at 10 N..... 74

Figure 4.32 Shallow craters on the pin surface indicating severe delamination with applied loads for Mg/(0.7Y_2O_3 + 0.3Ni) at (a) 15 N; (b) 20 N; and (c) 25 N..... 75

Figure 4.33 Presence of large flakes in the wear debris of Mg/(0.7Y_2O_3 + 0.3Ni) at 15 N..... 76

Figure 4.34 EDX analysis of flakes in the wear debris indicating increase in oxidation of the pin surface with increase in load (a) 15 N and (b) 30 N..... 76

Figure 4.35 SEM image of Mg/(0.7Y_2O_3 + 0.6Ni) at 25 N. 77

Figure 4.36 SEM image of Mg/(0.7Y_2O_3 + 0.6Ni) at 30 N. 77

Figure 4.37 Large sheet of wear debris collected from wear track indicative of adhesion for Mg/(0.7Y_2O_3 + 1.0Ni) at 30 N. 78

Figure 4.38 Variation in wear rate with applied load at a constant sliding speed of 1 m/s for Mg/(Y_2O_3 + Cu) nanocomposites. 80

Figure 4.39 Grooves and scratch marks on the pin surface indicating abrasion for Mg/(0.7Y_2O_3 + 0.3Cu) at 10 N. 83

Figure 4.40 Flake like wear particles in the wear debris of Mg/(0.7Y_2O_3 + 1.0Cu) due to delamination of oxidized surface layers. 83

Figure 4.41 Steel strip in the wear debris of the Mg/(0.7Y_2O_3 + 0.3Cu) due to abrasive wear of tool-steel counterface at 10 N. 84

Figure 4.42 Oxidation of the Mg/(0.7Y_2O_3 + 0.3Cu) hybrid nanocomposite pin surface at 10 N. 84

Figure 4.43 Optical microscopic examination of the wear track indicating transfer of material from the surface of Mg/(0.7Y_2O_3 + 0.3Cu) nanocomposite at 25 N. 85

Figure 4.44 Series of cracks perpendicular to the sliding direction indicating delamination for Mg/(0.7Y_2O_3 + 1.0Cu) at 15 N. 85

Figure 4.45 Large crater on pin surface due to delamination for Mg/(0.7Y_2O_3 + 1.0Cu) at 20N. 86

Figure 4.46 SEM image indicating softening for the Mg/(0.7Y_2O_3 + 0.3Cu) at 30 N. 86

Figure 4.47 SEM image of Mg/(0.7Y_2O_3 + 0.6Cu) hybrid nanocomposite at 30 N. 87

Figure 4.48 SEM image of Mg/(0.7Y_2O_3 + 1.0Cu) at 30 N. 87

Figure 4.49 Comparison between Mg/(Y_2O_3+Ni) and Mg/(Y_2O_3+Ni) hybrid nanocomposites. 89

ABSTRACT (ENGLISH)

Full Name : SYED ZABIULLAH

Thesis Title : WEAR BEHAVIOR OF MAGNESIUM BASED NANOCOMPOSITES

Major Field : MECHANICAL ENGINEERING

Date of Degree : December 2012

In the present work, wear behavior of magnesium based nanocomposites reinforced with different nanoparticles were investigated by using pin-on-disc configuration under dry sliding conditions.

In the first group of materials, dry sliding wear behavior of AZ31 magnesium alloy and its nanocomposites reinforced with 1.5 vol.% Al_2O_3 and 1 vol.% CNT were studied within a load range of 5-20 N at sliding speeds of 1, 2 and 5 m/s for sliding distance up to 2500 m. The test results showed that the wear rates of the magnesium alloy increases with the addition of reinforcement. Scanning electron microscopy (SEM) identified abrasion, oxidation, delamination, adhesion and thermal softening as the dominant wear mechanisms. The high wear rates in the nanocomposites were attributed to higher ductility, porosity and mismatch of thermal expansion coefficients between the reinforcement and matrix alloy.

In the second group of materials, dry sliding wear behavior of Mg/Y_2O_3 nanocomposites reinforced with varying amounts of nickel from 0.3-1.0 vol.% were studied within a load range of 5-30 N at a constant sliding speed 0.5 m/s for sliding distance up to 1000 m. The test results showed that the wear rates of the Mg/Y_2O_3

nanocomposites decreases with increase in amount of Ni. The improvement in wear resistance of the nanocomposites was attributed to the improved hardness and strength of the material with increase in Ni content. Scanning electron microscopy (SEM) identified abrasion, oxidation, delamination, adhesion as the dominant wear mechanisms.

In the third group of materials, dry sliding wear behavior of Mg/Y_2O_3 nanocomposites reinforced with varying amounts of copper from 0.3-1.0 vol.% were studied within a load range of 5-30 N at a constant sliding speed 1 m/s for sliding distance up to 1000 m. The test results showed slight improvement in the wear resistance of Mg/Y_2O_3 nanocomposite with 1.0 vol.% Cu. The improvement in wear resistance of the nanocomposites was attributed to the improved hardness of the material with increase in Cu content. Scanning electron microscopy (SEM) identified abrasion, oxidation, adhesion and mild delamination as the dominant wear mechanisms.

ABSTRACT (ARABIC)

ملخص العربية

الإسم : **سيد ظبي الله**

عنوان الرسالة : **سلوك البرى لمادة ملماغنسيوا النانو مركبة**

الخصص العام : **ألهندسة الكانيكية**

تأريخ التخرج : **1434هـ - (ديسمبر2013 م)**

في هذا العمل، تم دراسة سلوك البرى للمواد النانو مركبة / الماغنسيوم والمدعمة بجسيمات نانوية مختلفة باستخدام دبوس على قرص تحت ظروف الانزلاق الجافة.

في المجموعة الأولى من المواد ، تمت دراسة سلوك البرى لسبائك AZ31 من خليط الماغنسيوم والمدعمة بجسيمات نانوية مختلفة ١,٥ vol.% Al٢O٣ و ١ vol.% من انابيب الكربون نانوية باستخدام حمل فى مدى ٥-٢٠ نيوتن وسرعة الانزلاق ١، ٢ و ٥ m/s ومسافة انزلاق تصل إلى ٢٥٠٠ م. وأظهرت نتائج الاختبار أن معدلات البرى لسبائك المغنيسيوم زادت بزيادة نسبة المواد الداعمة. وحدد المسح الضوئي المجهر الإلكتروني (SEM) ان آليات البرى هى التاكل و الأكسدة، والالتصاق وتليين الحرارية .ان معلات التاكل العالية فى المواد النانومركبه ترجع الى الممطوليه العاليه ، المسامية وعدم تطابق معاملات التمدد الحراري بين المواد الداعمة و مصفوفة السبيكة.

في المجموعة الثانية من المواد، تمت دراسة سلوك البرى الجاف لمواد نانو مركبة من Mg/Y_2O_3

مدعمة بمقادير متفاوتة من النيكل من ٠,٣-١,٠ vol.% تمت الدراسة باستخدام باستخدام حمل فى مدى ٥-30 نيوتن وسرعة ثابته للانزلاق ٠,٥ m/s. ومسافة انزلاق تصل إلى ١٠٠٠ م. اوضحت نتائج الاختبار ان معدل التاكل .يتناقص مع زيادة نسبة النيكل. تحسين مقاومة البرى للمواد النانو مركبه يعزى إلى تحسين صلابة ومقاومة المواد مع زيادة نسبة النيكل. وحدد الميكروسكوب الإلكتروني اوضحت ان آليات البرى هى التاكل و الأكسدة، والالتصاق

في المجموعة الثالثة ، تمت دراسة سلوك البرى الجاف لمواد نانو مركبة من Mg/Y_2O_3

مدعمة بمقادير متفاوتة من النحاس بنسب ٠,٣-١,٠ vol.% تمت الدراسة باستخدام حمل فى مدى ٥-30 نيوتن وسرعة ثابته للانزلاق ١ .m/s ومسافة انزلاق تصل إلى ١٠٠٠ م. أظهرت نتائج الاختبار تحسنا طفيفا في مقاومة البرى مع ١,٠ vol.% Cu.تحسين مقاومة للمواد نانو مركبة يعزى إلى تحسين صلادة المواد مع زيادة في محتوى Cu. المسح الضوئي المجهر الإلكتروني (SEM) حدد البرى و الأكسدة والالتصاق وتنسل الأطراف كاليات للبرى .

CHAPTER 1

INTRODUCTION

The development of metal matrix composites (MMCs) has been one of the major innovations in materials which are rapidly replacing conventional materials in various applications such as automotive, aerospace, defense, sports, appliance and other industries. When compared to monolithic metallic materials, MMCs offer better physical, mechanical, thermal and tribological properties such as low density, high specific strength, high specific modulus, better fatigue resistance, improved wear resistance etc [1-3]. Generally, MMCs are defined as matrix materials (either metals or metallic alloys) that are reinforced with metals, ceramics, refractory metal, inter-metallic or semiconductor to combine the properties of reinforcing material with that of the matrix materials such that the resultant properties of the composite material are better than the properties of unreinforced materials. These MMCs are further divided into three main categories based on the shape of their reinforcement such as particles, fibers or whiskers. Among these three types of MMCs, particulate reinforced composites are of significant interest because (a) they exhibit isotropic properties, (b) can be successfully fabricated by using conventional metallurgical process, (c) can be machined using conventional

methods and (d) low cost. The most commonly used particulate reinforcement for MMCs are ceramics such as silicon carbide and alumina because of their high strength, hardness and low cost. Depending upon the application, the end properties of these materials can be tailored based on some key factors such as type of processing, matrix constitution, type, size, amount, morphology, distribution and orientation of reinforcement, nature of matrix-reinforcement interface and heat treatment procedure. Among all these factors, compatibility of reinforcement with that of metallic matrix is of greater importance in realizing the best properties from the resultant composite [4-6].

From past few decades, MMCs with lightweight matrix materials are showing considerable interest because of their superior mechanical and tribological properties in many engineering applications [7-8]. As shown by many researchers, use of ceramic particulates such as SiC, Al_2O_3 as reinforcement reduced wear and friction of aluminum based MMCs both at room and elevated temperatures making them strong candidate material for a number of tribological applications such as piston, cylinder liners, engine blocks, brakes, power transfer system elements etc., in automobile industry [9-11]. However, continuous attempt by aerospace and automobile industries to push performance limits, constantly presents the crucial issue of weight reduction. In this connection, magnesium is 35% lighter than aluminum and is attracting more attention as the lightest structural material because of its low density and high specific strength and stiffness, which make them strongest applicant and an alternative to aluminum in many tribological applications in near future. However, pure magnesium cannot be directly used for tribological applications due to their low thermal stability and poor resistance to wear. To overcome these difficulties significant research work has been done over the

last few decades to improve the performance of magnesium beyond traditional alloying using discontinuous reinforcement. Recently, magnesium based composites with nano-sized particulate reinforcements are receiving high attention due to their improved mechanical properties [12-14]. However, the study on the tribological properties of magnesium based MMCs with nano-particles as reinforcement are very less in the open literature.

Accordingly, the primary aim of the present study was to investigate the tribological behavior of magnesium based nanocomposites containing nano-size Al_2O_3, CNT, (Y_2O_3 + Cu) and (Y_2O_3 + Ni) particulate reinforcements. The effects of load, sliding speed and particulate content on the wear performance are investigated using a laboratory pin-on-disc wear tester designed and fabricated in Mechanical Engineering Department at KFUPM.

In the present work, Chapter 2 discusses the magnesium based metal matrix composites and their tribological behavior, and Chapter 3 describes experimental procedure used in the present study. Wear data obtained from the wear testing are presented in Chapter 4. And the wear mechanisms as identified by SEM and EDX analysis and their comparison with the obtained results are discussed in Chapter 5. Finally, the thesis ends with the main conclusions and recommendations for future work in chapter 6.

CHAPTER 2

LITERATURE REVIEW

The main motivation behind the development of composites is the utilization of advantageous properties of constituent materials to meet specific demands in many applications. The term “composite” is defined as the combination of two or more materials in which one of the material is termed as the reinforcing phase, which is in the form of fibers, whiskers, or particles, and is embedded in the other material termed as matrix phase (present in greater quantity in the composite) [15]. Typically, these materials have the ability to combine the properties of reinforcing phase with that of the matrix such that the resultant properties of the composite materials are better than the properties of monolithic counterparts. As a result of this, composite materials have the capability to serve a wide spectrum of applications [5, 16]. Composites can be broadly classified into three categories based on their matrix material namely: Metal Matrix Composites (MMCs), Polymer Matrix Composites (PMCs), and Ceramic Matrix Composites (CMCs). Among these three different types of composites, MMCs are one of the promising candidates for use in applications which require high strength and stiffness, particularly at elevated temperatures and for wear resistance applications [17].

2.1 Metal Matrix Composites and Nanocomposites

Metal matrix composite materials have been subject of scientific investigation and applied research from past few decades in the field of material science. These MMCs consists of two or more components namely: Matrix material (metal or metallic alloy) and Reinforcement (ceramics, metallic or refractory metal). Generally, the matrix is a "soft" phase (with excellent ductility, formability and thermal conductivity) in which "hard" reinforcements (with high stiffness and low thermal expansion) are embedded to improve its mechanical properties [6, 16, 18-20]. Previous studies on MMCs suggest particulate based reinforcement with size 1 to 100 microns as the most commonly used reinforcement due to their availability at competitive cost, well-developed cost effective fabrication process, ability to be machined using conventional methods and due to their isotropic nature [19]. Recently, more research in the field of production of nanocomposites is going on to explore the properties of MMCs when reinforced with nanoparticles (< 100 nm) instead of micron-sized particles. The challenge in developing these nanocomposites is to find different ways to create macroscopic components that benefit from the unique physical and mechanical properties of nanoparticles within them. The creation of these nanocomposites using nanoparticles as reinforcement has been investigated from past few years, and the development of these materials have shown comparable or greater strength and stiffness when compared to its micron sized MMCs [12-14, 22-23].

Today, increasing demand for the reduction of fuel consumption and environmental problems has led to intensive research efforts into design and development of lightweight

structural materials for automobile and aerospace applications. And it can be achieved by replacing denser materials and even aluminum based materials by lightweight magnesium materials which has gained significant interest due to its low density which is about two-thirds of the density of aluminum and one-quarter of that of steel to justify the growing demand of lightweight materials for various applications such as automotive, aerospace, marine, electronic, biomedical, sports etc., However, these materials are not used directly due to their lower thermal stability and poor resistance to corrosion and wear. To overcome these difficulties significant research work has been done over the last few decades to improve the performance of magnesium beyond traditional alloying using discontinuous reinforcement. And the major challenge in the developing magnesium based MMCs are to achieve improvement in strength without compromising the intrinsic limited ductility. Interestingly, recent studies on magnesium based MMCs with nanoparticles as reinforcement reported simultaneous improvement in strength and ductility. As a result, magnesium based MMCs are receiving high attention as a replacement to Al due to their improved mechanical properties [12-14].

2.2 Tribology of particulate reinforced metal matrix composites

Tribology can be defined as the ‘science and technology of interacting surfaces in relative motion and of related subjects and practices’, and is a field of engineering that deals with the technology of lubrication, control of friction and prevention of wear [24]. In tribological applications, the control of friction and wear is very important for economic reasons and long term reliability. Wear can be defined as the progressive loss of material resulting from mechanical interaction between two contacting surfaces that are in relative

motion, either by sliding or rolling or under load, whereas friction is the resistance to this movement of one body over another that are in contact [25]. Wear is a serious problem in many engineering applications such as moving parts, engine parts etc., and can completely destroy the mechanical functioning of these parts. It can also cause structural failure which can enlarge the tolerances and destroy the surface finish, thus forcing for early replacement of components. And, friction is the main principle that causes energy to be dissipated in various deformation processes that leads to wear of the contacting surfaces and their eventual degradation to an extent where replacement of whole components becomes necessary. Wear is also a very large component to the economic importance of friction, because without friction the contacting surfaces would not wear [26].

Earlier studies on wear behavior of MMCs had clearly shown that wear is never an intrinsic property of the material. MMCs exhibit different tribological behaviors and the principal tribological factors that control friction and wear performance of discontinuously reinforced MMCs can be classified into two categories [27-28]:

1. Mechanical and Physical factors (extrinsic to the material undergoing surface interaction). These include the following:
    1. Effect of load normal to the tribo-contact
    2. Sliding velocity
    3. Sliding distance
    4. Reinforcement orientation of non-equiaxed particulates
    5. Environment and temperature
    6. Surface finish of the counterpart

2. Material Properties (intrinsic to the material undergoing surface interaction). These include the following:
    1. Properties of the reinforcing phase
        i. Reinforcement type
        ii. Reinforcement size and size distribution
        iii. Reinforcement shape and hardness
        iv. Reinforcement volume fraction
    2. Properties of the matrix
        i. Matrix microstructure
        ii. Hardness and ductility
    3. Characteristics of bonding between the reinforcing phase and the matrix.

Understanding the relationship between the material properties and wear behavior is very important step for the design and selection of materials for any tribological applications [27]. MMCs containing hard particulates offer superior operating performances and resistance to wear due to their improved strength, hardness and high modulus at room and elevated temperatures. The factors that significantly influence the wear rates of MMCs are second phase particle dimension, interparticle spacing and particle/matrix interfacial bond strength [28]. To reduce wear in MMCs, it is important to understand the wear mechanisms by which it occurs.

2.3 Wear behavior of Mg based MMCs

The usage of Magnesium for tribological applications are limited because of their inferior mechanical properties such as low thermal stability and poor resistance to wear, which

prevented them from being used as widely as Al. Therefore, many researchers developed magnesium based composites i.e., reinforcement of magnesium with hard ceramic particles was done to obtain lightweight materials with excellent mechanical and tribological properties. In this connection, particulate reinforcements such as SiC, Al_2O_3, and TiC have been successfully employed to improve the wear resistance of magnesium and its alloys.

2.3.1 Mg – SiC MMCs

There has been considerable study regarding the effect of silicon carbide (SiC) particles on the wear properties of magnesium and its alloys. For example, Lim et al. [29] reported slight improvement in the wear resistance of AZ91 alloy when reinforced with 8 vol.% of SiC (14 μm) under lower load of 10 N, however the wear rates were not conclusive under higher load of 30 N. They reported oxidation as the dominant wear mechanism under lower load of 10 N and with increase in load to 30 N transition to delamination and abrasion were observed. Abachi et al. [30] studied the wear behavior of QE22 magnesium alloy reinforced with 10-25 vol.% of SiC (7.5 μm) particles with three different shapes i.e., sharp, blocky and round under different sliding conditions and they reported improvement in the wear resistance of QE22 alloy except under some cases (with higher SiC content), in which wear resistance of the composite decreased due to increased delamination. Moreover, increasing the load and sliding speed led to more weight loss in all the materials. They observed abrasion, oxidation and delamination as operative in combination in most of the test conditions. Huang et al. [31] investigated the wear behavior of AZ91D magnesium alloy reinforced with 3 vol.% SiC with particle size ranging from 5 to 15 μm and reported improvement in the wear resistance of the

composites with increase in particle size. They observed moderate abrasion, moderate oxidation, and slight delamination as operative under lower loads, and slight abrasion, moderate oxidation, heavy delamination, and moderate adhesion and moderate softening/melting under higher loads. In most recent studies, Jo et al. [32] also found similar results i.e., increase in the wear resistance of AZ91/SiC composites with increase in particle size from 1 to 20 μm. They observed transition from abrasive/adhesive wear at lower loads of 5 and 15 N to severe abrasive wear under higher load of 30 N.

2.3.2 Mg – Al_2O_3 MMCs

Lim et al. [33], studied the dry sliding wear behavior of magnesium reinforced with up to 1.11 vol.% nano-sized alumina (50 nm) under various sliding speeds at a constant load of 10 N and they reported increase in wear resistance of the nanocomposites with increase in amount of reinforcement. It was found that the wear rate reduces with increase in sliding speed. However, an optimum speed was seen beyond which the wear rate increased. Moreover, they observed abrasion, adhesion and thermal softening as the dominant wear mechanisms. Habibnejad et al. [34], using Mg and AZ31 alloy reinforced with 2 wt.% alumina (100 nm) nanoparticles, reported improvement in the wear resistance of nanocomposites due to improved strength and hardness. Different wear mechanism of abrasion, oxidation and delamination were observed in this study. Shanthi et al. [35] investigated dry sliding wear behavior of AZ31B–Al_2O_3/Ca nanocomposites under different sliding conditions and reported increase in the wear resistance of nanocomposites with increase in amount of calcium from 1 to 3 wt.% due to improved hardness and strength. They observed abrasion, adhesion as the dominant wear mechanisms under lower speeds with transition to thermal softening only under highest

sliding speed. Recently, Srinivasan et al. [36], also reported improvement in the wear resistance of AZ31B–Al_2O_3/Ca nanocomposite compared to unreinforced AZ31B alloy. They observed mix-up of ploughing, rows of furrows, delamination and oxidation wear mechanisms.

2.3.3 Mg reinforced with other particulate reinforcements

Several other types of particulate reinforcements and their combination on the wear behavior of Mg and its alloys have also been examined by many researchers. Sharma et al. [37] investigated the tribological behavior of AZ91 alloy reinforced with feldspar particles of size 30-50 μm with up to 5 wt.% and found that the wear rates decreased with increase in reinforcement content. They observed abrasive wear as the dominant wear mechanism at low loads and delamination under high loads. Aydin and Findik [38] studied the wear behavior of Mg reinforced with different particle-sized SiO_2 under dry friction conditions and reported decrease in wear rate with reduction in particle size from 500 to 10 μm. Also, increase in wear rate was observed with increase in sliding parameters (load, speed and sliding distance). Furthermore, they observed abrasion as the at low loads and delamination under high loads. Xiu et al. [39] reported increase in the wear resistance of AZ91 magnesium alloy with increase in TiC particulate content from 5 to 15 wt.%. Ploughing groove, adhesion and oxidation were observed as the dominant wear mechanisms in both unreinforced and reinforced materials. In this study, wear by delamination was not evident as the TiC particulates served as a hard barrier that enhance the resistance to plastic deformation. Yao et al. [40] also observed better wear resistance for AZ91/TiC composite with increasing TiC content from 3 to 10 wt.%. However, in this study wear by delamination was observed to be dominant under higher load while

oxidation was dominant at low loads. Umeda et al [41] studied the effect of Mg_2Si hard particles and Carbon Nano Tubes (CNTs) on the wear resistance of sintered magnesium material. Material was fabricated using powder metallurgy technique in which the elemental mixture of pure magnesium powders and amorphous porous silica particles containing CNTs were used as a starting material. The specimens were prepared in the form of disc whereas SUS304 stainless steel ball was used as counterface. They reported that the wear rate decreased with increasing the content of CNTs (0-10 wt.%) and Mg_2Si and friction coefficient was low and stable. Hard Mg_2Si dispersoids and self-lubricating effect by network CNTs were considered as a main cause in decreasing the wear rate and friction coefficient.

2.4 Wear regimes

Classification of wear regimes can be broadly done into two qualitative categories [42]:

1. Mild Wear
2. Severe Wear

The main external features that characterize these wear types are the size and shape of the wear particles, worn surfaces and wear rates. The presence of fine wear particles, smooth wear scars with fine features and low normalized wear rates indicate mild wear behavior whereas the presence of large wear particles, rough wear scars with coarse features and high normalized wear rates indicate the severe wear. The transition of wear from mild to severe is essential in design of wear components for tribological applications and it depends on the variation of the testing conditions that cause sudden jump in the wear rate, properties of the material subjected to wear, mechanical and thermal properties of the

counterface. In order to achieve desired lifetime of the wear components, the wear behavior must be in mild region because in mild form surfaces wear away slowly throughout the life of the machine while in severe form the surfaces tear away extensively and wear is so rapid that machines cannot be allowed to run in this condition [40]. Table 2.1 shows the distinction between mild and severe wear.

Table 2.1 Difference between mild and severe wear [42]

Mild wear	**Severe wear**
Results in very smooth surfaces - often smoother than original	Results in rough, deeply torn surfaces – much rougher than the original
Wear debris will be very small, typically only 100 nm diameter	Large metallic wear debris, typically up to 0.01 mm diameter
High contact resistance, little true metallic contact	Low contact resistance, true metallic junctions formed

2.5 Wear Mechanisms in MMCs

Wear mechanisms are the classification of wear in terms of the way in which material is either lost, displaced or damaged as a result of relative motion between two surfaces and are identified by considering complex changes during friction [24]. A wear mechanism can be either single or a combination of mechanisms, so understanding each wear mechanism in each wear of mode becomes important. Common wear mechanisms that are generally observed in MMCs include:

- Abrasive wear [42-44]
- Adhesive wear [43, 45]
- Delamination wear [26, 43]
- Oxidation wear [44]
- Melt wear [27]

Abrasive wear

Abrasive wear can be defined as wear that occurs whenever asperities of a rough, hard surface or hard particles have relative motion with a softer surface and damage the interface by plastic deformation or fracture. There are two general modes of abrasive wear namely: two body and three body abrasive wear.

Two body abrasive wear occurs when one of the two rubbing surfaces that are brought into contact have harder surface than the other. While in case of three body abrasive wear, the hard surface is a third body, which when trapped between two other surfaces is able to remove material from either one or both of the mating surfaces. During abrasion,

plastic deformation of a surface resulting into material removal can occur by three modes which include ploughing, wedge formation and cutting. In ploughing, series of grooves are formed and the material is displaced on both sides of the grooves without removal of material, while in wedge forming, an abrasive particle ploughs a groove resulting into worn of tiny wedge shaped fragments from the surface. In cutting, an abrasive tip ploughs a groove resulting into removal of material in the form of small fragments or ribbon shaped debris particles. Further, the friction coefficient increases with an increase in degree of penetration which is critical in transition from ploughing and wedge formation to cutting [42-44].

Archard's abrasive wear model [24] is given by

$$W = \frac{K_{abr}.L.v.B}{H}$$

W = Wear rate (m^3/s)

L = Normal force (N)

K_{abr} = Non-dimensional coefficient

H = Hardness of the softer surface (N/m^2)

v = Sliding Velocity (m/s)

$B = 2 \cot \theta / \pi$

Adhesive Wear

When two surfaces move relative to one another, adhesion occurs at the asperity contacts at the interface that are sheared by sliding which may lead to detachment of a fragment from one surface and attachment to the another surface. As the sliding continues, the transferred fragments may come off the surface on which they are transferred and be transferred back to the original surface or else form loose wear debris particles. Also, researchers have found that the increasing temperature during sliding contact may result in greater amount of material transfer [43]. Different wear scar features are indicative of this mechanism such as presence of transferred material between the mating surfaces, wear debris (particles like, rather than platelets or flakes). Some of the parameters on which adhesion of the materials depend are material roughness, modulus of elasticity, hardness and ductility [45].

Delamination Wear

Delamination wear was reported to have occurred by the following steps [28]:

1. Cyclic plastic deformation of surface layers by normal and tangential loads.
2. Crack or void nucleation in the deformed layers at inclusions or second-phase particles.
3. After the crack nucleation, further loading and deformation causes them to extend and to propagate nearly parallel to the surface.
4. These cracks finally shear the surface which results into formation of thin and long wear sheets as debris and their removal by extension of cracks to the surface.

Analysis made on microstructures having hard reinforcing particles revealed that if sufficient plastic deformation occurred during sliding wear, then it results in crack nucleation at these particles. Crack propagation controlled the wear rate as the inter-particle spacing is an important variable in this observation. Void formation was due to the plastic flow of the matrix around these reinforced hard particles and it occurred very readily around these particles but crack propagation occurred very slowly. The depth at which the void nucleation was initiated intended to increase the void size with increased coefficient of friction and applied load [46]. Earlier studies on crack nucleation at particle/matrix interface reported that the following conditions mentioned below were necessary for crack nucleation [28].

1. Tensile stress across the interface should go beyond the interfacial bond strength.
2. Elastic strain energy released upon decohesion of the interface should be sufficient to account for the surface energy of the crack created.

Oxidation Wear

Oxidation wear occurs whenever frictional heating increases the contact temperature of the two mating surfaces that are in sliding motion. It is reported that a threshold sliding velocity must be passed before asperity flash temperatures become high enough for oxidation to take place at a rate that is able to sustain a load bearing film of adequate thickness. Oxidation wear mechanism is dependent on the ability of the wearing material to undergo oxidation and also depends on the availability of oxygen in the immediate vicinity of the sliding contact [47].

Melt wear

Melt wear is caused by frictional heating at the sliding interface. When the applied load and sliding speed reach certain critical thresholds, flash temperatures at the contacting asperities could go beyond the melting point of the matrix, thus raising the bulk temperature and causing gradual softening of the matrix. Further, increase in load and speed would increase the temperature more, leading to melting of the material [29].

2.6 Summary

Based on the literature survey carried out, it was found that most of the magnesium based MMCs were developed by using micron-size ceramic reinforcements fabricated by various processing methods. The development of these materials led to improvement in strength and reduction of ductility. To improve the ductility of Mg based MMCs, researchers were prompted to use reinforcements of nano size. Recently, the use of ceramics as well as metal reinforcements of nano size in magnesium showed significant improvement in strength, work of fracture and ductility. Also, development of magnesium based MMCs with nanoparticles as reinforcement have exhibited comparable or greater strength and stiffness when compared to its micron sized MMCs. Despite the potential of Mg nanocomposites, very less investigation has been made so far on the tribological behavior of these nanocomposites with Al_2O_3 as reinforcement. And, no study has been conducted on wear behavior of CNT reinforced magnesium nanocomposites and (Y_2O_3 + Cu), (Y_2O_3 + Ni) reinforced hybrid nanocomposites. Accordingly, in the present study attempts have been made to explore the tribological properties of magnesium based nanocomposites with Al_2O_3, CNT, (Y_2O_3 + Cu) and

(Y_2O_3 + Ni) particulate reinforcements. The major tasks of this work includes the investigation of the sliding conditions which include applied load, sliding speed, effect of particle content on wear rate and identification of dominant wear mechanisms under each sliding conditions.

CHAPTER 3

EXPERIMENTAL PROCEDURE

3.1 Materials

Three different types of materials namely: Magnesium alloy (AZ31), AZ31-alumina (AZ31/Al_2O_3), AZ31-Carbon Nanotubes (AZ31/CNT) and two different groups of hybrid nanocomposite materials namely: Mg-yttria + copper (Mg/Y_2O_3 + (0.3-1.0) vol.% Cu) and Mg-yttria + nickel (Mg/Y_2O_3 + (0.3-1.0) vol.% Ni) were tested under dry sliding conditions. The base material magnesium alloy (AZ31) and its nanocomposites were synthesized using a innovative method known as disintegrated melt deposition (DMD) technique [48-49] whereas all the hybrid nanocomposites were synthesized by using powder metallurgy technique [50-51]. All the materials were subsequently hot extruded at 350 ˚C. Details of the fabrication process and microstructural characterization taken from published articles are presented in the next sections.

For the first group of materials, Magnesium Alloy AZ31 (nominally 2.5-3.5 wt% Al, 0.6-1.4 wt% Zn, 0.15-0.4 wt% Mn, 0.1 wt% Si, 0.05 wt% Cu, 0.01 wt% Fe, 0.01 wt% Ni balance Mg) was used as the base material, and 1.5 vol. % alumina (50 nm size), 1.0 vol.

% Carbon Nanotubes (vapor grown, 94.7% purity, 40-70 nm outer diameter) were used as reinforcement.

In one group of hybrid nanocomposite materials, pure magnesium (98.5% purity) was used as the matrix material in which 0.7 vol.% of yttria (30-50 nm) and Nickel (20 nm) of three different amounts (0.3, 0.6 and 1.0 vol.%) were used as reinforcement. Whereas in other group of hybrid nanocomposite materials, Copper (25 nm) of similar amounts was used as a reinforcement in place of copper.

3.2 Processing Technique

All the materials used in the present study were fabricated by using two different processing methods namely: Disintegrated Melt Deposition (DMD) and Powder Metallurgy technique at National University of Singapore, Singapore.

3.2.1 Disintegrated Melt Deposition Technique for AZ31/Al_2O_3 and AZ31/CNT Nanocomposites

In the present investigation, the base material (AZ31) and its nanocomposites were synthesized using Disintegrated melt deposition (DMD) technique**.** In this process, the base material and the desired amount of reinforcement particulates (for the composite) are firstly weighed and placed in a graphite crucible. The materials are then superheated to 750˚C in an inert gas atmosphere using resistance heating furnace. The crucible was equipped with an arrangement for bottom pouring. After attaining the superheat temperature, the molten slurry was agitated for 2.5 min at 460 rpm using a twin blade mild steel impeller to have uniform distribution of reinforcement particulates in the

molten mixture. The impeller is coated with Zirtex 25 to avoid iron contamination of the molten metal. The melt was then released through a 10 mm diameter orifice at the base of the crucible and disintegrated by the two argon gas jets, oriented normal to the melt stream. The disintegrated molten slurry was subsequently deposited onto a metallic substrate located 500 mm from the disintegrated point. An ingot of 40 mm diameter was obtained. The synthesis of base material AZ31 was carried out using similar steps except that no reinforcement particulates were added. The deposited base material and reinforced nanocomposites were machined to 35 mm diameter and hot extruded on a 150 ton hydraulic press. Rods of 8 mm were obtained after extrusion [48-49]. The schematic diagram of DMD technique is shown in figure 3.1.

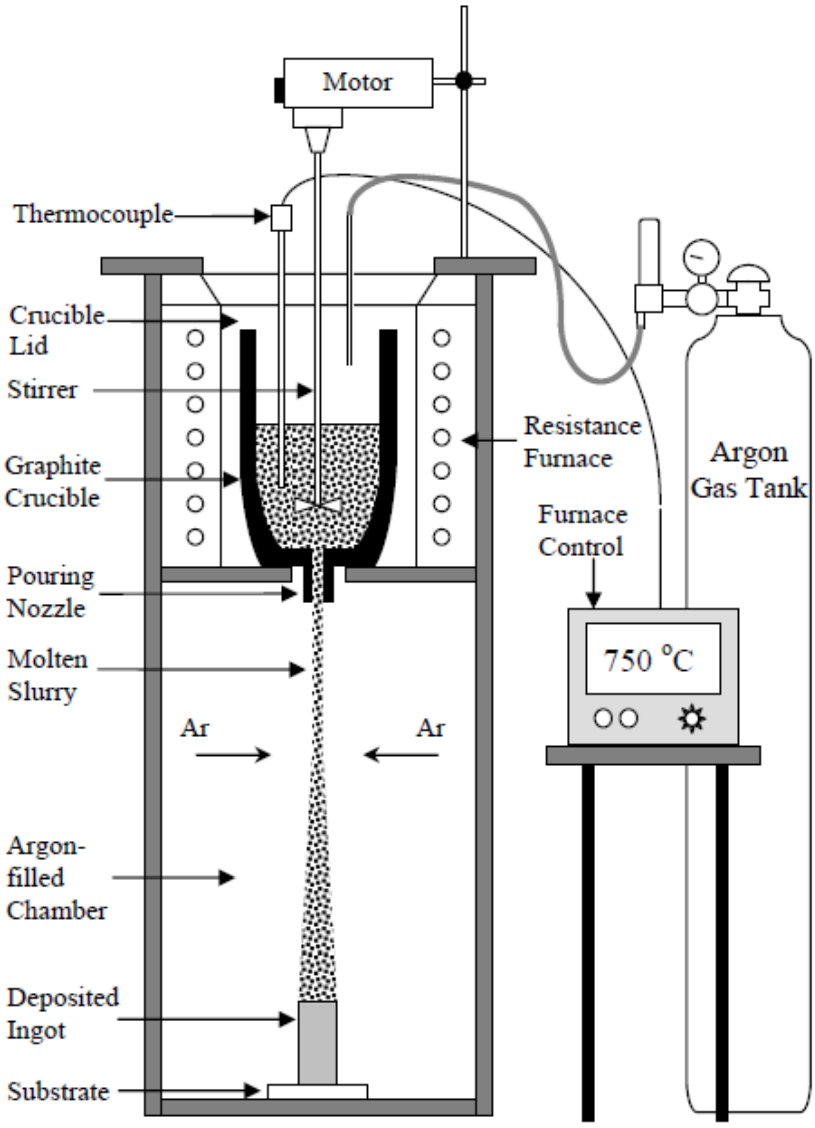

Figure 3.1 Schematic Diagram of DMD process [5].

3.2.2 Powder Metallurgy Technique for Mg/(Y_2O_3+Cu) and Mg/(Y_2O_3+Ni) Hybrid Nanocomposites

All the Magnesium based hybrid nanocomposites that were used in the present study for wear tests were fabricated by using powder metallurgy technique in the following procedure. Blending of pure magnesium matrix and reinforcement powders were done in a mechanical alloying machine at 200 rev/min for 1 hour followed by compaction at a pressure of 97 bars using a 100 ton press to form a billet of 35 mm diameter and 40 mm height. All the compacted billets were immediately sintered by using an innovative microwave sintering at 643 ˚C for 13 min. The sintered billets were hot extruded at a temperature of 350˚C at an extension ratio of 25:1 [50-51].

3.3 Material Characterization

Physical, microstructural and mechanical properties characterization of the developed materials used in the present work was done at National University of Singapore (NUS), Singapore. Density measurements of all the materials were performed by using Archimedes's principle. SEM analysis of all the materials indicated that the reinforcement distribution in the nanocomposite was reasonably uniform, with minimal porosity. Tensile tests were conducted on round specimens in accordance with ASTM E8M-05. Also, Microhardness tests were performed on all the samples using Vicker's indenter under a test load of 25gf and a dwell time of 15 s in accordance with the ASTM standard E384-99. Some mechanical properties of the pin materials used in the present study are summarized in Table 3.1.

Table 3.1 Some important properties of pin materials used in the present work [48-51].

Material	Porosity (vol.%)	Microhardness (HV)	0.2% Yield Strength (MPa)	Ultimate Tensile Strength (MPa)	Ductility (%)	Work of Fracture (MJ/m^3)	Density (g/cm^3)
AZ31	0.11	64 ± 4	172 ± 15	263 ± 12	10.4 ± 3.9	26 ± 9	1.794
AZ31/1.5Al_2O_3	1.09	83 ± 5	204 ± 8	317 ± 5	22.2 ± 2.4	68 ± 7	1.804
AZ31/1.0CNT	0.53	95 ± 4	190 ± 13	307 ± 10	17.5 ± 2.6	50 ± 8	1.78
Mg/(0.7Y_2O_3 + 0.3Cu)	0.45	55 ± 2	215 ± 20	270 ± 22	11.1 ± 1.0	29.8 ± 2.7	1.775
Mg/(0.7Y_2O_3 + 0.6Cu)	0.77	58 ± 3	179 ± 7	231 ± 13	11.1 ± 0.7	25.4 ± 0.9	1.792
Mg/(0.7Y_2O_3 + 1.0Cu)	1.04	62 ± 5	-	-	-	-	1.811
Mg/(0.7Y_2O_3 + 0.3Ni)	0.34	54 ± 4	221 ± 7	262 ± 6	9.0 ± 0.9	23.7 ± 2.1	1.778
Mg/(0.7Y_2O_3 + 0.6Ni)	0.21	60 ± 4	232 ± 8	272 ± 2	9.5 ± 0.9	25.9 ± 2.3	1.802
Mg/(0.7Y_2O_3 + 1.0Ni)	0.3	63 ± 4	228 ± 8	271 ± 6	5.5 ± 0.7	15.4 ± 2.3	1.829

3.4 Experimental Apparatus

The tribometer that was used in the present work for wear testing is a pin-on-disc type tribometer designed in King Fahd University of Petroleum and Minerals (KFUPM). The apparatus and other materials that were used in the present study include:

1. Apparatus equipped with Pin-on-disc tribometer that were used in the present study are as follows
    - Frictional (Force or Torque) indicator
    - Programmable Timer
    - Frequency controller (to control the Speed)
2. Electronic balance with ±0.05 mg accuracy (was used to measure the mass of pin before and after each test)
3. Heat treated AISI 4140 tool steel hardened to 53 HRC.
4. Abrasive SiC papers (400 and 600 grit) were used for grinding the pin specimen before each test
5. Alcohol was used to clean the specimen before and after the test

3.4.1 Pin-on-Disc tribometer

The Pin-on-Disc tribometer that will be used in the present study has following specifications:

- Vertical Load upto 200 N can be applied.
- Continuous bidirectional rotation of disc over a large range of sliding speeds (0.1 rpm to 13000 rpm).

- High temperature capabilities (upto 500˚C ± 5˚C).
- Maximum torque upto 10 N-m with an accuracy of 0.0025 N-m.
- Dry and Lubricated tests capabilities
- Controlled gas environment non-reactant with stainless steel or tool steel.
- Temperature measurement capability with an accuracy of ± 0.5˚C.
- Capability to control oscillation over a range of amplitudes.

A view of the tribometer is shown in figure 3.2.

Figure 3.2 Pin-on-Disc tribometer at KFUPM

3.5 Wear Tests

3.5.1 Pin Specimen Preparation

The as-extruded 8-mm rods were machined to a diameter of 6 mm and then cut into 15 mm long pins in a lathe (to approximately 0.4 µm surface finish). The end surfaces of the pins were prepared by grinding against abrasive SiC papers (400 and 600 grit) to ensure that both ends are flat and smooth. For dry wear tests, final polishing was performed by using diamond paste of 0.1 µm size.

3.5.2 Disc Preparation

The disc specimens were machined from commercially available AISI 4140 tool steel to a diameter of 125 mm and thickness of 20 mm. Heat treatment of the disc was done and a hardness of 53 HRC was obtained. The disc surface was flatly ground to give a surface finish with an average R_a value of approximately 0.3 µm using alumina abrasive wheel.

3.5.3 Experimental Conditions

AZ31 Magnesium alloy and its nanocomposites AZ31/Al_2O_3 and AZ31/CNT were tested at three sliding speeds of 1, 2 and 5 m/s under the applied loads of 5, 10, 15 and 20 N for a sliding distance of 2500 m. The other group of materials i.e., Mg/Y_2O_3-(0.3-1) vol.% Cu hybrid nanocomposites were tested at a constant sliding of 1 m/s whereas Mg/Y_2O_3-(0.3-1) vol.% Ni) were tested at a constant sliding speed of 0.5 m/s under the applied loads of 5, 10, 15, 20, 25 and 30 N for a sliding distance of 1000 m.

3.5.4 Experimental Procedure

1. Preparing the pin and cleaning the contact surfaces of the pin (by grinding against 600 grit silicon carbide paper and then cleaning with alcohol) followed by measuring and recording the initial weight with high accuracy.

2. Cleaning the surface of the AISI 4140 tool steel disc (having surface finish 0.3μm) using alcohol.

3. Loading the stationary pins securely and vertically on to a rotating AISI 4140 tool steel disc using pin holder.

4. Adjusting the speed to the desired value while holding the pin specimen out of contact with the disc.

5. Applying the load on the pin and closing the door of the tribometer properly.

6. Starting the test with the specimen in contact under load without interrupting until the completion of desired number of revolutions.

7. Any noise, vibration or any other unusual behavior of the specimen that were observed are noted.

8. After the completion of desired number of revolutions, specimens were removed and wear debris was collected, if any. Existence of features on or near the wear scar such as: protrusions, displaced metal, discoloration, micro-cracking or spotting were noted.

9. In most cases, the materials of the pins were pushed to the sides during sliding and got resolidified along the periphery. Since these resolidified materials were considered as the material worn out during sliding, they were filed off carefully after each run prior to weighing in order to avoid error in measured weights.

10. Cleaning the pin specimen with alcohol after the test.

11. Weights of the specimen were measured again after each test to find out the weight loss.

12. Experiments were repeated with more specimens to obtain sufficient and reliable results.

3.5.5 Wear measurements

Wear rate is defined as the volume loss of the pin specimen per unit sliding distance and its units are expressed as mm^3/km. The volume loss will be calculated from the ratio of mass difference of the pin measured before and after the test to the density.

Volume loss = (mass loss of the pin (g) / Density (g/cm^3)) x 1000

$$\Delta \mathbf{V} = \frac{\Delta \boldsymbol{m}}{\boldsymbol{\rho}}$$

Volumetric wear rate = Volume loss (mm^3) / Sliding distance (km)

3.5.6 Scanning Electron Microscopic and Energy Dispersive X-ray Analysis

The worn surfaces of the pin specimen and collected wear debris were examined using the scanning electron microscope (SEM) and energy dispersed X-ray analysis (EDX). An optical microscope was used to examine the wear track on the disc under various sliding conditions.

3.6 Uncertainty Analysis

Uncertainty analysis was carried out as the accuracy of the wear rate depends on several parameters. The symbols used in the present analysis are as follows [52]:

w = Wear rate (mm^3/km)

ΔV = Volume loss of pin during wear test (mm^3)

ρ = Density of the material (g/cm^3)

m_1 = Mass of pin before wear test

m_2 = Mass of pin after wear test

v = Sliding speed (m/s)

R = Radius of circular wear track (mm)

N = RPM of counterface disc

t = Wear test duration (s)

The wear rate 'w' is defined as the volume loss per sliding distance and hence it is expressed as

$$w = \frac{\Delta V}{vt}$$

Where

$$\Delta V = \frac{m_1 - m_2}{\rho}$$

And

$$v = \frac{2\pi RN}{60}$$

Therefore

$$w = \frac{9.5(m_1 - m_2)}{\rho RNt} \ldots\ldots (1)$$

The data reduction equation expresses wear rate as a function of measured parameters in the form

$$w = f(m_1 , m_2 , \rho , R , N)$$

Uncertainty with time has been neglected.

The variables m_1 and m_2 are fully correlated since they are measured using same instrument. Hence the Bias in wear rate 'B_w' is given by

$$B_w^2 = \left(\frac{\partial w}{\partial m_1}\right)^2 B_{m_1}^2 + \left(\frac{\partial w}{\partial m_2}\right)^2 B_{m_2}^2 + 2\left(\frac{\partial w}{\partial m_1}\right)\left(\frac{\partial w}{\partial m_2}\right) B_{m_1} B_{m_2}$$

$$+\left(\frac{\partial w}{\partial R}\right)^2 B_R^2 + \left(\frac{\partial w}{\partial N}\right)^2 B_N^2 + \left(\frac{\partial w}{\partial \rho}\right)^2 B_\rho^2$$

Dividing whole equation by w^2, we get

$$\left(\frac{B_w}{w}\right)^2 = \left(\frac{1}{w}\frac{\partial w}{\partial m_1}\right)^2 B_{m_1}^2 + \left(\frac{1}{w}\frac{\partial w}{\partial m_2}\right)^2 B_{m_2}^2 + 2\left(\frac{1}{w}\frac{\partial w}{\partial m_1}\right)\left(\frac{1}{w}\frac{\partial w}{\partial m_2}\right) B_{m_1} B_{m_2}$$

$$+\left(\frac{1}{w}\frac{\partial w}{\partial R}\right)^2 B_R^2 + \left(\frac{1}{w}\frac{\partial w}{\partial N}\right)^2 B_N^2 + \left(\frac{1}{w}\frac{\partial w}{\partial \rho}\right)^2 B_\rho^2 \ldots\ldots (2)$$

From (1), the partial derivatives are obtained as follows

$$\frac{\partial w}{\partial m_1} = \frac{w}{m_1 - m_2}$$

$$\frac{\partial w}{\partial m_2} = \frac{w}{m_1 - m_2}$$

$$\frac{\partial w}{\partial R} = -\frac{w}{R}$$

$$\frac{\partial w}{\partial N} = -\frac{w}{N}$$

$$\frac{\partial w}{\partial \rho} = -\frac{w}{\rho}$$

Substituting these partial derivatives in (2), we get

$$\left(\frac{B_w}{w}\right)^2 = \left(\frac{B_R}{R}\right)^2 + \left(\frac{B_N}{N}\right)^2 + \left(\frac{B_\rho}{\rho}\right)^2 \ldots\ldots (3)$$

Bias in m_1 and m_2 gets cancelled out due to correlation between them.

The precision in wear rate (P_w) is given by

$$P_w^2 = \left(\frac{\partial w}{\partial m_1}\right)^2 P_{m_1}^2 + \left(\frac{\partial w}{\partial m_2}\right)^2 P_{m_2}^2 + \left(\frac{\partial w}{\partial R}\right)^2 P_R^2 + \left(\frac{\partial w}{\partial N}\right)^2 P_N^2 + \left(\frac{\partial w}{\partial \rho}\right)^2 P_\rho^2$$

Dividing equation by w^2, we get

$$\left(\frac{P_w}{w}\right)^2 = \left(\frac{1}{w}\frac{\partial w}{\partial m_1}\right)^2 P_{m_1}^2 + \left(\frac{1}{w}\frac{\partial w}{\partial m_2}\right)^2 P_{m_2}^2 + \left(\frac{1}{w}\frac{\partial w}{\partial R}\right)^2 P_R^2 + \left(\frac{1}{w}\frac{\partial w}{\partial N}\right)^2 P_N^2 + \left(\frac{1}{w}\frac{\partial w}{\partial \rho}\right)^2 P_\rho^2$$

Substituting partial derivatives, we get

$$\left(\frac{P_w}{w}\right)^2 = \left(\frac{P_{m_1}}{m_1 - m_2}\right)^2 + \left(\frac{P_{m_2}}{m_1 - m_2}\right)^2 + \left(\frac{P_R}{R}\right)^2 + \left(\frac{P_N}{N}\right)^2 + \left(\frac{P_\rho}{\rho}\right)^2 \ldots\ldots (4)$$

In the present work, values of 'm_1' and 'm_2' were recorded by using a Shimadzu AUW220D dual range electronic balancer. In this instrument, the scale has a resolution of 0.1 mg for a range of 220 g and a resolution of 0.01 mg for a range of 82 g. And, the device has a linearity of 0.2 mg for a range of 220 g and a linearity of 0.1 mg for a range of 82 g. Since a range of 82 g was used, a linearity of 0.1 mg is used as bias. The manufacturer's data sheet lists a repeatability of 0.1 mg for a large range and a repeatability of 0.05 mg for a small range. A repeatability of 0.05 mg is thus used as precision.

The track radius ‘R’ was set using a specially designed arm having graduations in mm which were made during arm fabrication. The accuracy was insured using a Starret 721A electronic digital calliper having accuracy of 0.03 mm which is taken as bias. The pin holder is adjusted manually with the graduation. So in this adjustment, the human error of 0.25 mm is taken as precision.

The bias in ‘N’ is based on the work carried out previously [53] in which 1 Hz of input frequency corresponds to 41 rpm using same tribometer setup as in current work. The bias in that work was found to be 13 rpm and precision as 0 rpm. In present work, 1 Hz of input frequency corresponds to 18 rpm. So the current bias in N can be calculated as (18/41)*13 = 5 rpm (approx.). The precision remains same as 0 rpm.

The density ‘ρ’ of specimens was measured using MD 300 electronic densimeter for which the error in measurements could be 0.001 g/cm^3 according to manufacturer’s data sheet. So this value is taken as bias. In density measurement, the density of the same specimen varied by 0.001 g/cm^3 during repetitions and hence this value was taken as precision.

Table 3.2 summarizes the bias, precision and nominal values for all the variables.

Substituting values from Table 3.2 in (3) and (4), we get

$$\left(\frac{B_w}{w}\right)^2 = 2.01 \times 10^{-4}$$

$$\left(\frac{P_w}{w}\right)^2 = 8.98 \times 10^{-4}$$

Therefore, uncertainty in wear rate 'U_w' is given by

$$\left(\frac{U_w}{w}\right)^2 = \left(\frac{B_w}{w}\right)^2 + \left(\frac{1}{\sqrt{n}}\frac{P_w}{w}\right)^2$$

Where 'n' is the number of repetitions for the same experiment and its value is 3.

Substituting in the above equation, we get

$$\left(\frac{U_w}{w}\right)^2 = 5.002 \times 10^{-4}$$

$$\frac{U_w}{w} = 0.0224$$

$$U_w = 2.24\ \%$$

Hence, the uncertainty in reported wear rate is 2.24 percent.

Table 3.2 Bias, Precision and Nominal values for different variables.

Variable	Bias	Precision	Nominal Value
m_1	0.1 mg	0.05 mm	0.5880×10^3 mg
m_2	0.1 mg	0.05 mm	0.55156×10^3 mg
R	0.03 mm	0.25 mm	27 mm
N	5 rpm	0 rpm	354 rpm
ρ	0.001 g/cm^3	0.001 g/cm^3	1.794 g/cm^3

CHAPTER 4

RESULTS

To get a better understanding of the tribological behaviour of nanocomposites, it is necessary to explore different extrinsic parameters that affect its wear performance. In the present investigation, there are three parameters that are of great importance; they are: normal load, sliding speed and particulate content. Wear data of all the specimens obtained from the wear tests will be presented individually for the three different groups of nanocomposites i.e., in the first group results of AZ31 and its nanocomposites AZ31/Al_2O_3, AZ31/CNT are presented, then the results of other two groups i.e., Mg/(Y_2O_3 + Ni) and Mg/(Y_2O_3 + Cu) hybrid nanocomposites are presented in the following sections.

4.1 Magnesium alloy (AZ31) based Nanocomposites

4.1.1 Wear Rate of AZ31 and its AZ31/Al_2O_3 nanocomposite

The variations in wear rate with applied loads of 5 to 20 N with an increment of 5 N at sliding speeds of 1, 2 and 5 m/s for both monolithic AZ31 and its AZ31-1.5 vol.% Al_2O_3 nanocomposite are shown in Fig. 4.1. Under all the sliding conditions, addition of nano-

sized alumina particulates did not show any reduction in the wear rates of AZ31 magnesium alloy. Rather, the nanocomposite displayed higher wear rates compared to unreinforced alloy. From the Fig. 4.1, it is also clearly evident that the wear rates of AZ31 and its nanocomposite gradually increased with an increase in applied load from 5 to 20 N under all sliding speeds.

Fig. 4.2 shows the volumetric wear rates for AZ31 and its AZ31-1.5 vol.% Al_2O_3 nanocomposite plotted against sliding speeds under normal loads of 5-15 N. It is clearly evident that in all the conditions, nanocomposite has higher wear rates than the unreinforced material and also there is a gradual reduction in the wear rate of AZ31 and its nanocomposite with increase in sliding speed from 1 to 5 m/s under all the applied loads of 5-15 N.

The present experimental results show that the reinforcement of nano-sized alumina particulates increases the wear rate of AZ31 magnesium alloy. These results are perhaps surprising since mechanical properties such as hardness and strength of the composite are significantly better than its monolithic counterpart. The reasons for this are discussed in later sections.

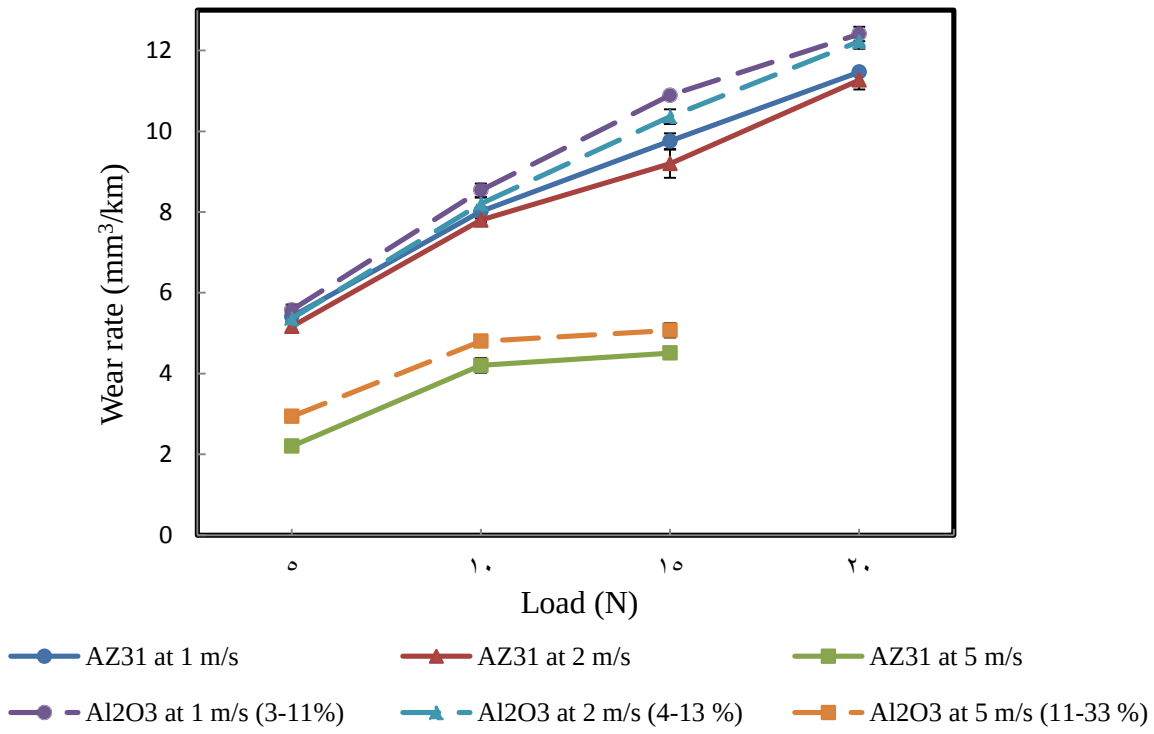

Figure 4.1 Variation of wear rate with applied load at different sliding speeds for AZ31 and its AZ31/Al_2O_3 nanocomposite.

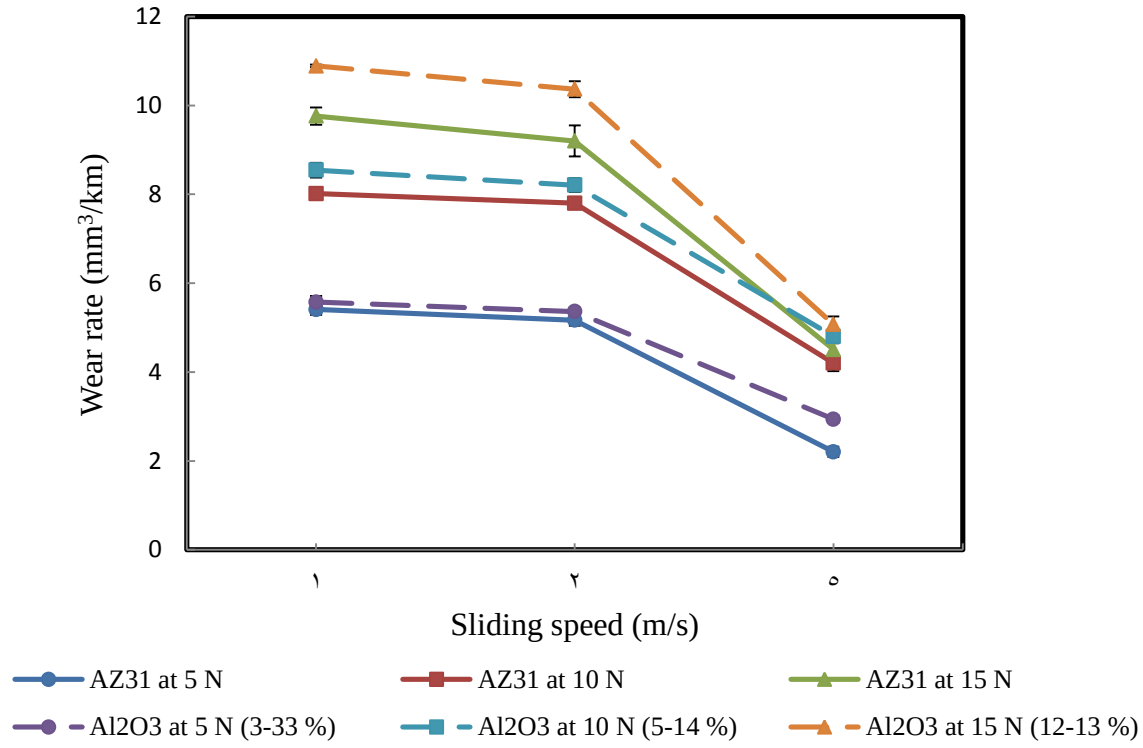

Figure 4.2 Effect of sliding speed on the wear rate at various applied loads for AZ31 and its AZ31/Al_2O_3 nanocomposite.

4.1.2 Wear Mechanisms in AZ31 and its AZ31/Al_2O_3 nanocomposite

Abrasion

Scanning Electron Microscopic (SEM) examination of worn pin surfaces of both unreinforced alloy and its nanocomposite tested under sliding speeds of 1 and 2 m/s at a normal load of 5 and 10 N revealed continuous long grooves and scratch marks parallel to the sliding direction (Fig. 4.3). However, discernible difference between the extent of abrasion on the unreinforced alloy and its Al_2O_3 reinforced nanocomposite is observed under the same sliding conditions (Fig. 4.4). The reasons for this are discussed in the later sections. Moreover, small fragments and ribbon shaped strips of material are seen in the wear debris (Fig. 4.5). And, EDX analysis of the wear debris of the nanocomposite exhibited presence of thin steel strips indicating abrasion of the tool-steel counterface (Fig. 4.6). All these features suggested abrasive wear as the dominant wear mechanism under these sliding conditions.

Under lower sliding speed of 1 m/s, deep grooves are observed on the pin surface with minimum displacement of material on either side of the grooves. At the same time, more amount of wear debris is collected, which altogether suggested more removal of material due to cutting mode of abrasion under these sliding conditions [33].

As the sliding speed is increased, transition from deeper grooves to shallow scratches along with plastic deformation is observed, with material displacement on either side of the grooves on the pin surface. At the same time, long and small wear particles due to breaking of ridges during sliding are observed in the wear debris (Fig. 4.7), which altogether suggested abrasion via ploughing at high speeds [33].

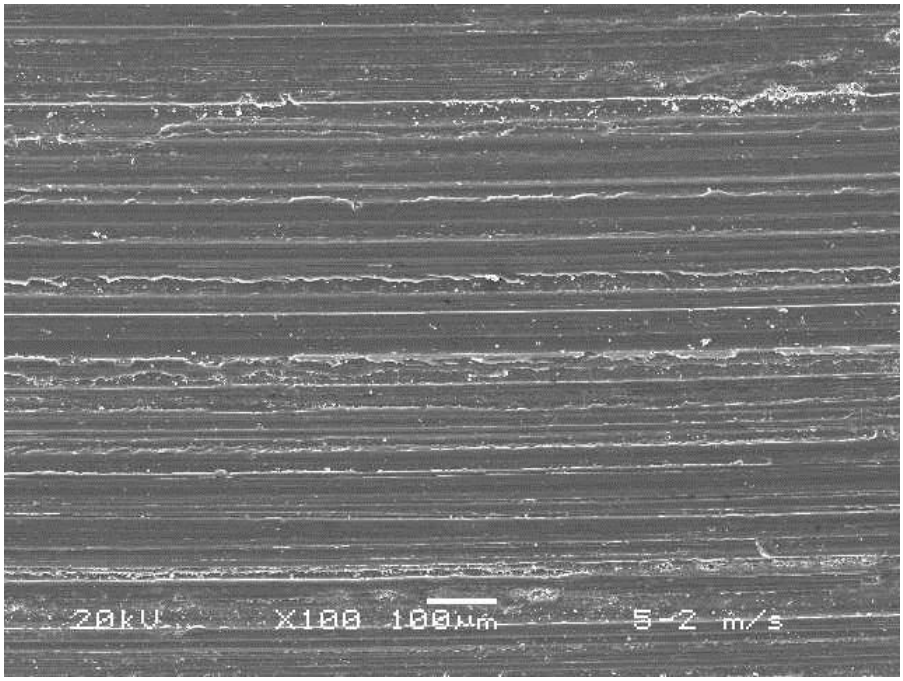

Figure 4.3 Grooves and scratches on the pin surface indicating abrasive wear for the AZ31/Al_2O_3 nanocomposite at 2 m/ sliding speed and 5 N applied load.

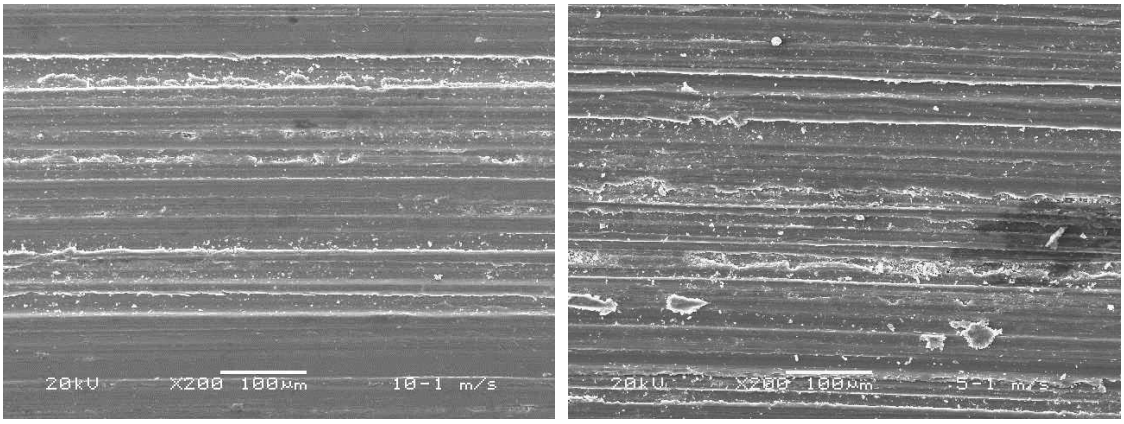

(a) (b)

Figure 4.4 Difference in extent of abrasion on the pin surfaces of (a) unreinforced alloy and (b) Al_2O_3 reinforced nanocomposite at 1 m/s sliding speed and 10 N applied load.

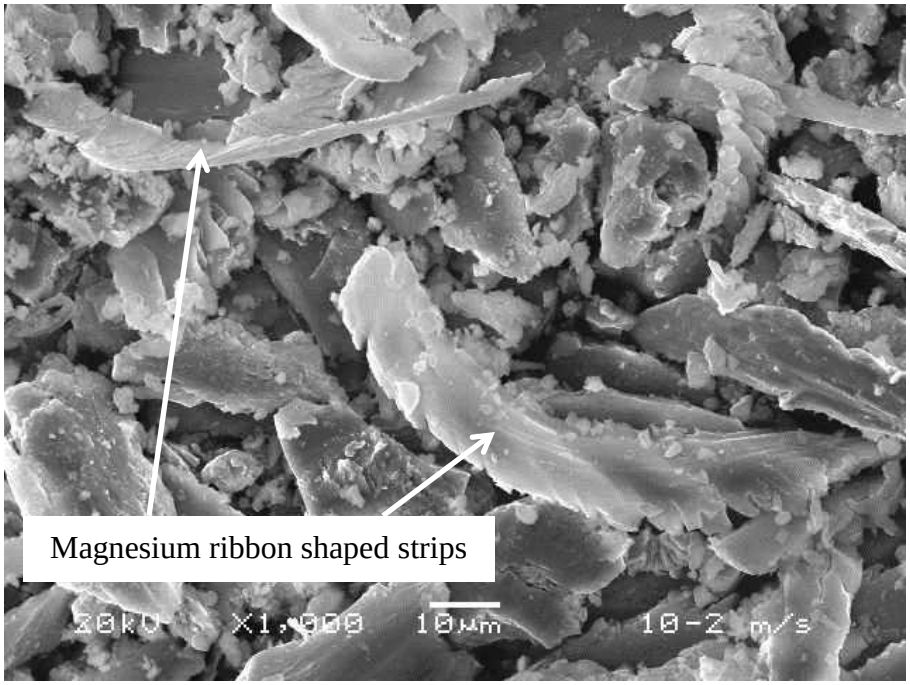

Figure 4.5 Magnesium ribbon shaped strips in the wear debris of AZ31/Al2O3 nanocomposite showing cutting action of an abrasive particle at 10 N and 2 m/s.

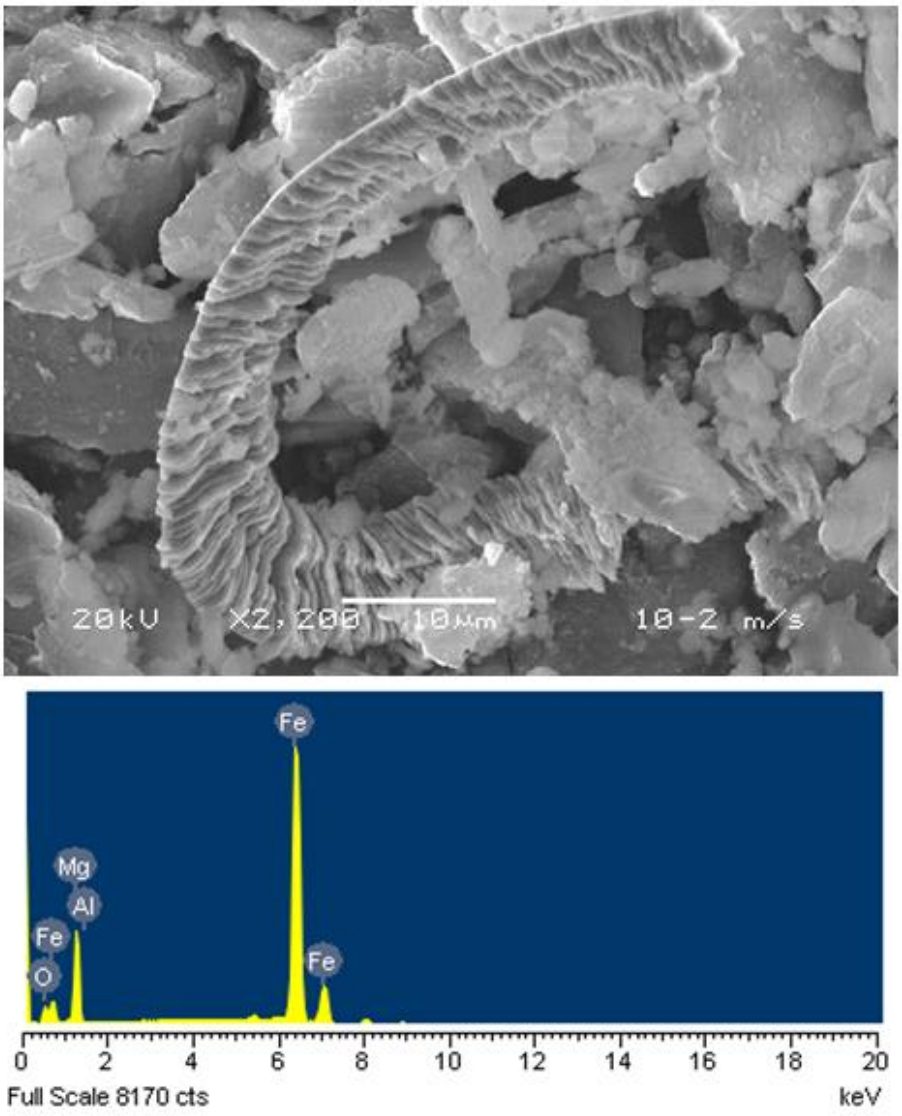

Figure 4.6 Steel strip in the wear debris of the AZ31/Al_2O_3 nanocomposite due to abrasive wear of tool-steel counterface at 2 m/s sliding velocity and 10 N applied load.

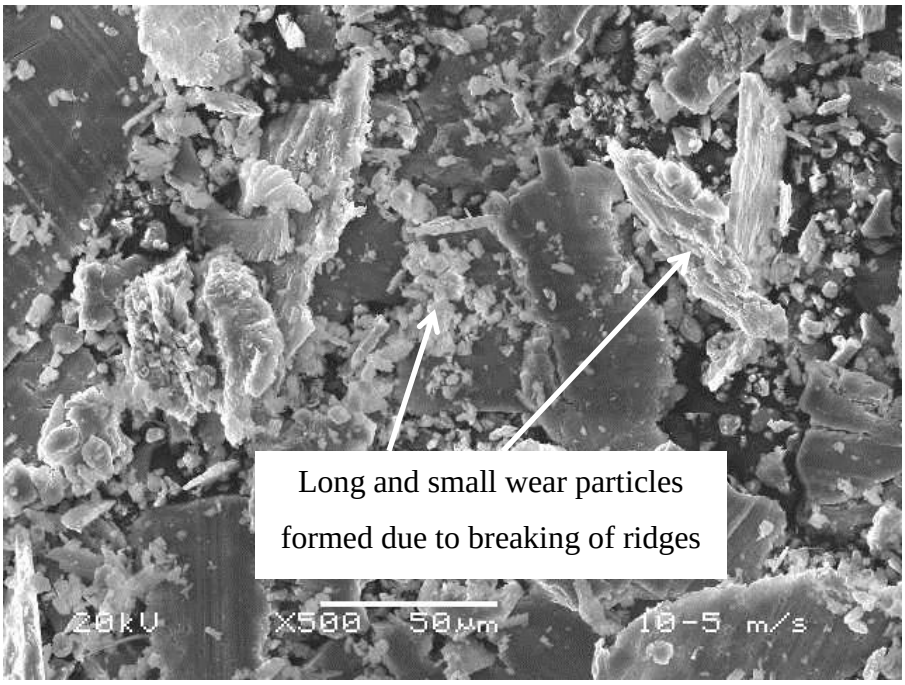

Figure 4.7 Long and small wear particles formed due to breaking of ridges showing ploughing action of AZ31 at 10 N and 5 m/s.

Delamination

Detailed analysis of worn pin surfaces tested under sliding speeds of 2 and 5 m/s at normal loads of 5 and 10 N showed a series of cracks perpendicular to the sliding direction (Fig. 4.8). At the same time, shallow craters (Fig. 4.9) are seen on the pin surfaces due to the propagation of these cracks in the subsurface region resulting in removal of material in the form of flakes or thin sheets, which are evident from the EDX analysis (Fig. 4.10). All these features suggested delamination wear mechanism as effective under these sliding conditions. Moreover, delamination appeared slightly extensive in nanocomposite compared to the base material. The reasons for this are discussed in later sections.

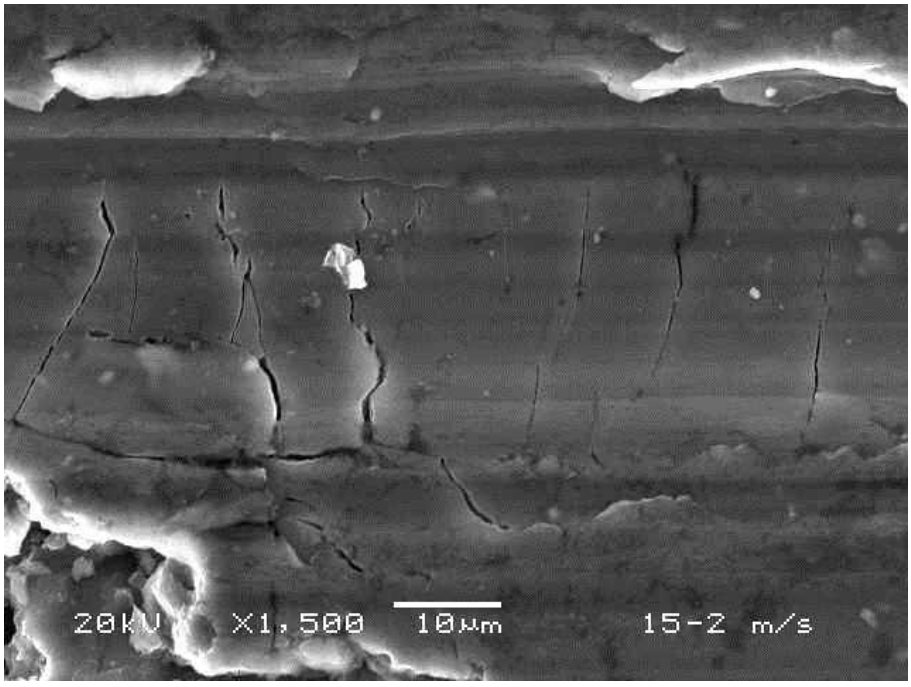

Figure 4.8 Series of cracks perpendicular to the sliding direction indicating delamination in the AZ31/Al_2O_3 nanocomposite under a load of 15 N at 2 m/s sliding speed.

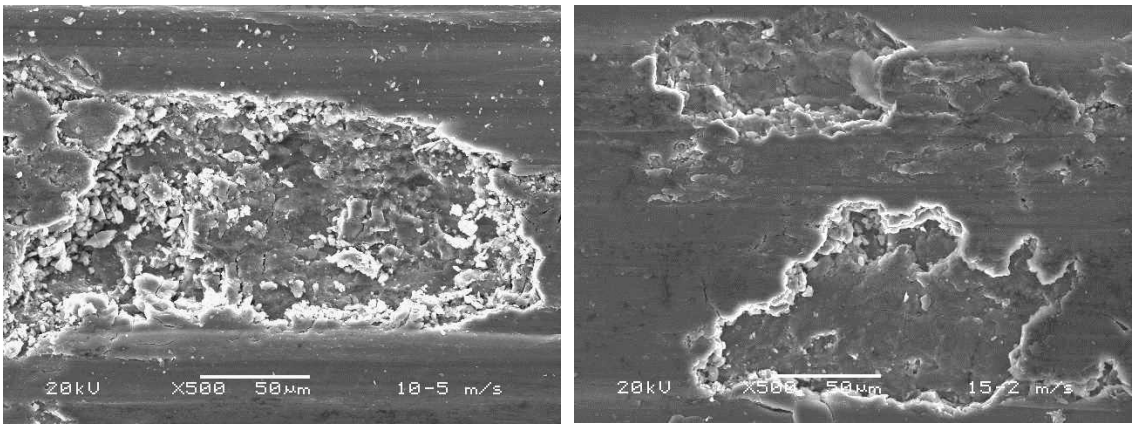

(a) (b)

Figure 4.9 Large crater on the pin surface due to delamination for (a) AZ31/Al_2O_3 at a load of 10 N and 5 m/s sliding speed. (b) AZ31 magnesium alloy at a load of 15 N and 2 m/s sliding speed.

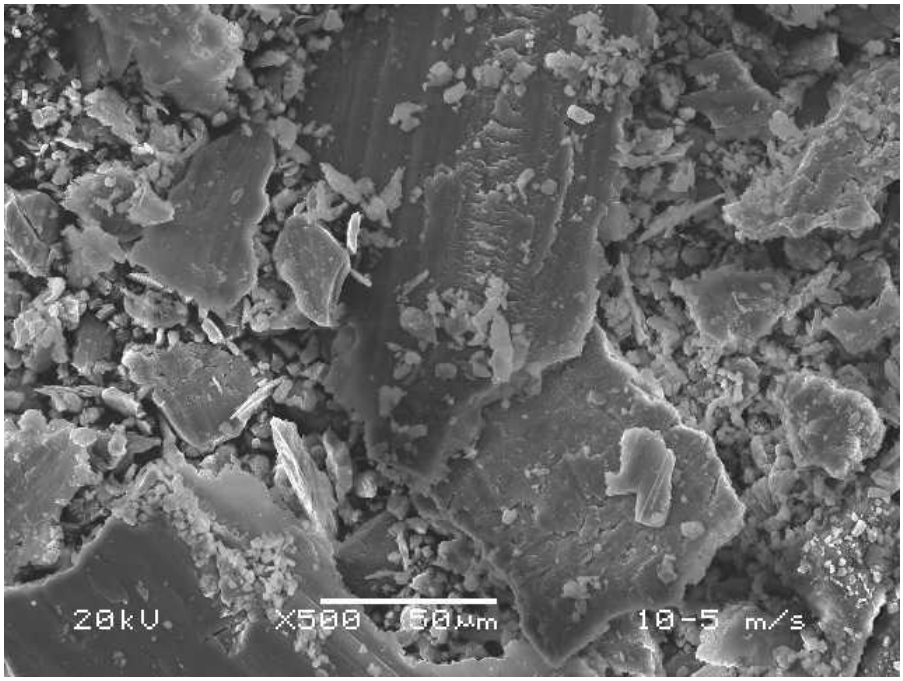

Figure 4.10 Wear debris of the AZ31/Al_2O_3 nanocomposite showing large sheet-like wear particles at 10 N and 5 m/s.

Adhesion

At the sliding speed of 2 and 5 m/s under normal loads of 10 N and above, rows of furrows as well as signs of smearing and plastic deformation are seen on the worn pin surfaces (Fig. 4.11). Analysis of wear track at these sliding conditions showed transfer of material from the pin surface to the disc (Fig. 4.12). And as the sliding speed and load is increased, more amount of transferred material is seen on the wear track. Furthermore, less amount of wear debris is collected when compared with conditions where other mechanisms were dominant. All these features are associated with adhesive wear which increased with increase in sliding parameters. Moreover, adhesive wear is observed to be more severe in case of nanocomposites. The reasons for this are discussed in later sections.

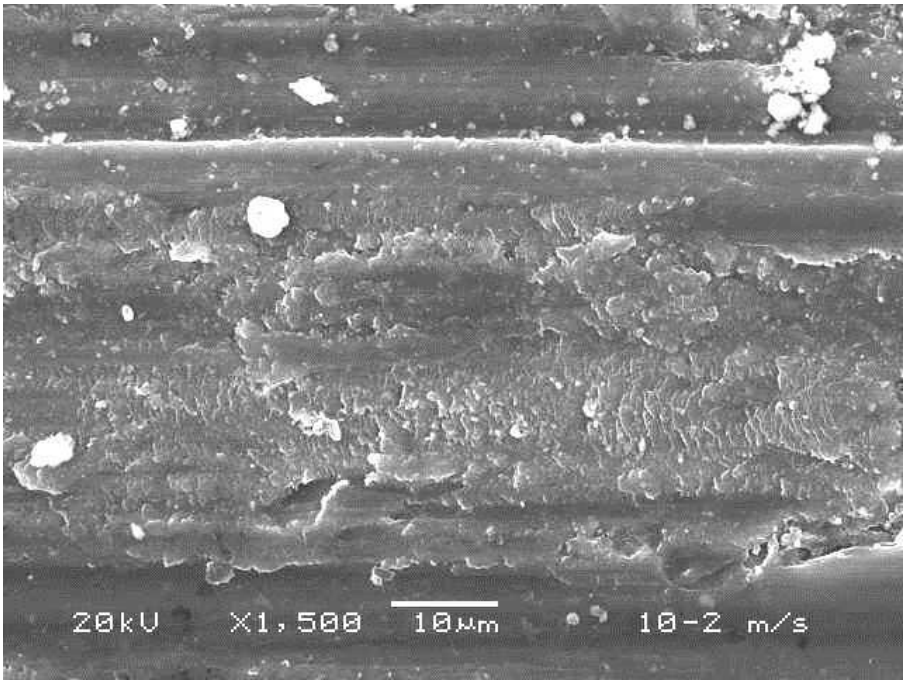

Figure 4.11 Rows of furrows indicating adhesive wear of AZ31/Al_2O_3 nanocomposite under a load of 10 N and 2 m/s sliding speed.

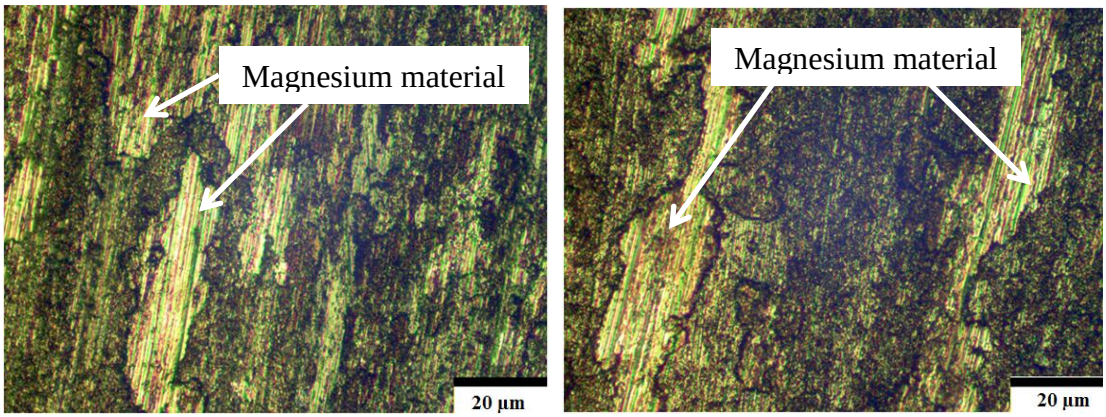

Figure 4.12 Optical microscopic examination of the wear track indicating transfer of material from the surface of AZ31/Al_2O_3 nanocomposite at a normal load of 20 N and 2 m/s sliding speed.

Thermal Softening

Under the most severe sliding condition of 20 N, gross plastic deformation of the pin surface occurs and material is extruded from the interface before re-solidifying around the periphery of the pin (Fig. 4.13). At the same time, the worn pin surfaces of the specimen appeared much smoother than those worn under other sliding conditions. Also, large amount of material transfer is clearly seen on the wear track of the disc. These features are associated with softening and melting of the material caused at higher sliding parameters due to frictional heating at the sliding interface.

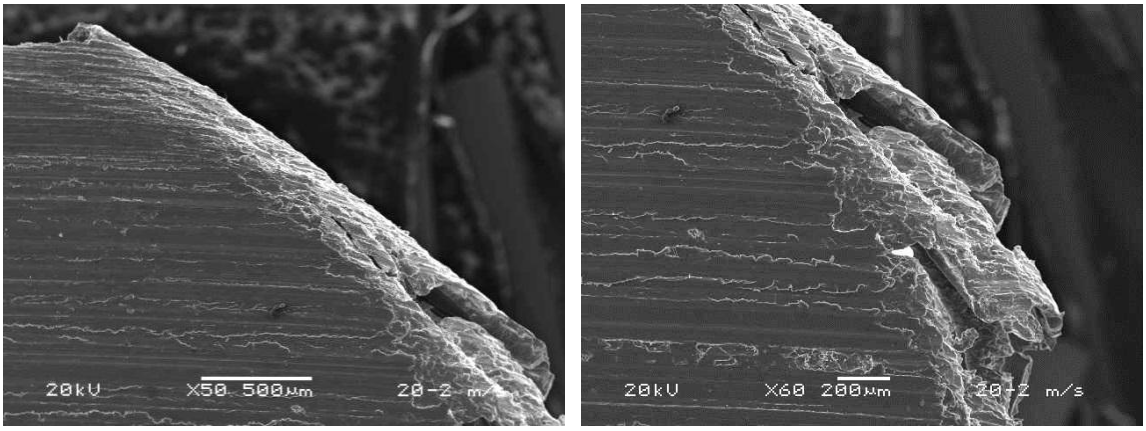

(a) (b)

Figure 4.13 Material extrusion from the interface that have re-solidified around the periphery of AZ31/ Al_2O_3 nanocomposite under a load of 20 N and 2 m/s sliding speed.

Oxidation wear

Apart from the above mentioned mechanisms, oxidation wear is also observed under all the sliding conditions. However, this wear mechanism appeared more dominant under high sliding speeds. This is because increase in sliding speed leads to increase in contact temperature between the two surfaces which oxidizes the pin surface (Fig. 4.14). This was evident from the EDX analysis of the wear debris which showed the presence of strong oxygen peak in addition to the magnesium peak (Fig. 4.15).

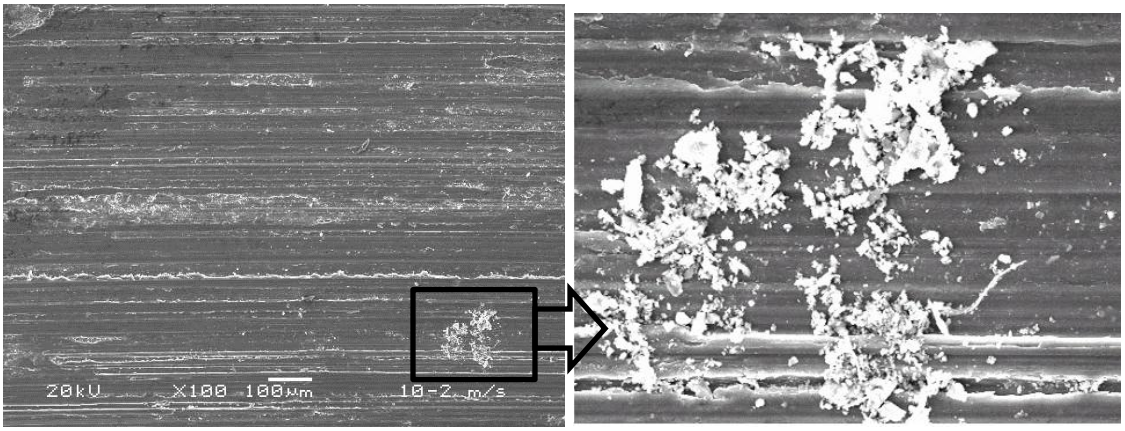

(a) (b)

Figure 4.14 (a) Presence of oxide particles on the surface of AZ31 nanocomposite at a load of 10 N and 2 m/s sliding speed. (b) High magnification of the box area of (a).

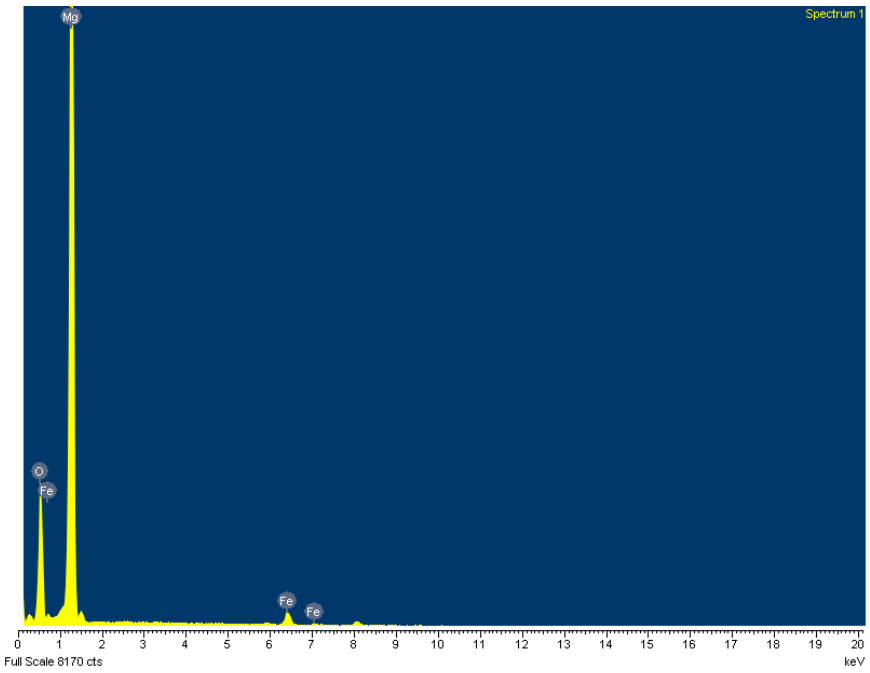

Figure 4.15 EDX analysis of oxide particles indicating presence of magnesium oxide on the surface of AZ31/Al_2O_3 nanocomposite at a load of 10 N and 5 m/s sliding speed.

4.1.3 Wear Rate of AZ31 and its AZ31/CNT nanocomposite

The volumetric wear rates for monolithic material AZ31 and AZ31/CNT nanocomposite are plotted against applied loads (5-20 N) at various sliding speeds in Fig.4.16. It is clearly evident that in all the conditions, nanocomposite has higher wear rates than the unreinforced material. Also, gradual increase in the wear rate of AZ31 and its nanocomposite are observed with increase in load under all sliding speeds. The reasons for this are discussed in later sessions.

The wear rates for monolithic AZ31 and AZ31-1 vol.% CNTs are plotted in Fig. 4.17 as a function of the sliding speed. For both materials, wear rate values showed the maximum value during sliding at 1 m/s and it gradually decreased with increase in sliding speed from 1 to 5 m/s. The lower wear rates were observed at a sliding speed of 5 m/s under all loads.

The present results obtained i.e., increase in wear rates as a result of CNT addition to AZ31 magnesium alloy are unexpected since mechanical properties such as hardness and strength of the composite are significantly better than its monolithic counterpart. The reasons for this will be discussed in later sections.

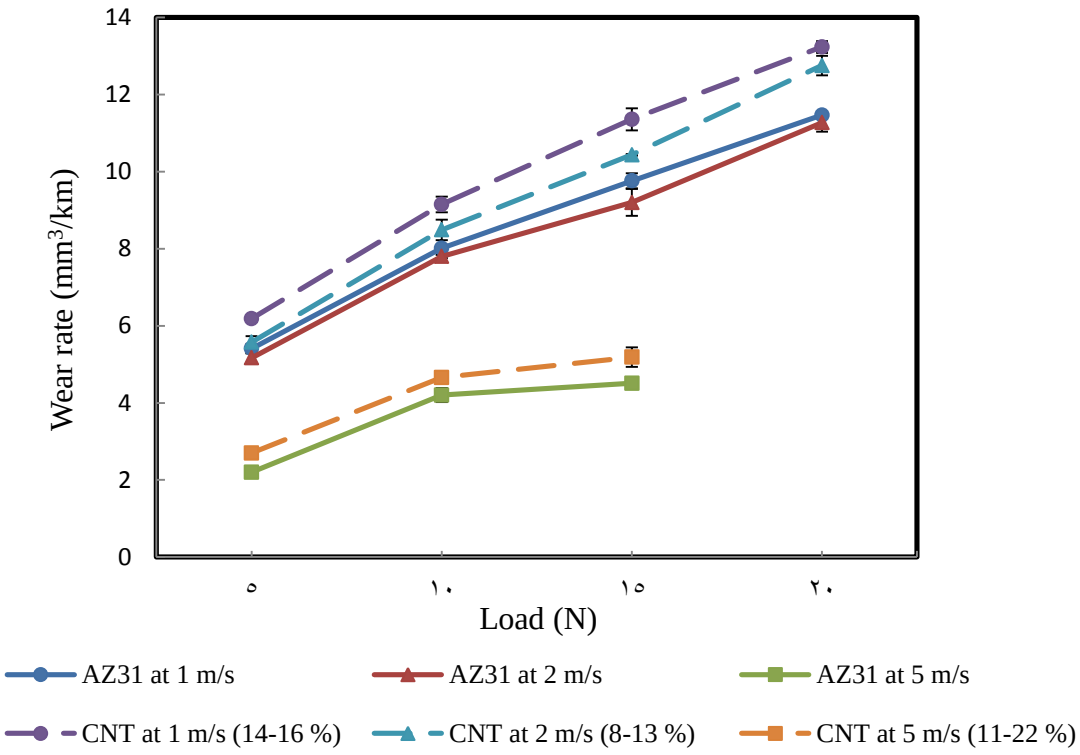

Figure 4.16 Variation of wear rate with applied load at different sliding speeds for AZ31 and its AZ31/CNT nanocomposite.

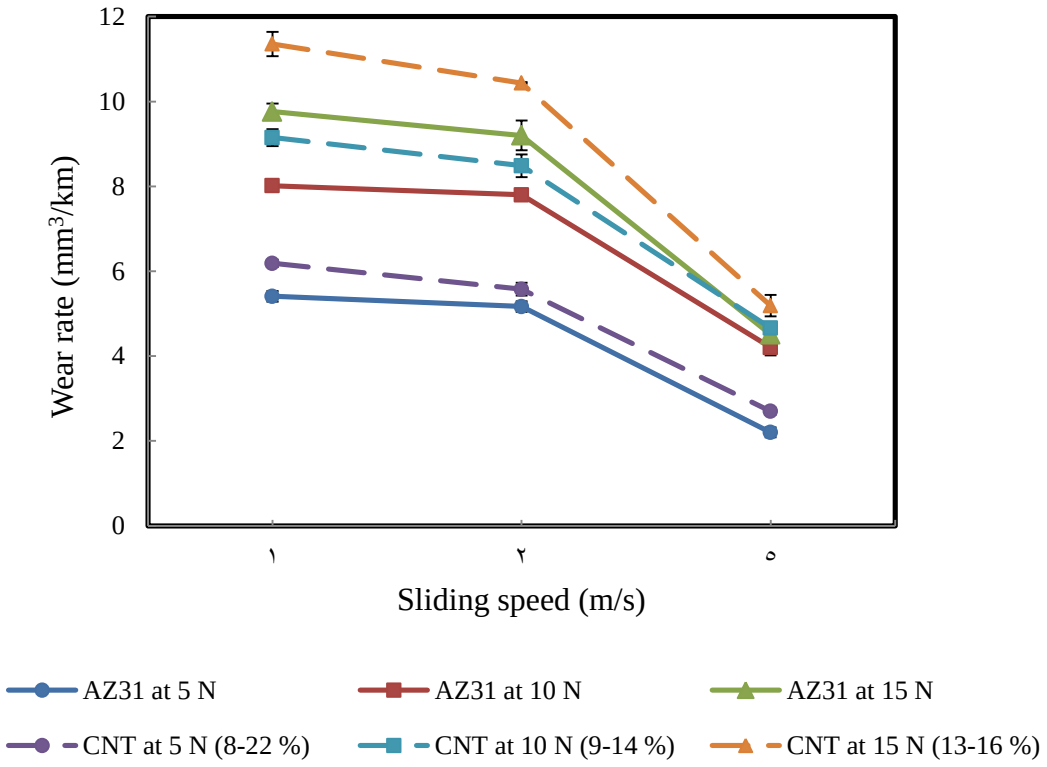

Figure 4.17 Effect of sliding speed on the wear rate at various applied loads for AZ31 and its AZ31/CNT nanocomposite.

4.1.4 Wear Mechanisms in AZ31 and its AZ31/CNT nanocomposite

Abrasion

Scanning Electron Microscopic (SEM) examination of worn pin surfaces of both unreinforced alloy and its nanocomposite tested under sliding speeds of 1 and 2 m/s at a normal load of 5 and 10 N revealed continuous long grooves and scratch marks parallel to the sliding direction (Fig. 4.18). At the same time, small fragments and ribbon shaped strips of material are seen in the wear debris (Fig. 4.19). All these features suggested abrasive wear as the dominant wear mechanism under these sliding conditions, in which material is removed from the pin surface in the form of small fragments or ribbon-like strips of material by hard asperities on the steel counterface, or hard particles that are trapped between the pin and disc which either plough or cut into the surface [44].

Under lower sliding speed of 1 m/s, deep grooves are observed on the pin surface with minimum displacement of material on either side of the grooves. At the same time, more amount of wear debris is collected, which altogether suggested more removal of material due to cutting mode of abrasion under these sliding conditions. And as the sliding speed is increased, transition from deeper grooves to shallow scratches along with plastic deformation is observed, with material displacement on either side of the grooves on the pin surface indicating abrasion via ploughing at high speeds.

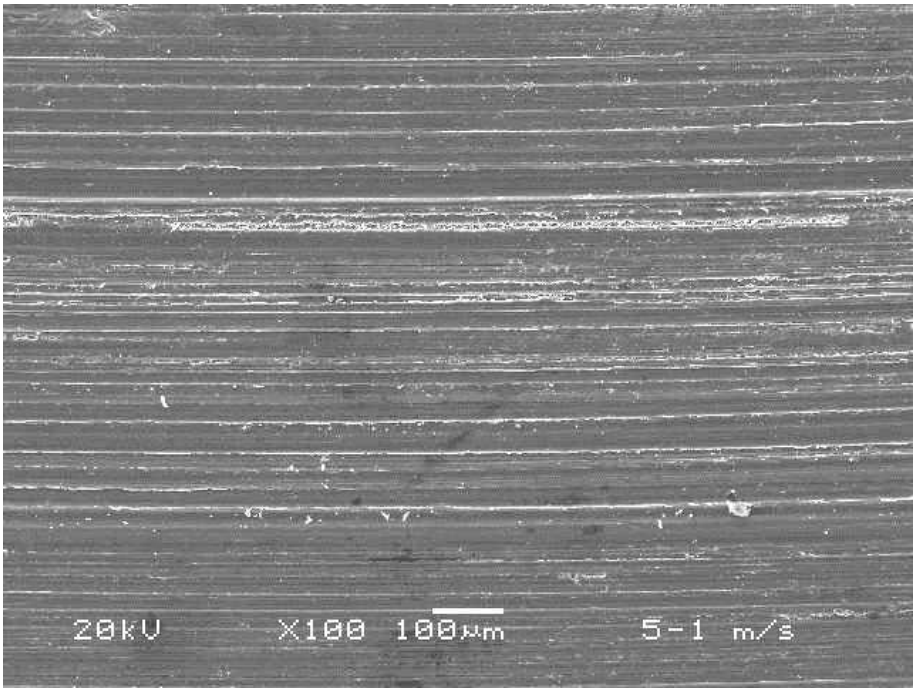

Figure 4.18 Grooves and scratches on the pin surface indicating abrasive wear for the AZ31/CNT nanocomposite at 1 m/ sliding speed and 5 N applied load.

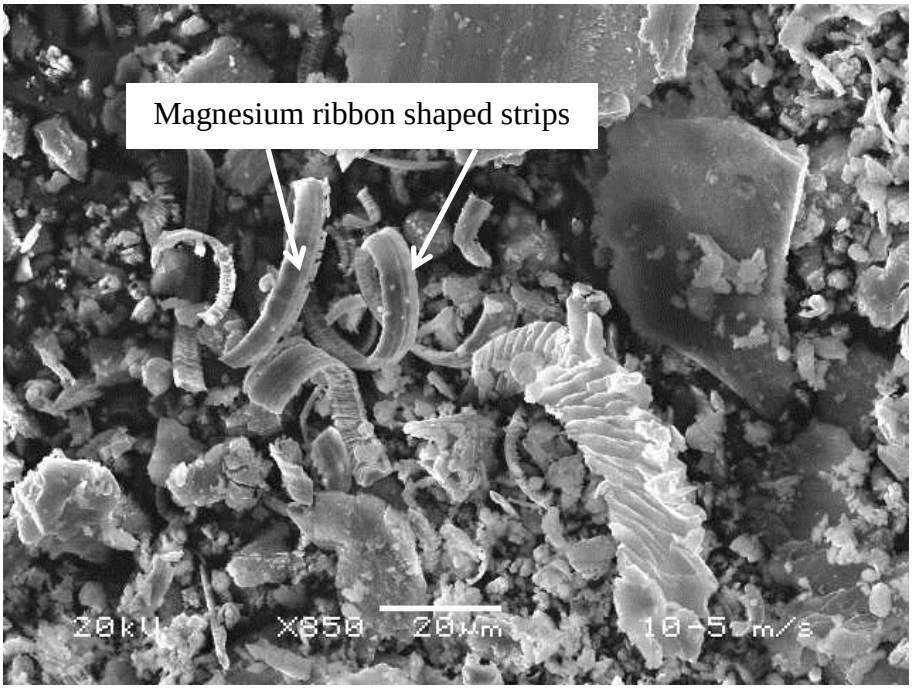

Figure 4.19 Magnesium ribbon shaped strips in the wear debris of AZ31/CNT nanocomposite showing cutting action of an abrasive particle at 10 N and 5 m/s.

Delamination

Detailed analysis of worn pin surfaces tested under sliding speeds of 1, 2 and 5 m/s at normal loads of 10 N and above showed a series of cracks perpendicular to the sliding direction (Fig. 4.20). Also, shallow craters are seen on the pin surfaces due to the propagation of these cracks in the subsurface region resulting in removal of material in the form of flakes or thin sheets (Fig. 4.21). All these features suggested delamination wear mechanism as effective under these sliding conditions. Moreover, delamination appeared slightly extensive in nanocomposite compared to the base material. The reasons for this are discussed in later sections.

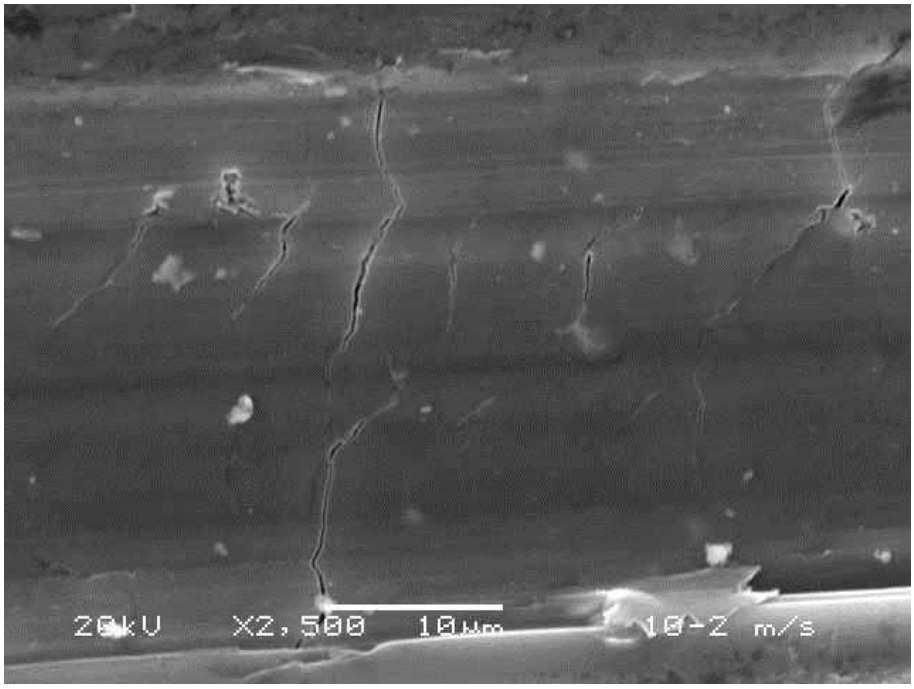

Figure 4.20 Series of cracks perpendicular to the sliding direction indicating delamination in the AZ31/CNT nanocomposite under a load of 10 N at 2 m/s sliding speed.

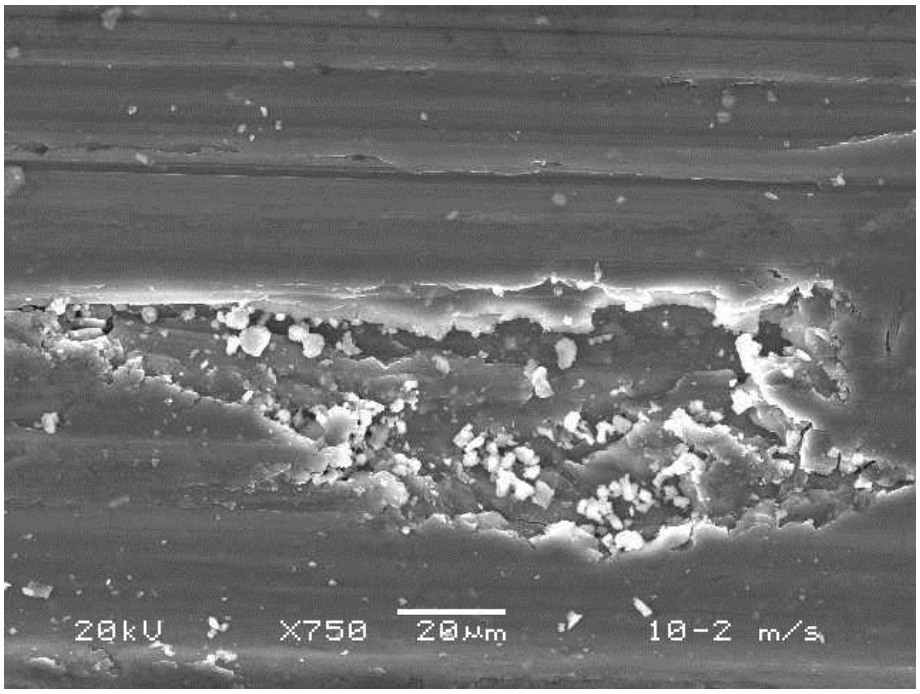

Figure 4.21 Large crater on the pin surface due to delamination for AZ31/CNT at a load of 10 N and 2 m/s sliding speed.

Adhesion

At the sliding speed of 2 and 5 m/s under normal loads of 10 N and above, rows of furrows as well as signs of smearing and plastic deformation are seen on the worn pin surfaces (Fig. 4.22). Analysis of wear track at these sliding conditions showed transfer of material from the pin surface to the disc (Fig. 4.23). And as the sliding speed and load is increased, more amount of transferred material is seen on the wear track. Furthermore, less amount of wear debris is collected when compared with conditions where other mechanisms were dominant. All these features are associated with adhesive wear which increased with increase in sliding parameters. Moreover, adhesive wear is observed to be more severe in case of nanocomposites. The reasons for this are discussed in later sections.

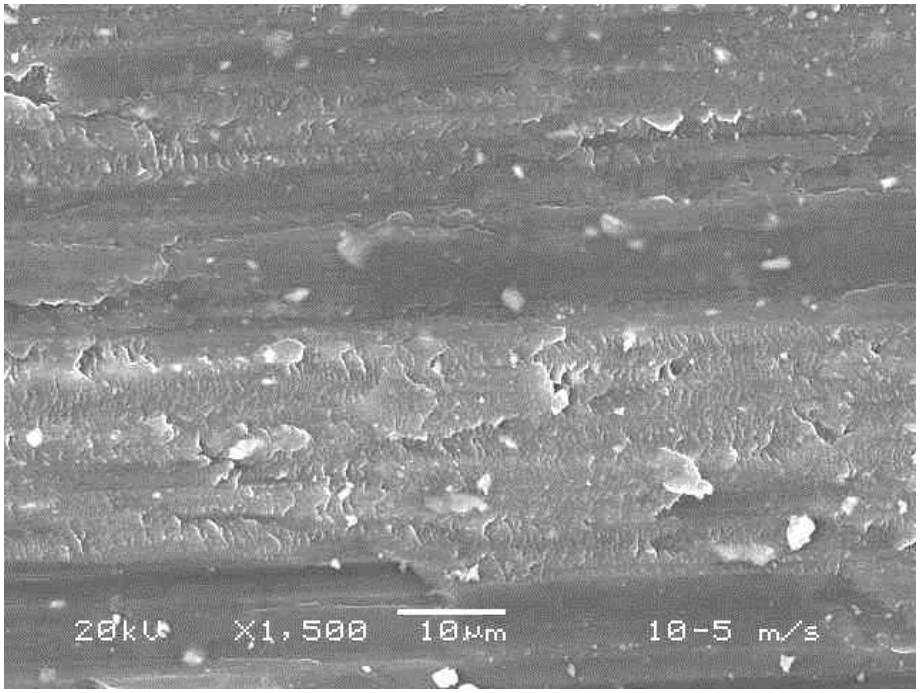

Figure 4.22 Rows of furrows indicating adhesive wear of AZ31/CNT nanocomposite under a load of 10 N and 5 m/s sliding speed.

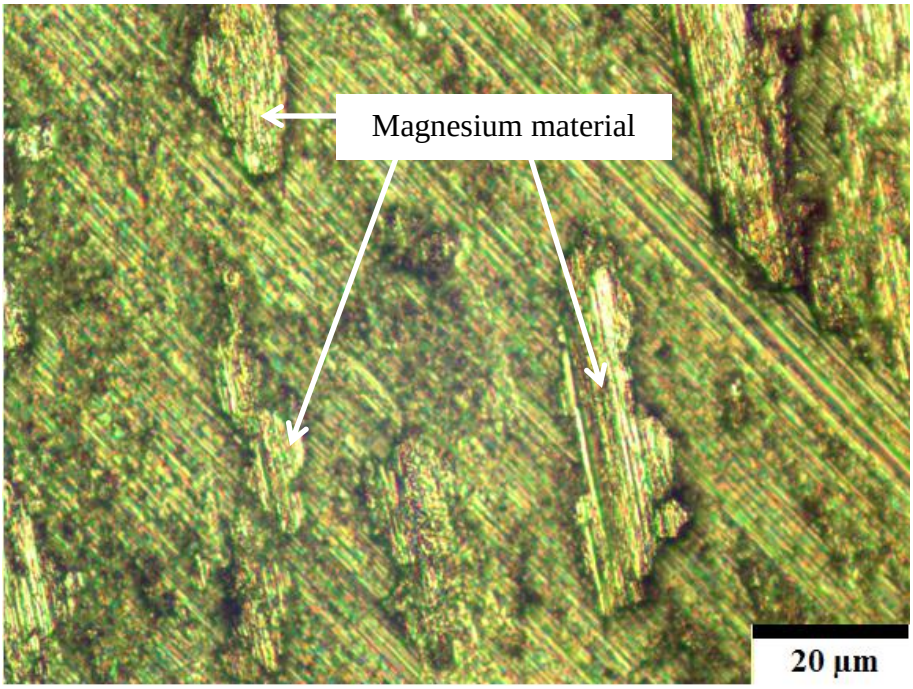

Figure 4.23 Optical microscopic examination of the wear track indicating transfer of material from the surface of AZ31/CNT nanocomposite at a normal load of 15 N and 5 m/s sliding speed.

Thermal Softening

Under the most severe sliding condition of 20 N, gross plastic deformation of the pin surface occurs and material is extruded from the interface before re-solidifying around the periphery of the pin (Fig. 4.24). At the same time, the worn pin surfaces of the specimen appeared much smoother than those worn under other sliding conditions. Also, large amount of material transfer is clearly seen on the wear track of the disc. These features are associated with softening and melting of the material caused at higher sliding parameters due to frictional heating at the sliding interface.

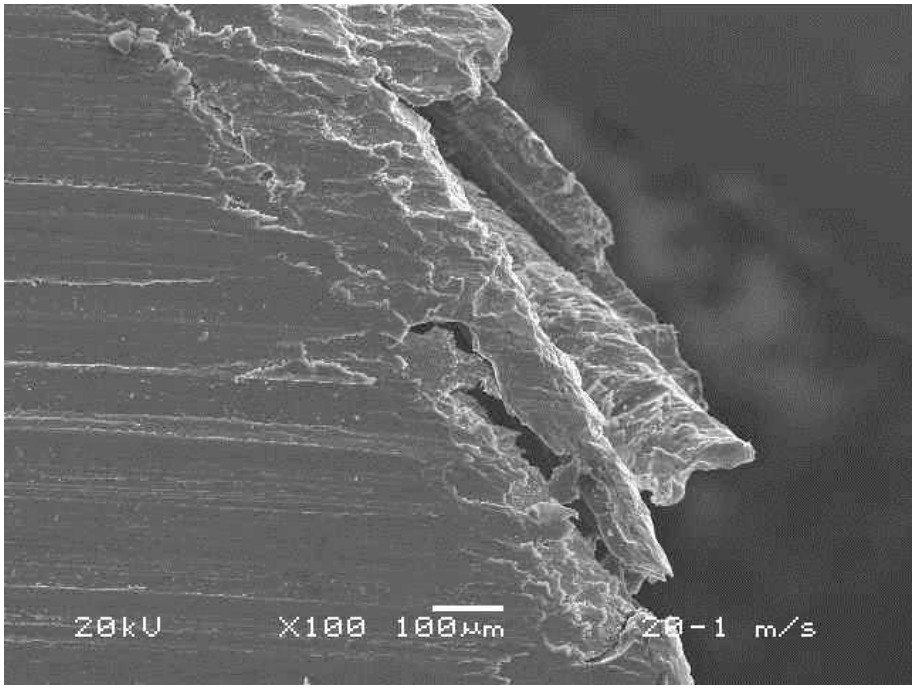

Figure 4.24 Material extrusion from the interface that have re-solidified around the periphery of AZ31/ CNT nanocomposite under a load of 20 N and 1 m/s sliding speed.

Oxidation wear

Apart from the above mentioned mechanisms, oxidation wear is also observed under all the sliding conditions. However, this wear mechanism appeared more dominant under high sliding speeds. This is because increase in sliding speed leads to increase in contact temperature between the two surfaces which oxidizes the pin surface (Fig. 4.25). This was evident from the EDX analysis of the wear debris which showed the presence of strong oxygen peak in addition to the magnesium peak (Fig. 4.26).

.

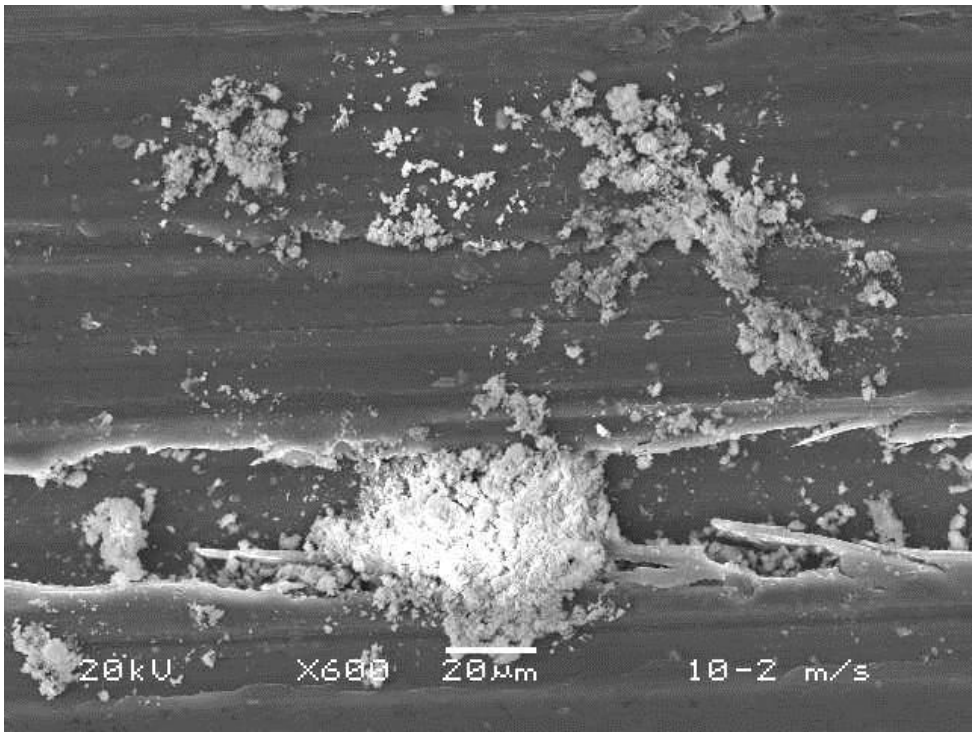

Figure 4.25 Presence of oxide particles on the surface of AZ31/CNT nanocomposite at a load of 10 N and 2 m/s sliding speed.

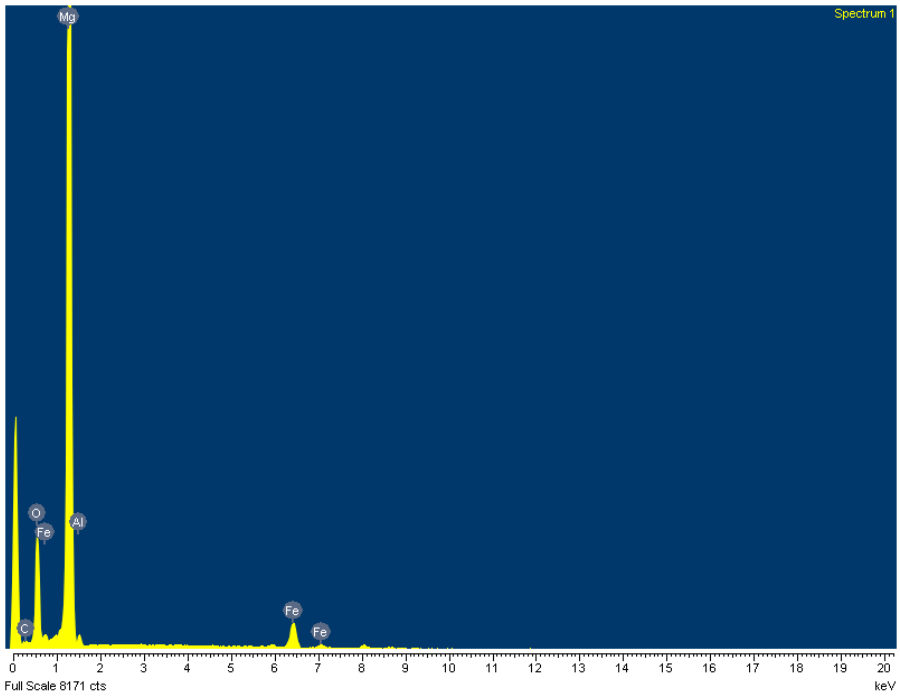

Figure 4.26 EDX analysis of oxide particles indicating presence of magnesium oxide on the surface of AZ31/CNT nanocomposite at a load of 10 N and 2 m/s sliding speed.

4.1.5 Comparison between AZ31/Al_2O_3 and AZ31/CNT Nanocomposites

From the discussion earlier on the wear data and wear mechanisms, it is evident that under all the sliding conditions, Magnesium alloy (AZ31) based nanocomposites with Al_2O_3 and CNT as reinforcement are not beneficial when compared with unreinforced alloy. In this section, the wear behavior of the AZ31/1.5 vol.% Al_2O_3 nanocomposite will be compared with AZ31/1.0 vol.% CNT nanocomposite to identify and explore the best wear resistant material. The sliding parameters chosen for this comparison are 5-20 N load at sliding speeds of 1.2 and 5 m/s. Fig. 5.42 shows the comparison of these nanocomposites, in which dotted lines represent AZ31/CNT and solid line represents AZ31/Al_2O_3 hybrid nanocomposites.

Under all the sliding conditions except at 5 m/s, AZ31/Al_2O_3 nanocomposite shows improved wear resistance when compared to the AZ31/CNT nanocomposite. At a sliding speed of 1 m/s, AZ31/Al_2O_3 nanocomposite showed an improvement of about 4-7 % when compared with AZ31/CNT nanocomposite. As the sliding speed is increased to 2 m/s, improvement in the wear resistance of AZ31/Al_2O_3 nanocomposite reduced to 1-4 % when compared with AZ31/CNT nanocomposite. However, wear rates of both the materials remained almost same at 5 m/s.

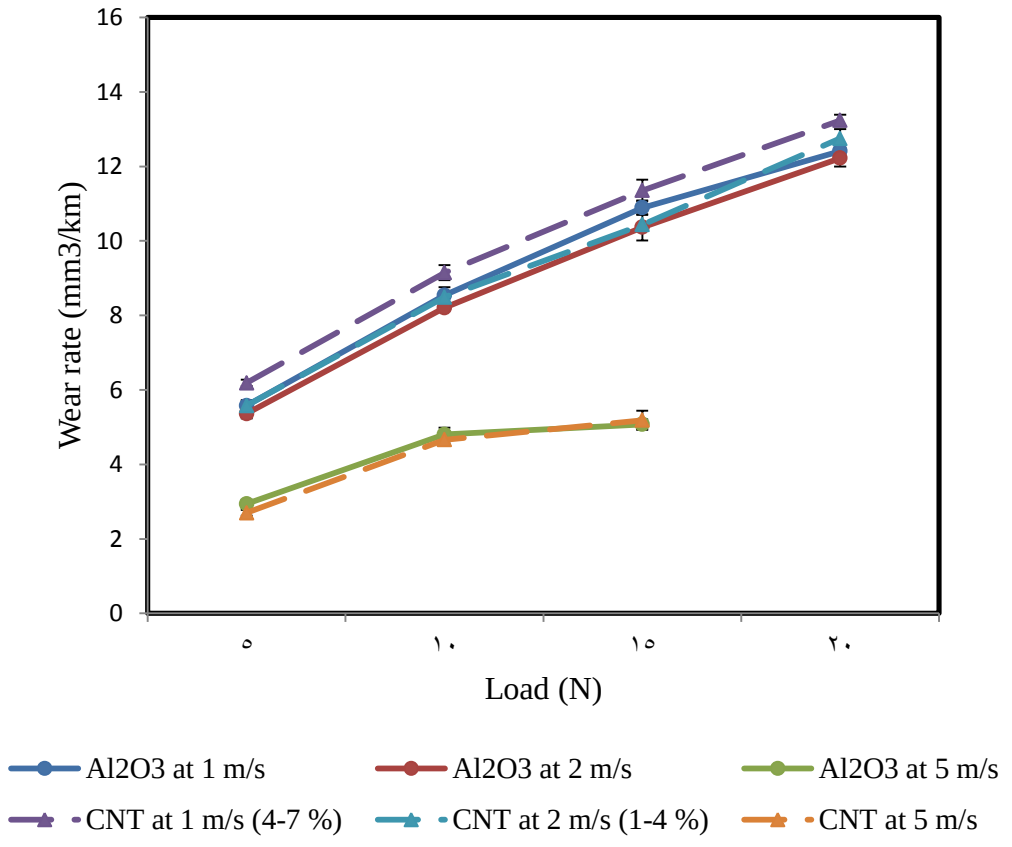

Figure 4.27 Variation of wear rate with applied load at different sliding speeds for AZ31/Al_2O_3 and its AZ31/CNT nanocomposite.

4.2 Magnesium/(yttria + nickel) Hybrid Nanocomposites

4.2.1 Wear Rate for Mg/(0.7Y_2O_3 + (0.3-1.0Ni) Nanocomposites

The volumetric wear rates for magnesium/(yttria + nickel) hybrid nanocomposites (Mg/Y_2O_3 + (0.3-1.0) vol.% Ni) are plotted against applied loads in Fig.4.28. It is clearly evident that there is consistent increase in the wear resistance with increasing amounts of nickel as reinforcement. It is also observed that there is a gradual increase in the wear rates of the nanocomposites with increase in applied load from 5 to 30 N under a constant sliding speed of 0.5 m/s.

The wear regimes in the current study can be classified into low load regime (5-10 N) and high load regime (15-30 N). At low load regime of 5 N and 10 N, the nanocomposite with 1 vol.% Ni showed slight improvement in wear resistance compared to the nanocomposite with 0.3 and 0.6 vol.% Ni. At high load regime of 15-30 N, the nanocomposite with 1 vol.% Ni showed better improvement in the wear resistance than other materials. The wear resistance of Mg/(0.7Y_2O_3 + 1.0Ni) nanocomposite improved up to 17% under low load regime to 36% under high load regime when compared to Mg/(0.7Y_2O_3 + 0.3Ni). This improvement in wear performance can be attributed to rise in hardness and strength of the nanocomposites with reinforcement level (see table 3.1). The current observation agrees with Archard's proposal which states that the hardness of the material is inversely proportional to wear rate [60]. The hardness table (see table 3.1) shows that Mg/(0.7Y_2O_3 + 1.0Ni) is harder than the other two materials with lesser amount of Ni. Thus, it is evident from the present study that the increase in amount of

nickel from 0.3 to 1 vol.% is beneficial in lowering the wear rates of the Mg/Y_2O_3 nanocomposites under all loads.

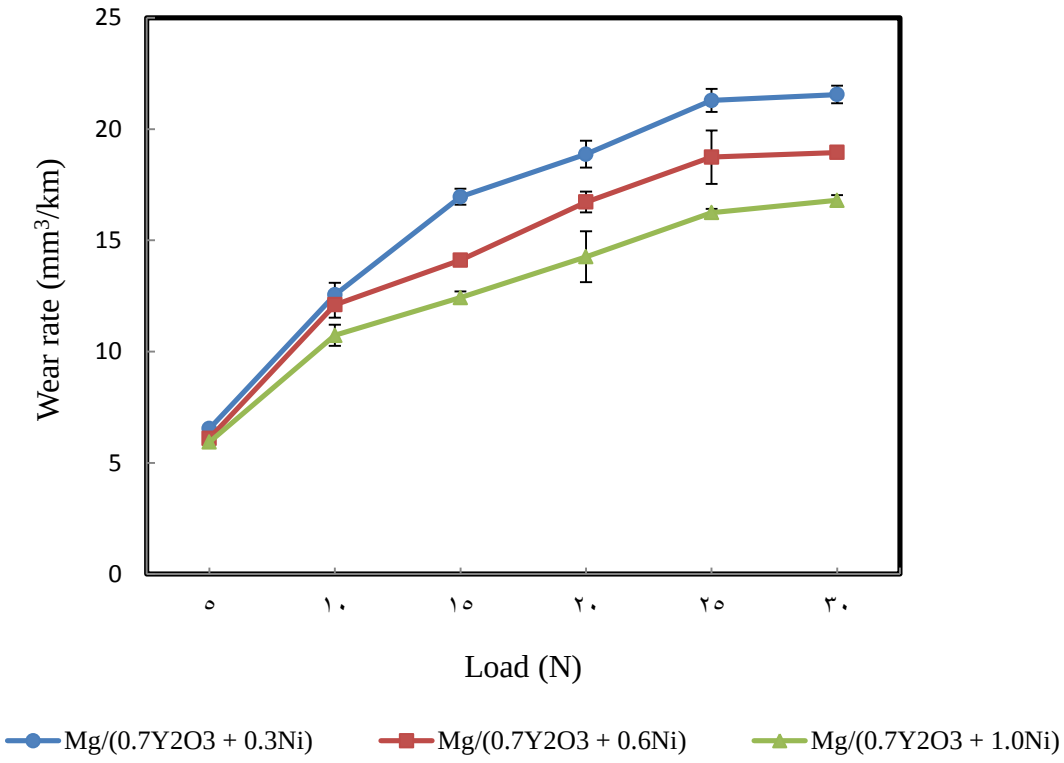

Figure 4.28 Variation of wear rate with applied loads at a constant sliding speed of 0.5 m/s for $Mg/(Y_2O_3 + Ni)$ nanocomposites.

4.2.2 Wear Mechanisms in Mg/($0.7Y_2O_3$ + (0.3-1.0Ni) Nanocomposites

Analysis of worn pin surfaces for all three composites tested under lower load of 5 N, showed continuous long grooves and scratch marks parallel to the sliding direction (Fig. 4.29). This suggests abrasion as the operating wear mechanism under these sliding conditions. However, the intensity of abrasion is observed to be less severe with increasing amount of reinforcement level due to increase in hardness. Meanwhile, fine particles were observed on the pin surface. And, EDX analysis of these particles clearly showed presence of magnesium oxide indicating oxidation wear (in addition to abrasion) as operative under this load (Fig. 4.30). Further, as the load is increased 10 N, series of cracks roughly perpendicular to the sliding direction began to appear in all materials which suggested presence of slight delamination in addition to abrasion (Fig. 4.31)

Fig. 4.32a shows the worn surface of Mg/($0.7Y_2O_3$ + 0.3Ni) at an applied load of 15 N. And it indicates delamination either due to spallation of oxidized surface layers or due to the propagation of cracks in the subsurface region. EDX analysis of the wear debris revealed presence of large flakes or thin sheets under these sliding conditions (Fig. 4.33). Also, presence of oxygen peak in addition to magnesium peak during the analysis of these particles in the wear debris suggested that the pin surfaces were slightly oxidized (Fig. 4.34a).

As the load is increased to 20 N, severe delamination is seen in all the nanocomposites (Fig. 4.32b). However, delamination appeared to be less severe in the nanocomposite with 1 vol.% Ni compared to other nanocomposites with 0.3 and 0.6 vol.% Ni reinforcement. This may be attributed to increase in the hardness and strength of the

material with the increasing amount of nickel content. And also due to reduction in porosity of the material with increasing Ni content (see table 3.1). Consequently, improvement in wear resistance of nanocomposite was seen with increasing amount of nickel.

Fig. 4.35 shows the SEM images of worn surfaces of the Mg/($0.7Y_2O_3$ + 0.6Ni) nanocomposites at an applied load of 25 N. It indicates that the worn surfaces are characterized by severe delamination and with some adhesion. This is because increase in load will hasten the process of delamination which involves subsurface deformation, crack nucleation and crack propagation. And an increase in load further will hasten these process and results in greater wear [28]. Moreover, delamination in case of nanocomposite with 0.3 vol.% Ni was more severe when compared to other materials. This could be attributed to its high porosity (0.34 vol.%), which promotes the process of delamination by creating additional crack nucleation and crack propagation sites.

Under the higher load of 30 N, frictional heating led to softening of the pin surface (Fig. 4.36) and resulted in material transfer from the pin surface to the disc (Fig. 4.37). This indicates adhesive wear as operative under these sliding conditions. However, adhesive wear is observed to be slightly less severe for the nanocomposite with 1 vol.% of Ni. As discussed earlier, this observation is in agreement with Archard's proposal that the wear rate of a material is inversely proportional to its hardness [60]. The other important reason for lower adhesion in case of 1 vol.% of Ni is due to its lower ductility when compared with other materials (See table 3.1) [45]. Furthermore, EDX analysis of the wear debris revealed increase in oxidation of the pin surface with increase in load (Fig. 4.34b).

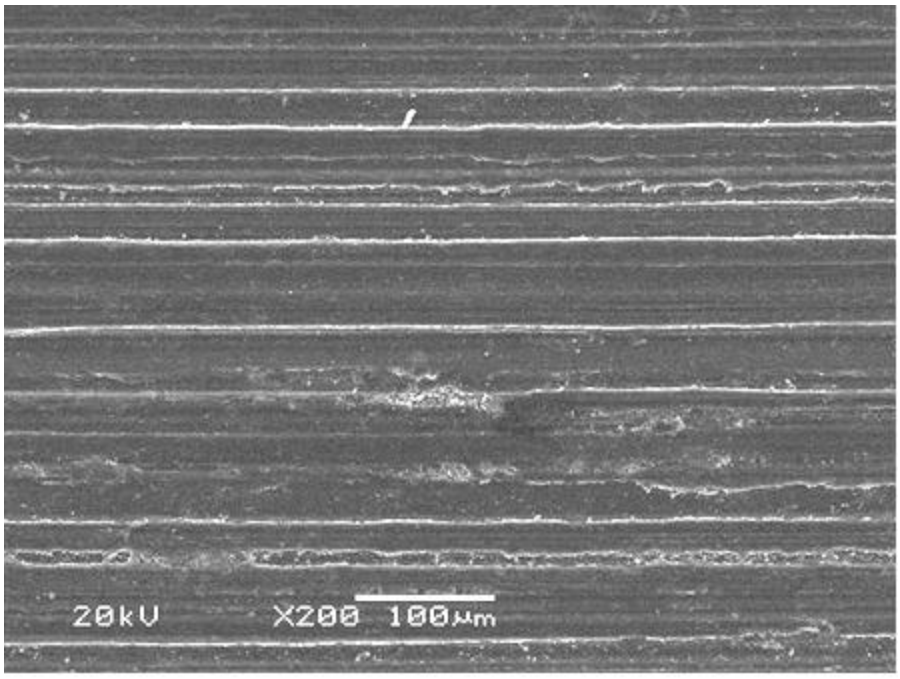

Figure 4.29 SEM image of Mg/($0.7Y_2O_3$ + 0.6Ni) indicating abrasion at a load of 5 N.

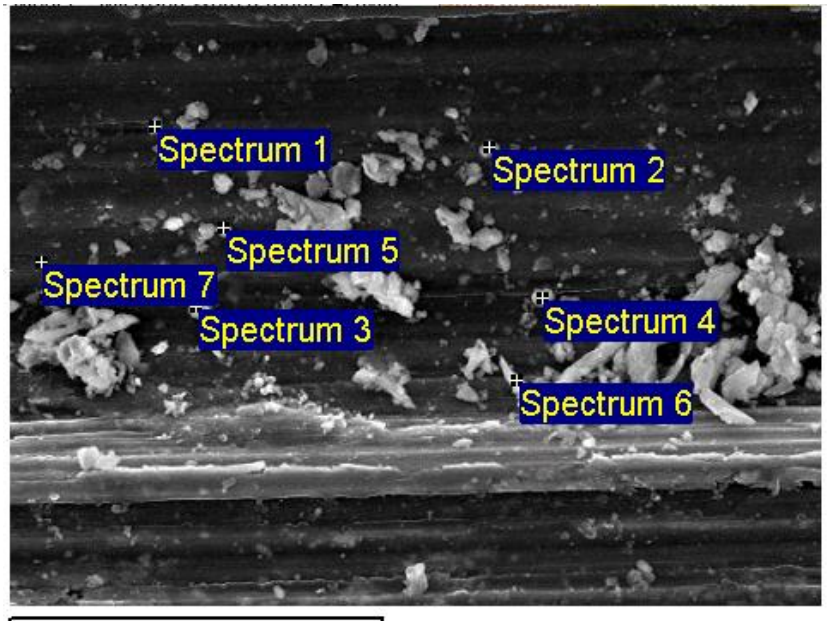

Spectrum	O	Mg	Fe	Ni	Y	Total
Spectrum 1	33.60	64.66	1.74	0.00	0.00	100.00
Spectrum 2	26.15	72.58	1.28	0.00	0.00	100.00
Spectrum 3	20.74	75.05	4.21	0.00	0.00	100.00
Spectrum 4	29.90	68.69	1.41	0.00	0.00	100.00
Spectrum 5	34.18	61.02	3.49	1.31	0.00	100.00
Spectrum 6	15.98	82.89	1.13	0.00	0.00	100.00
Spectrum 7	24.07	69.05	6.88	0.00	0.00	100.00

Figure 4.30 EDX analysis of fine particles indicating oxidation of the pin surface at a load of 5 N.

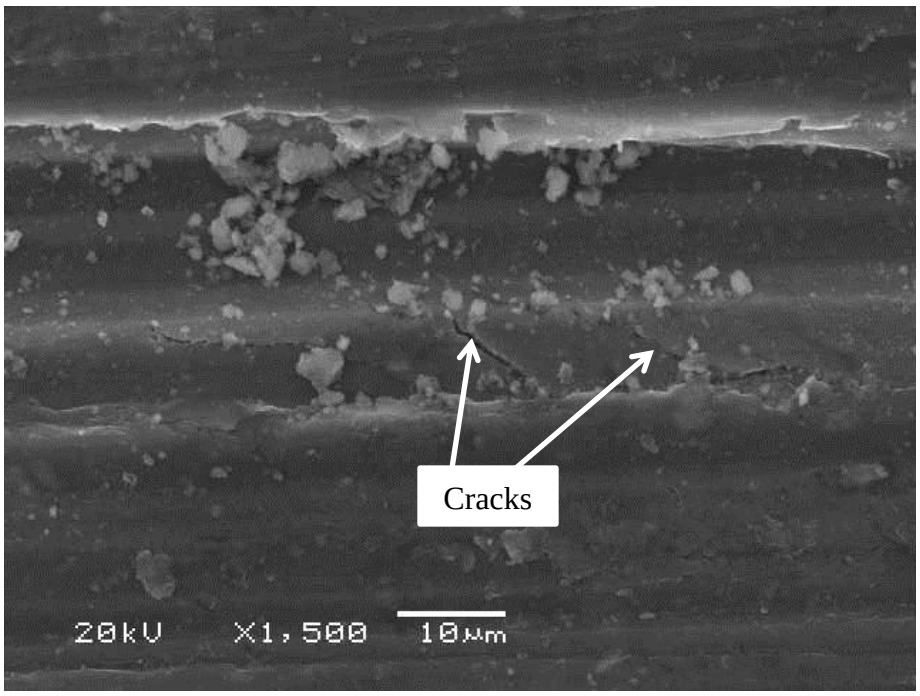

Figure 4.31 Perpendicular cracks indicating delamination in Mg/($0.7Y_2O_3$ + 0.3Ni) at 10 N.

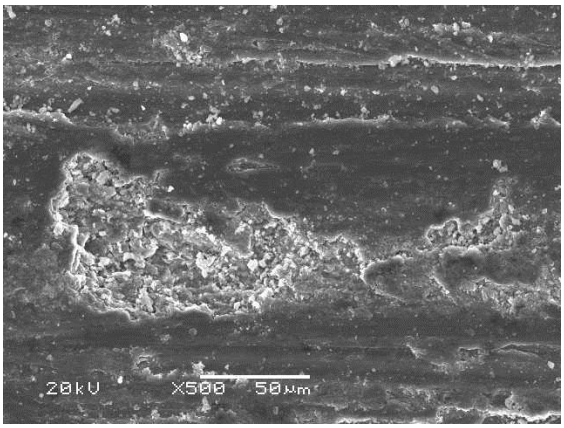

(a)

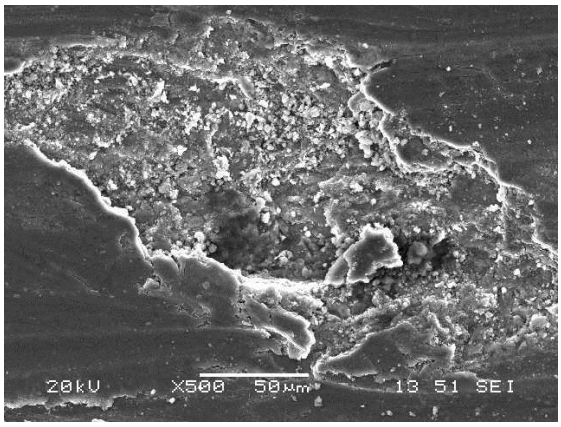

(b)

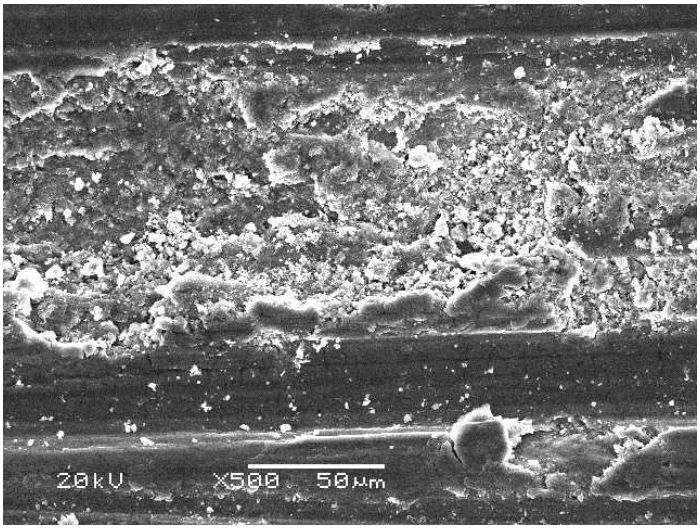

(c)

Figure 4.32 Shallow craters on the pin surface indicating severe delamination with applied loads for Mg/($0.7Y_2O_3$ + 0.3Ni) at (a) 15 N; (b) 20 N; and (c) 25 N.

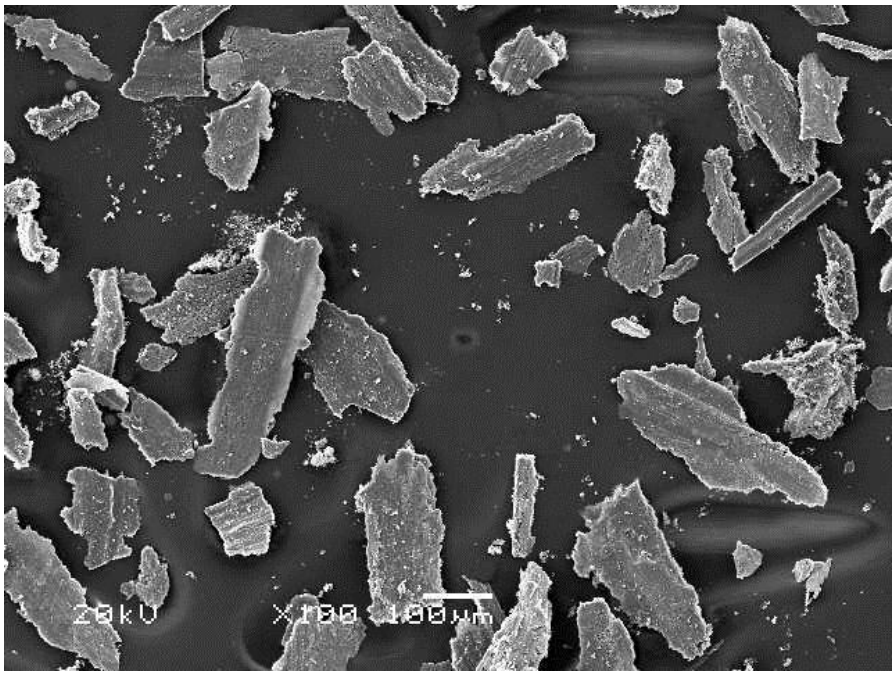

Figure 4.33 Presence of large flakes in the wear debris of Mg/(0.7Y_2O_3 + 0.3Ni) at 15 N.

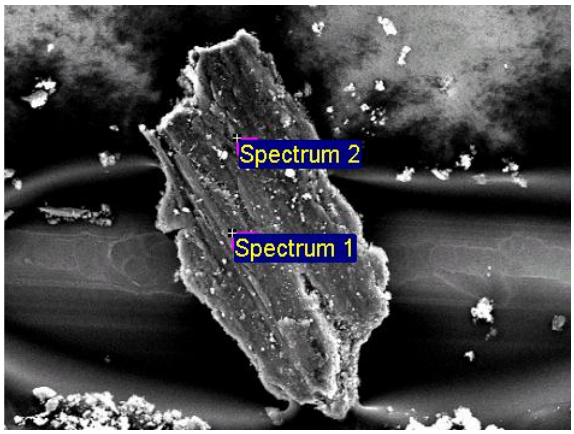

Spectrum	O	Mg	Fe	Ni	Total
Spectrum 1	13.11	73.90	7.36	4.42	100.00
Spectrum 2	10.82	70.21	11.86	7.11	100.00

(a)

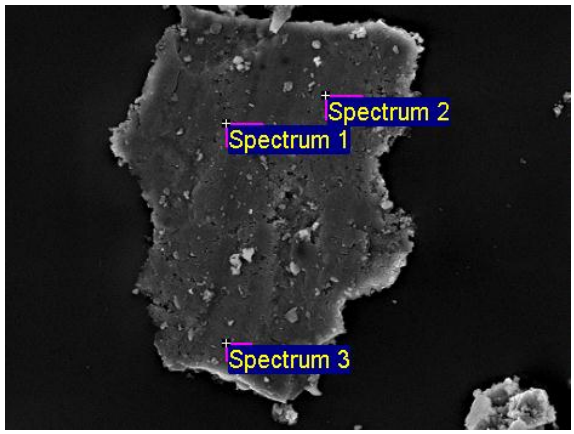

Spectrum	O	Mg	Fe	Ni	Total
Spectrum 1	20.17	70.79	1.40	7.65	100.00
Spectrum 2	24.04	69.81	1.75	4.40	100.00
Spectrum 3	15.82	79.79	1.16	3.23	100.00

(b)

Figure 4.34 EDX analysis of flakes in the wear debris indicating increase in oxidation of the pin surface with increase in load (a) 15 N and (b) 30 N.

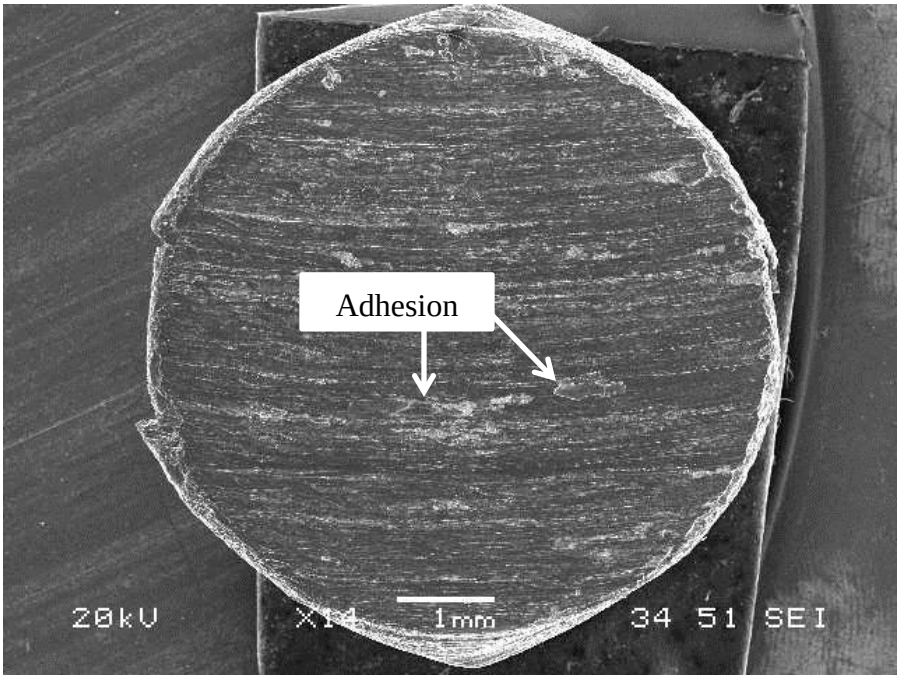

Figure 4.35 SEM image of Mg/($0.7Y_2O_3$ + 0.6Ni) at 25 N.

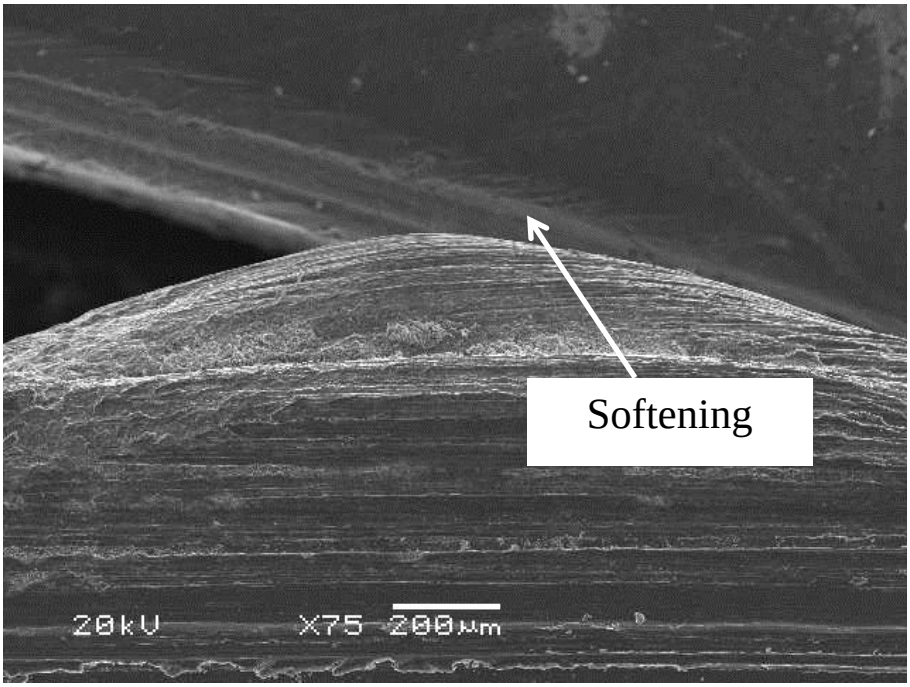

Figure 4.36 SEM image of Mg/($0.7Y_2O_3$ + 0.6Ni) at 30 N.

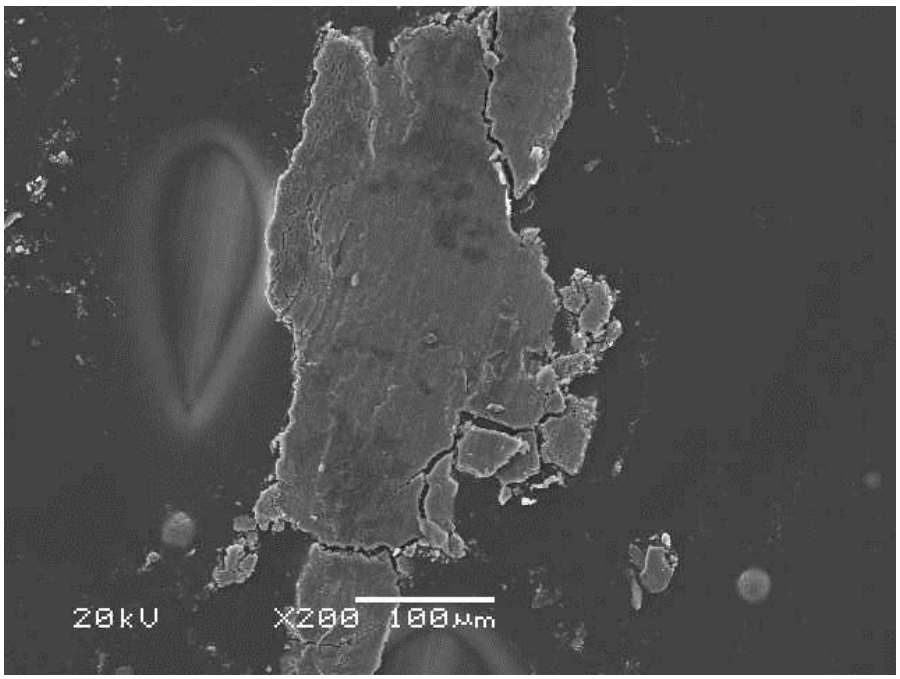

Figure 4.37 Large sheet of wear debris collected from wear track indicative of adhesion for Mg/(0.7Y_2O_3 + 1.0Ni) at 30 N.

4.3 Magnesium/(yttria + copper) Hybrid Nanocomposites

4.3.1 Wear Rate for Mg/(0.7Y_2O_3 + (0.3-1.0Cu) Nanocomposites

The volumetric wear rates for magnesium/(yttria + copper) hybrid nanocomposites (Mg/Y_2O_3 + (0.3-1.0) vol.% Cu) are plotted against applied loads in Fig.4.38. It is evident that there is slight improvement in the wear resistance of the nanocomposite with 1 vol.% of Cu. It is also observed that there is a gradual increase in the wear rates of the nanocomposites with increase in applied load from 5 to 30 N under a constant sliding speed of 1 m/s. The reasons for this will be discussed in later sections.

Under lower loads of 5 and 10 N, no improvement is seen in the wear resistance with increasing amount of copper content. However, at higher loads of 15 to 25 N, the wear resistance of the nanocomposite with 1.0 vol.% Cu is slightly better than the other nanocomposites with lesser Cu content. And at the highest load of 30 N, the wear rates of all the nanocomposites remain same and no improvement is seen in the nanocomposite with increasing amount of copper up to 1 vol.%. The results also revealed that increasing the copper content from 0.3 to 0.6 vol.% shows very slight improvement in the wear resistance only under 20 and 25 N. However, slight improvement is seen in the nanocomposite with 1.0 vol.% Cu when compared to other materials in all conditions except at 30 N. Thus, it is evident from the present study that the addition of 1.0 vol.% copper as reinforcement to Mg/Y_2O_3 slightly improves the wear resistance compared to Mg/Y_2O_3 with 0.3 vol.% copper.

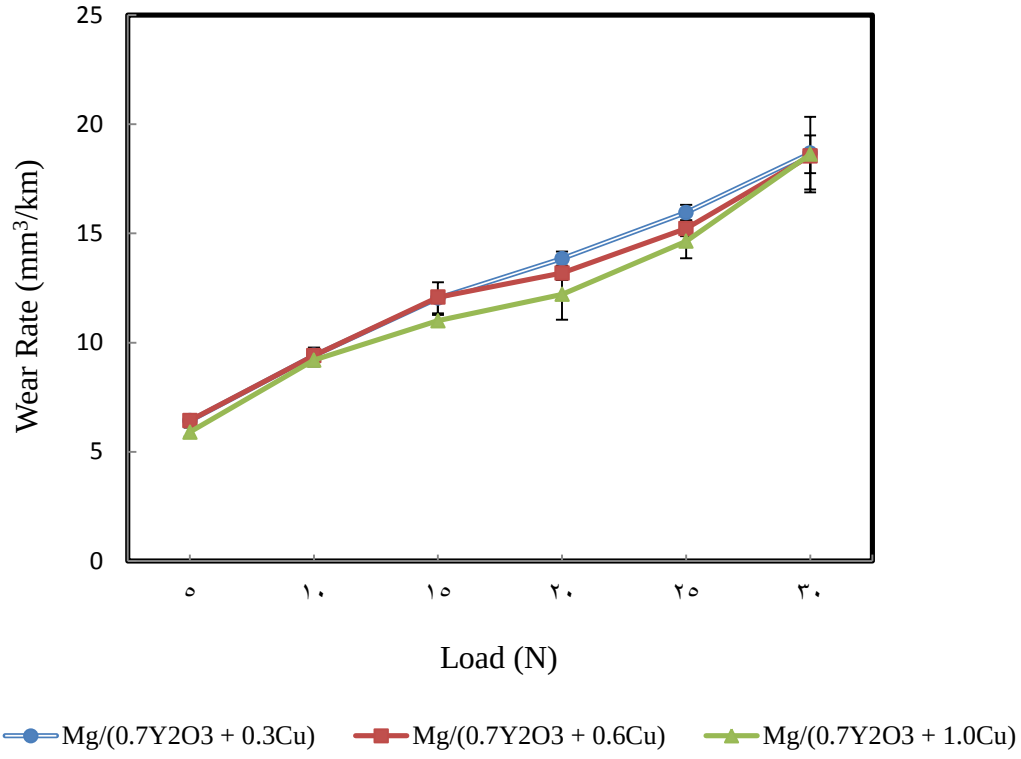

Figure 4.38 Variation in wear rate with applied load at a constant sliding speed of 1 m/s for Mg/(Y_2O_3 + Cu) nanocomposites.

4.3.2 Wear Mechanisms in Mg/(0.7Y_2O_3 + (0.3-1.0Cu) Nanocomposites

Analysis of worn pin surfaces tested under lower load of 5 N, showed continuous long grooves and scratch marks parallel to the sliding direction (Fig. 4.39). This suggests abrasion as the operating wear mechanism under these sliding conditions. However, the intensity of abrasion is observed to be less in the nanocomposite with 1.0 vol.% Cu.

As the load is increased 10 N, flakes were seen in the wear debris of the nanocomposite with 1.0 vol.% of Cu which suggested presence of delamination due to spallation of oxidized surface layers (Fig. 4.40). However, such type of behavior is not seen in other nanocomposites. Thus, no improvement is seen in the wear rate of the nanocomposite with 1.0 vol.% Cu due to presence of delamination in addition to abrasion. Moreover, analysis of wear debris of the nanocomposite with 0.3 vol.% of Cu revealed thin steel strips which suggested abrasion of the tool-steel counterface (Fig. 4.41). This could be due to the presence of hard intermetallic particles as a result of addition of copper which during sliding would have created deep grooves in the counterface by removing the material in the form of thin steel strips.

Under the higher loads of 15 to 25 N, abrasion, adhesion and slight delamination coexists on the pin surface. The worn pin surfaces under these sliding conditions revealed rows of furrows as well as signs of smearing and plastic deformation on the pin surface. At the same time, analysis of the wear track revealed material transfer from the pin surface to the disc (Fig. 4.43). And as the load is increased, more amount of transferred material is seen on the wear track which indicated severe adhesion with increase in load. Moreover, adhesion appeared slightly less severe for the nanocomposite with 1.0 vol.% Cu. This

observation is in accordance to Archard's proposal which states that the hardness is inversely proportional to wear rate of a material. Meanwhile, series of cracks roughly perpendicular to sliding direction (Fig. 4.44) and shallow craters formed due to propagation of these cracks in the subsurface region (Fig. 4.45) were seen in all the nanocomposites. However, presence of delamination is very less when compared to other mechanisms and no severity is seen in it with increase in load.

As the load is increased to 30 N, gross plastic deformation of the pin surface occurs and material is extruded from the interface before re-solidifying around the periphery of the pin (Fig. 4.46). At the same time, the worn pin surfaces of the specimen appeared much smoother than those worn under other sliding conditions. Also, large amount of material transfer is clearly seen on the wear track of the disc. Moreover, iron is observed on the pin surface due to extensive adhesion between pin and disc (Fig. 4.47). All these could be due to increase in frictional heating with increase in applied load. Meanwhile, more delamination is seen in Mg/Y_2O_3 with 1.0 vol.% Cu due to its high porosity (0.77 vol.%) which creates an additional crack nucleation and propagation paths (Fig. 4.48).

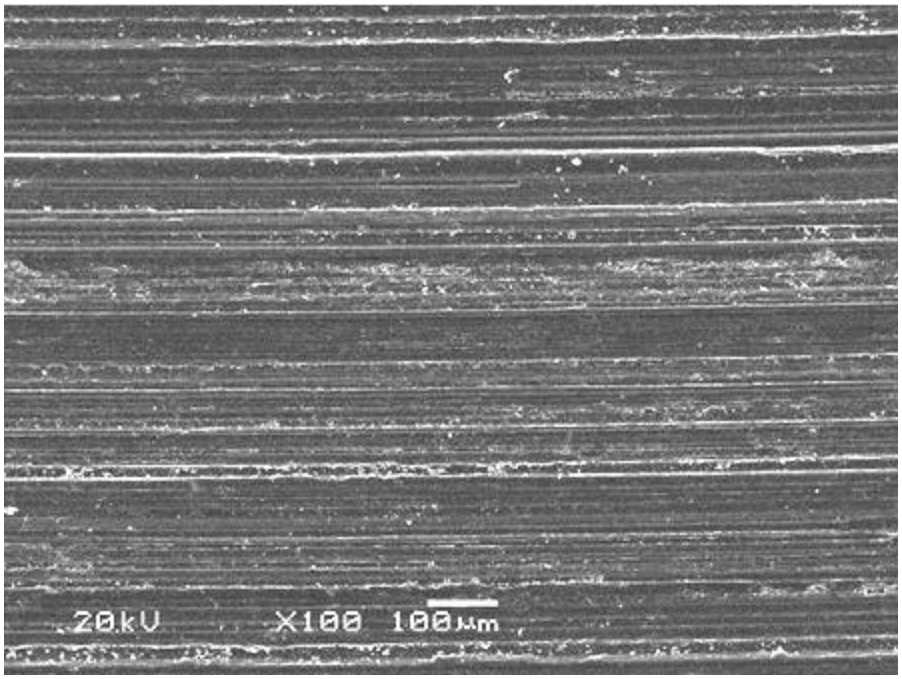

Figure 4.39 Grooves and scratch marks on the pin surface indicating abrasion for Mg/(0.7Y_2O_3 + 0.3Cu) at 10 N.

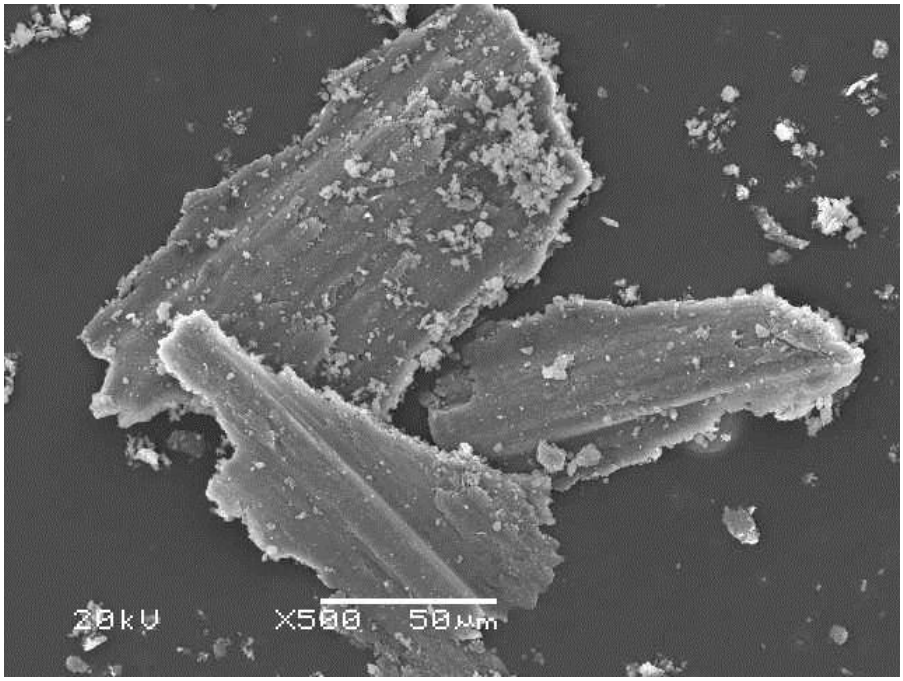

Figure 4.40 Flake like wear particles in the wear debris of Mg/(0.7Y_2O_3 + 1.0Cu) due to delamination of oxidized surface layers.

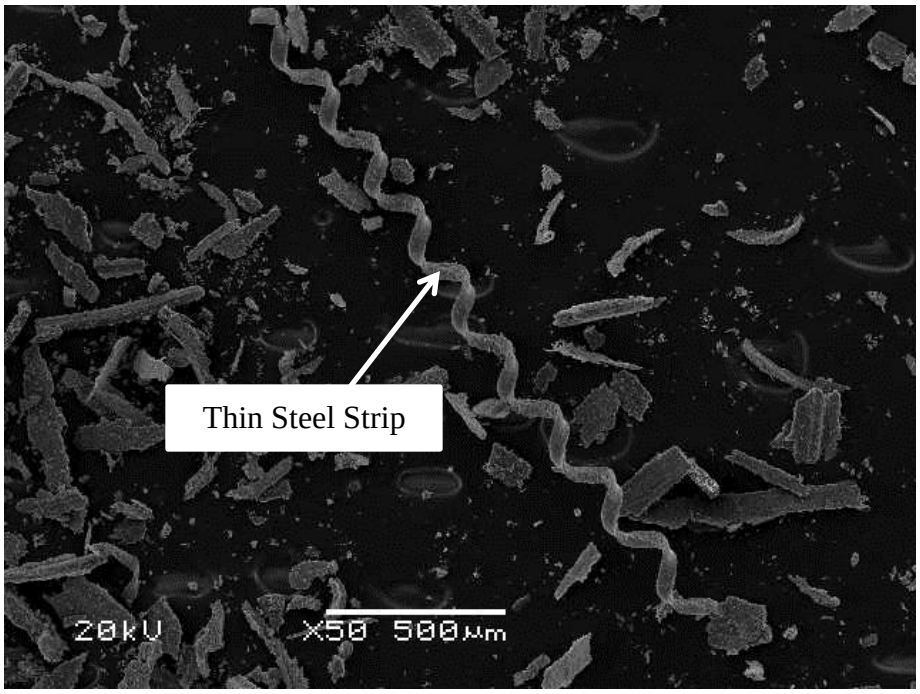

Figure 4.41 Steel strip in the wear debris of the Mg/($0.7Y_2O_3$ + 0.3Cu) due to abrasive wear of tool-steel counterface at 10 N.

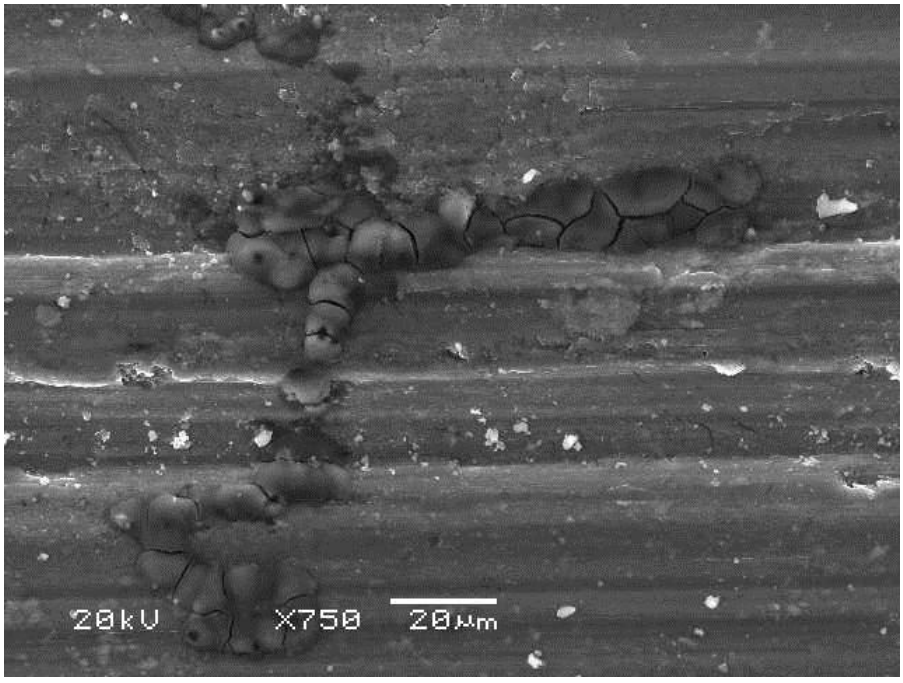

Figure 4.42 Oxidation of the Mg/($0.7Y_2O_3$ + 0.3Cu) hybrid nanocomposite pin surface at 10 N.

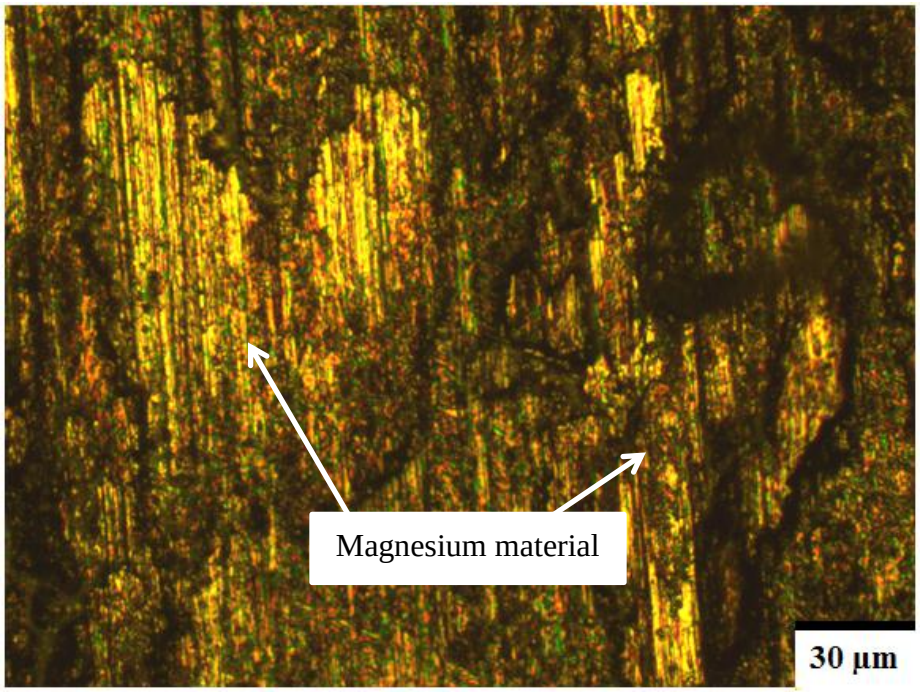

Figure 4.43 Optical microscopic examination of the wear track indicating transfer of material from the surface of Mg/(0.7Y_2O_3 + 0.3Cu) nanocomposite at 25 N.

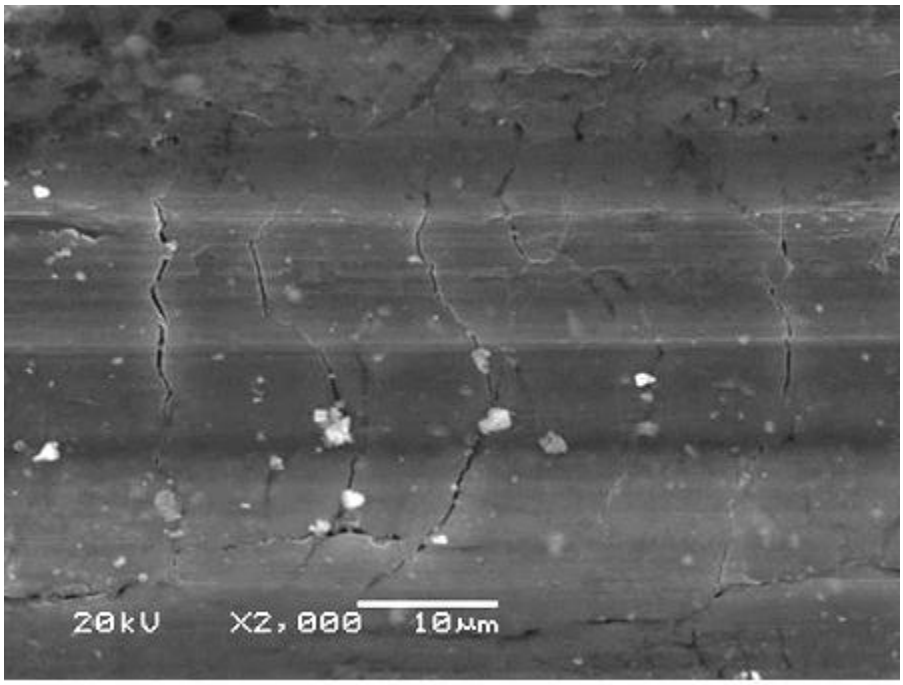

Figure 4.44 Series of cracks perpendicular to the sliding direction indicating delamination for Mg/(0.7Y_2O_3 + 1.0Cu) at 15 N.

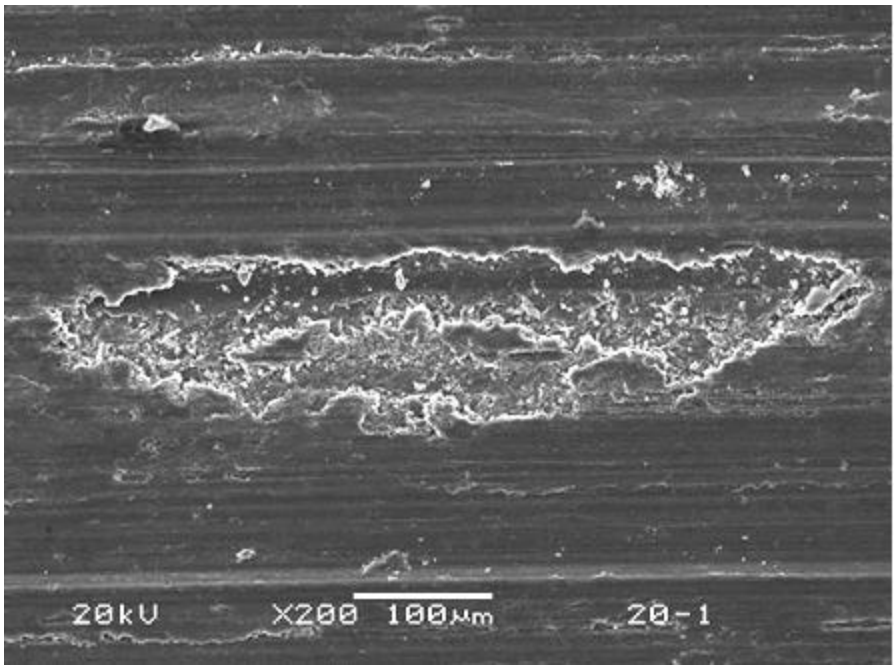

Figure 4.45 Large crater on pin surface due to delamination for Mg/(0.7Y_2O_3 + 1.0Cu) at 20N.

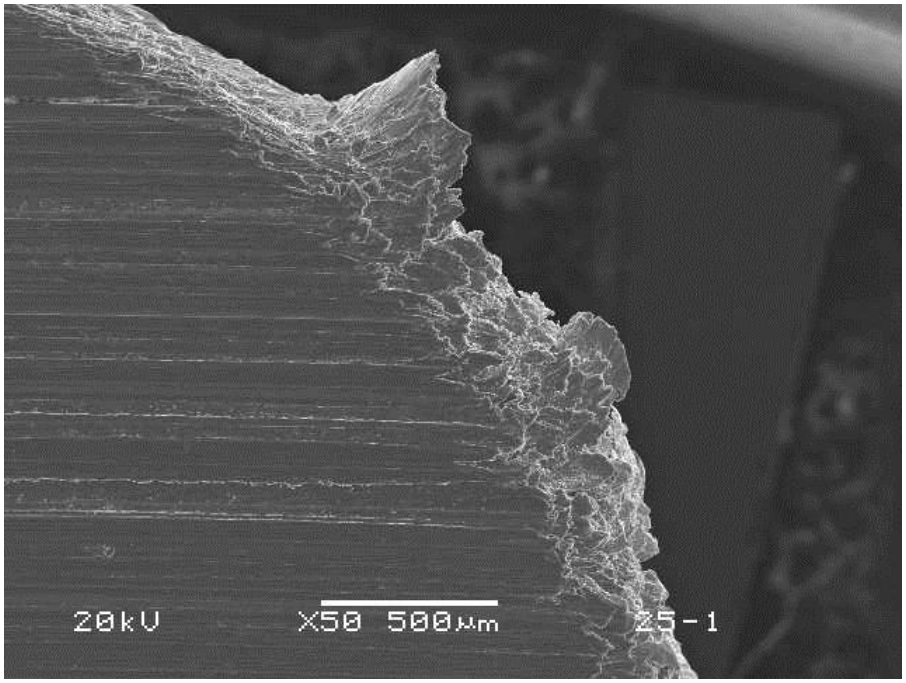

Figure 4.46 SEM image indicating softening for the Mg/(0.7Y_2O_3 + 0.3Cu) at 30 N.

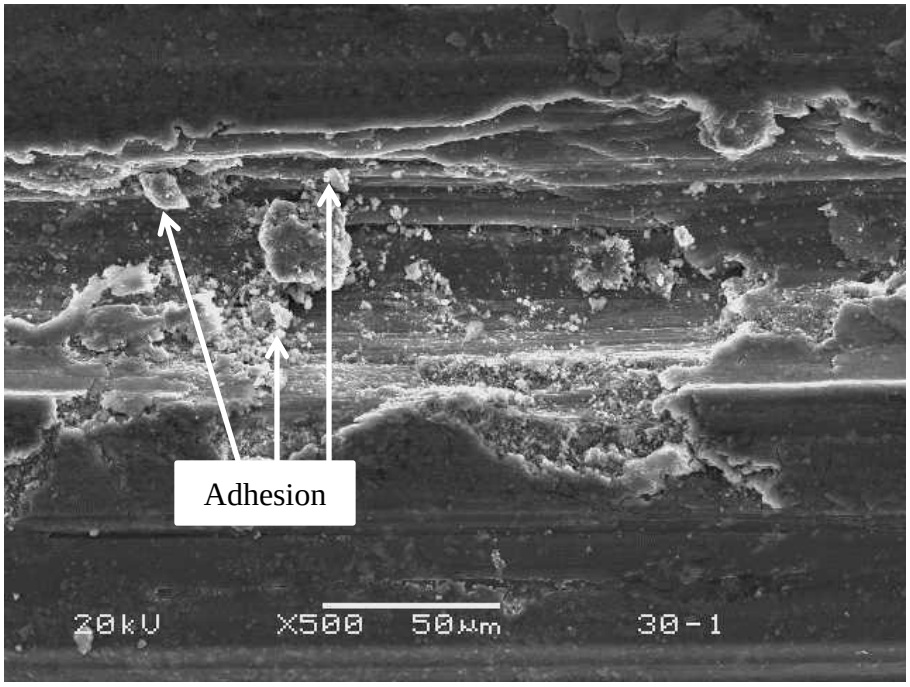

Figure 4.47 SEM image of Mg/($0.7Y_2O_3$ + 0.6Cu) hybrid nanocomposite at 30 N.

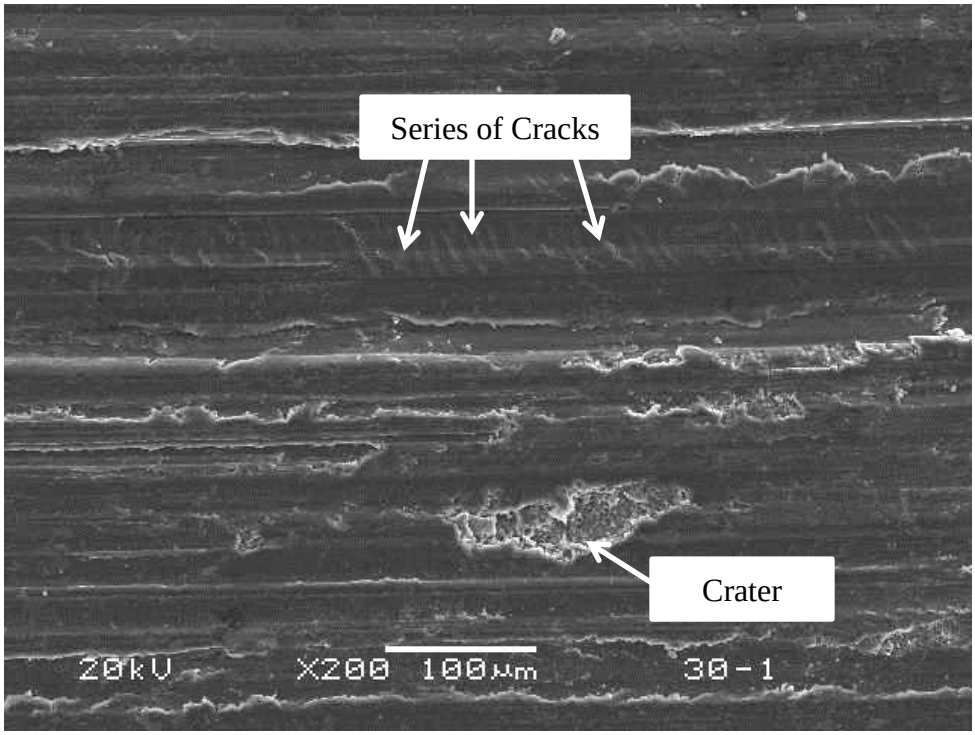

Figure 4.48 SEM image of Mg/($0.7Y_2O_3$ + 1.0Cu) at 30 N.

4.4 Comparison between Mg/(0.7Y_2O_3 + (0.3-1.0Ni) and Mg/(0.7Y_2O_3 + (0.3-1.0Cu) Hybrid Nanocomposites

From the discussion earlier on the wear data and wear mechanisms, it is evident that magnesium based hybrid nanocomposites are beneficial with increase in amount of reinforcement under all sliding conditions. In this section, the wear behavior of the three Mg/(Y_2O_3+Ni) nanocomposites will be compared with Mg/(Y_2O_3+Cu) nanocomposites to identify and explore the useful materials that can be valuable for practical applications. The sliding parameters chosen for this comparison are 5, 15 and 30 N loads at a constant sliding speed of 0.5 m/s. Fig. 5.42 shows the comparison of these hybrid nanocomposites, in which dotted lines represent Mg/(Y_2O_3+Cu) and solid line represents Mg/(Y_2O_3+Ni) hybrid nanocomposites.

At lower load of 5 N, both Mg/(Y_2O_3+Ni) and Mg/(Y_2O_3+Cu) nanocomposites showed nearly similar wear rates. As the load is increased to 15 and 30 N, negligible difference in wear rates are seen in both hybrid nanocomposites with 0.3 vol.% of reinforcement. However, the nanocomposites with 0.6 and 1.0 vol.% Ni as reinforcement showed better wear resistance when compared to the nanocomposite with similar compositions of Cu reinforcement. The improvement in 0.6 vol.% Ni nanocomposite was about 13 to 21% when compared to 0.6 vol.% Cu, while in case of 1.0 vol.% Ni nanocomposite an improvement of about 8 to 17% were observed when compared with 1.0 vol.% Cu.

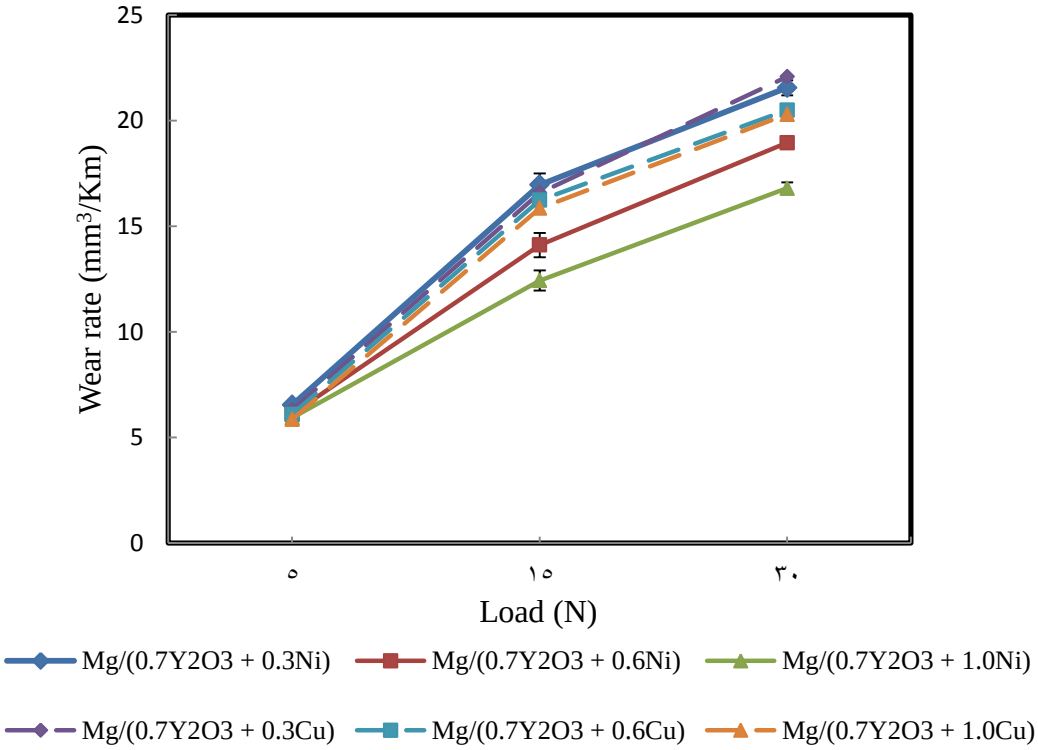

Figure 4.49 Comparison between Mg/(Y_2O_3+Ni) and Mg/(Y_2O_3+Ni) hybrid nanocomposites.

CHAPTER 5

DISCUSSION

5.1 Magnesium alloy (AZ31) based Nanocomposites

5.1.1 Wear Rate for AZ31 and its AZ31/Al_2O_3 Nanocomposite

The results of the present study revealed that the addition of nano-sized alumina particulates to the AZ31 magnesium alloy matrix led to high wear rates when compared to its unreinforced alloy tested under applied loads of 5-20 N and sliding speeds of 1, 2 and 5 m/s. The increase in wear rates of nanocomposite could be attributed to higher ductility, increased porosity and mismatch of thermal expansion coefficients between the reinforcement and matrix alloy. Moreover, conflicting results have been reported in the open literature. These conflicting results may come from the large number of variables, which can affect wear mechanisms and wear rates. For example, Habibnejad et al. [34] observed decrease in the wear rate of AZ31 when reinforced with Al_2O_3 nanoparticles (100 nm). Similarly, Lim et al. [33] found a continuous improvement in the wear resistance with increasing Al_2O_3 (50 nm) content from 0-1.11 vol.% in pure magnesium. However, other studies have reported that the composite has higher wear rate than that of

the unreinforced material. For example, Rohatgi et al. [54] have studied the dry sliding wear behavior of aluminum alloy A206-5 wt.% of Mg reinforced with 2 wt.% of Al_2O_3 (47 nm) nanoparticles by using pin-on-disc type apparatus and showed that the reinforcement caused increase in the wear rate of the alloy. Apparently, the wear resistance of the composite not only depends on the material properties but also on the nature of mechanical and physical factors [27].

The current results showed gradual increase in wear rates of both the materials with increase in applied loads at all sliding speeds. This behavior may be attributed to change in wear mechanisms of both the materials under different values of applied load. And these results are similar to previous investigations on Mg based composites which had also found increase in wear rates with increase in applied load [29-30, 34].

Moreover, decrease in wear rates are observed with increase in sliding speed due to the formation of magnesium oxide on the pin surface at high sliding speeds which acted as a protective layer from wear. Earlier studies on magnesium based composites had also found the presence of magnesium oxides at high sliding speed as beneficial in lowering the wear rates when compared to those at low sliding speeds [34-35]. For example, studies carried out by Habibnejad et al. [34] and Shanthi et al. [35], in which the addition of 1.5 vol.% of nano-sized alumina particulates (100 and 50 nm size) to magnesium alloys AZ31 and AZ31B dropped the wear rates with increase in sliding speed. In another study, Lim et al [33] conducted dry sliding wear tests of magnesium composites reinforced with up to 1.11 vol.% of nano-sized alumina particulates (50 nm size) and they reported that the wear rates decreased with increase in sliding speed up to 7 m/s beyond which the wear rate began to rise. However, the wear trends observed in the present study

are in contrast to the findings of Chen and Alphas [55], where increase in wear rates of AZ91 were seen with increase in sliding speed under loads of 5-20 N.

Furthermore, the intensity of oxidation wear appeared high in AZ31 alloy when compared to its nanocomposite. These observations are supported by the earlier studies conducted on the oxidation behavior of AZ31B alloy and its alumina reinforced nanocomposite which showed that AZ31B alloy tends to oxidize more quickly with increase in temperature compared to AZ31B/Al_2O_3 nanocomposite with upto 1.5 vol.% [65]. Thus, it can be concluded that less wear rates are seen in the base material AZ31 when compared to the AZ31/Al_2O_3 nanocomposite with increase in sliding speed.

5.1.2 Wear Mechanisms in AZ31 and its AZ31/Al_2O_3 Nanocomposite

At lower loads of 5 and 10 N and sliding speed of 1 m/s, abrasion is found to be the dominant wear mechanism in both the materials. However, abrasion appeared extensive in the nanocomposite as the alumina particles that are pulled-out during sliding acted as third body abraders, which when trapped between the pin specimen and counterface created deep grooves on the surface of the tool-steel counterface by removing the material in the form of thin steel strips (see Fig. 4.6). And as the sliding continued, these deep grooves formed in the counterface would have caused additional contribution to abrasive wear. Consequently, 3 to 5% increase in the wear rates of the nanocomposite were observed under these sliding conditions.

As the sliding speed is increased under lower loads, combination of mild abrasion, mild delamination and mild adhesion coexists on the pin surface. However, increase in the intensity of delamination was observed with increase in sliding parameters under lower

loads. This could be attributed to misfit strain that occurred during sliding as a result of difference between the thermal expansion coefficients of reinforcement (α = 7.4 x 10^{-6} /°K [66]) and matrix alloy (α = 26 x 10^{-6} /°K [67]). These misfit strains in the nanocomposites cause internal stresses which results in plastic deformation of the material. Further, as the sliding speed is increased, the internal stresses increases due to increase in surface temperature and exceeds the tensile strength of the material due to high misfit strain causing material rupture and also results in detachment of fragments with continuous sliding [63]. Consequently, high wear rates are seen in the nanocomposites with increase in sliding parameters under lower loads of 5 and 10 N, as the mismatch of thermal expansion coefficients together with porosity promoted the rate of delamination process by creating additional void nucleation sites and preferential crack propagation paths through a particle-matrix de-cohesion mechanism. Earlier studies had also found increase in wear rates of composite due to presence of delamination wear mechanism. For example, Lim et al. [29] reported increase in wear rates of Mg/SiC_p composites due to the presence of delamination wear.

As the load is further increased to 15 N, mild abrasion, mild delamination and adhesion coexists on the pin surface. However, with increase in load and speed, adhesion becomes severe and is extensive in nanocomposite than its monolithic counterpart. This could be due to the higher ductility of the nanocomposite which is almost twice the base material (see table 3.1). And, this high ductility of the material favors strong adhesion between the pin and disc with increase in surface temperature. This is because a material with high ductility will have greater elongation and less elastic recovery, which together with increase in real area of contact due to increase in load and duration results in high

adhesion of materials [45]. Thus, it might be reasonable to conclude that more amount of material transfer is seen due to increase in ductility of nanocomposites which resulted in severe adhesion with increase in sliding parameters. Consequently, 12-13% increase in wear rates of the nanocomposite are seen as a result of severe adhesion compared to its unreinforced alloy.

Under higher load of 20 N, increase in frictional heating led to softening of the pin surface which resulted in large amount of material transfer from the pin to the disc. Such type of behavior is also evident from earlier studies on Mg and Al composites which had also found presence of thermal softening at higher speeds and loads [33, 35, 62]. And they reported presence of particulate reinforcements as beneficial in lowering the wear rates by delaying the onset of thermally activated deformation processes to higher loads and speeds. However, the present results are contrary to previous findings i.e., the nanocomposites showed high wear rate compared to unreinforced alloy under these sliding conditions. As discussed earlier, this could be due to the more amount of material transfer in nanocomposites as a result of higher ductility under this sliding condition. Thus, the addition of 1.5 vol.% of nano-sized alumina particles to AZ31 magnesium alloy is not beneficial in lowering the wear rates when tested under normal loads of 5-20 N at sliding speeds of 1, 2 and 5 m/s.

5.1.3 Wear Rate for AZ31 and its AZ31/CNT Nanocomposite

The addition of carbon nanotubes (CNT) to the AZ31 magnesium alloy matrix led to high wear rates when compared to its unreinforced alloy tested under applied loads of 5-20 N and sliding speeds of 1, 2 and 5 m/s. The increase in wear rates of the nanocomposite could be attributed to higher ductility, increased porosity and mismatch of thermal expansion coefficients between the reinforcement and matrix alloy. These results are in contrast to previous studies on CNT reinforced Al MMCs that had shown improvement in both mechanical and tribological properties [56-59]. However, caution should be taken in making direct comparisons between the current and previous results, since material systems are different. Moreover, earlier research on MMCs suggests that the wear resistance of the composite not only depends on the material properties but also on the nature of mechanical and physical factors [27].

The results showed gradual increase in wear rates of both the materials with increase in applied loads at all sliding speeds. This behavior may be attributed to change in wear mechanisms of both the materials under different values of applied load. And, these results are similar to previous investigations on CNT reinforced MMCs which had also found increase in wear rates with increase in applied loads [56-59].

Moreover, decrease in wear rates are observed with increase in sliding speed due to the formation of magnesium oxide on the pin surface at high sliding speeds which acted as a protective layer from wear. And, these findings are similar to earlier studies carried out by Habibnejad et al. [34] and Shanthi et al. [35], in which the addition of 1.5 vol.% of nano-sized alumina particulates (100 and 50 nm size) to magnesium alloys AZ31 and

AZ31B dropped the wear rates with increase in sliding speed. In another study, Lim et al [33] conducted dry sliding wear tests of magnesium composites reinforced with up to 1.11 vol.% of nano-sized alumina particulates (50 nm size) and they reported that the wear rates decreased with sliding speed up to 7 m/s beyond which the wear rate began to rise. However, the wear trends observed in the present study are in contrast to the findings of Chen and Alphas [55], where increase in wear rates of AZ91 were seen with increase in sliding speed under loads of 5-20 N.

5.1.4 Wear Mechanisms in AZ31 and its AZ31/CNT Nanocomposite

Under all the sliding conditions except at 20 N, abrasion, delamination and adhesion coexists on the pin surface and at 20 N, thermal softening is observed. However, the intensity of these mechanisms varies with sliding parameters. At low sliding speed of 1 m/s and load of 5 and 10 N, abrasion is found to be the dominant wear mechanism. And, an increase in wear rate of about 8-9% was observed in the nanocomposite due to presence of slight delamination in addition to abrasion.

As the speed and load is increased the intensity of delamination and adhesion increases. The increase in intensity of delamination in case of nanocomposites could be attributed to misfit strain that occurred during sliding as a result of difference between the thermal expansion coefficients of reinforcement (α ⁼ 0 /°K [68]) and matrix alloy ($\alpha = 26 \times 10^{-6}$ /°K [67]). These misfit strains in the nanocomposites cause internal stresses which results in plastic deformation of the material. Further, as the sliding speed is increased, the internal stresses increases due to increase in surface temperature and exceeds the tensile strength of the material due to high misfit strain causing material rupture and also results

in detachment of fragments with continuous sliding [63]. Consequently, high wear rates are seen in the nanocomposites with increase in sliding parameters under lower loads of 5 and 10 N, as the mismatch of thermal expansion coefficients together with porosity promoted the rate of delamination process by creating additional void nucleation sites and preferential crack propagation paths through a particle-matrix de-cohesion mechanism. Earlier studies had also found increase in wear rates of composite due to presence of delamination wear mechanism. For example, Lim et al. [29] reported increase in wear rates of Mg/SiC_p composites due to the presence of delamination wear.

Under the normal load of 15 N, mild abrasion, delamination and adhesion coexists on the pin surface. However, with increase in load and speed, adhesion becomes severe and is extensive in nanocomposite than its monolithic counterpart. This could be due to the higher ductility of the nanocomposite which is almost twice the base material (see table 3.1). And, this high ductility of the material favors strong adhesion between the pin and disc with increase in surface temperature. This is because a material with high ductility will have greater elongation and less elastic recovery, which together with increase in real area of contact due to increase in load and duration results in high adhesion of materials [45]. Thus, it might be reasonable to conclude that more amount of material transfer is seen due to increase in ductility of nanocomposites which resulted in severe adhesion with increase in sliding parameters. Consequently, 13-16% increase in wear rates of the nanocomposite are seen as a result of severe adhesion compared to its unreinforced alloy.

Under higher load of 20 N, increase in frictional heating led to softening of the pin surface which resulted in large amount of material transfer from the pin to the disc. Such type of behavior is also evident from earlier studies on Mg and Al composites which had

also found presence of thermal softening at higher speeds and loads [33, 35, 62]. And they reported presence of particulate reinforcements as beneficial in lowering the wear rates by delaying the onset of thermally activated deformation processes to higher loads and speeds. However, the present results are contrary to previous findings i.e., the nanocomposites showed high wear rate compared to unreinforced alloy under these sliding conditions. As discussed earlier, this could be due to the more amount of material transfer in nanocomposites as a result of higher ductility under this sliding condition. Thus, the addition of 1.0 vol.% of Carbon Nanotubes (CNT) to AZ31 magnesium alloy is not beneficial in lowering the wear rates when tested under normal loads of 5-20 N at sliding speeds of 1, 2 and 5 m/s.

5.1.5 Comparison between AZ31/Al_2O_3 and AZ31/CNT Nanocomposites

At sliding speeds of 1 and 2 m/s, as the load is increased from 5 to 20 N, an increase in wear rate was observed with increase in applied load for both AZ31/Al_2O_3 and AZ31/CNT nanocomposite. This behavior may be attributed to change in wear mechanisms of both the materials under different values of applied load i.e., under lower loads of 5 and 10 N, combination of abrasion, delamination and slight adhesion was observed. And, with increase in load to 15 and 20 N, combination of abrasion, adhesion thermal softening and slight delamination was observed. Moreover, when compared to AZ31/Al_2O_3 nanocomposite, the wear rates of AZ31/CNT nanocomposite are 4-7 % higher. This may be attributed to presence of more delamination in AZ31/CNT nanocomposite due to large difference between thermal expansion coefficients of its reinforcement and matrix alloy when compared to AZ31/Al_2O_3.

At a sliding speed of 5 m/s, almost similar wear rates were observed for both AZ31/CNT and AZ31/Al_2O_3 nanocomposites under all applied loads. And, similar wear mechanisms i.e., combination of abrasion, adhesion, oxidation, delamination and thermal softening were seen in both the materials under these sliding conditions. Moreover, contrary to the results obtained under lower speeds, no improvement was observed in the wear resistance of AZ31/Al_2O_3 when compared with AZ31/CNT nanocomposite under this sliding condition. This may be attributed to increase in frictional heating which led to more amount of material transfer from pin to the disc i.e., more adhesion was observed in case of AZ31/Al_2O_3 nanocomposite due to its higher ductility when compared to AZ31/CNT (see table 3.1) [45]. Thus, the mechanism of reinforcing AZ31 magnesium alloy with 1.5

vol.% of Al_2O_3 is beneficial in improving the wear resistance when compared with AZ31 with 1.0 vol.% of CNT under low and moderate sliding speed of 1 and 2 m/s.

5.2 Mg/(0.7Y_2O_3 + (0.3-1.0Ni) Nanocomposites

5.2.1 Wear Rate for Mg/(0.7Y_2O_3 + (0.3-1.0Ni) Nanocomposites

The results of the present study revealed that increasing the amount of nickel (Ni) addition from 0.3 to 1.0 vol.% led to improvement in the wear resistance of Mg/0.7Y_2O_3 tested under applied loads of 5-30 N at a constant sliding speed of 0.5 m/s. The 1.0 vol.% Ni nanocomposite being the best performer shows an improvement in the wear resistance of 10 % at the lowest load of 5 N and 30% under high sliding condition of 30 N. The improvement in wear resistance of the nanocomposite could be attributed to improvement in the mechanical properties particularly hardness and strength (see table 3.1) with the increasing amount of nickel.

The results showed gradual increase in wear rates of both the materials with increase in applied loads. This behavior may be attributed to change in wear mechanisms with different values of applied load and also due to increase in real contact area between the pin and disc during sliding. Similar observations had been made in several previous studies on aluminum based hybrid composites [69-72].

5.2.2 Wear Mechanisms in Mg/(0.7Y_2O_3 + (0.3-1.0Ni) Nanocomposites

At low load of 5 N, abrasion (5.23) is found to be the dominant wear mechanism in all the materials. And the presence of oxide particles suggested oxidation wear as operative in addition to abrasion under this sliding condition. Moreover, abrasive wear appeared to be less severe in case of nanocomposite with increasing amount of Ni. This could be due to the increase in hardness of the materials with Ni content which resulted in reduction of wear rates. As the load is increased to 10 N, the nanocomposite with 1.0 vol.% Ni

continued to show better wear resistance, however the surface of all the nanocomposites were characterized by series of cracks roughly perpendicular to the sliding direction. At much higher load values of 15-20 N, the pin surfaces were oxidized and resulted in removal of material in the form of large sheet-like wear particles either due to delamination of the oxidized surface or due to crack propagation in the subsurface region. The increase in oxidation of the pin surface could be due to increase in frictional heating with increase in load [34-35]. Further, the delamination appeared more severe in case of nanocomposite with 0.3 vol.% Ni due to its high porosity which acted as an additional source for crack nucleation and propagation (see table 3.1). Accordingly, high wear rates are seen in the nanocomposite with 0.3 vol.% Ni when compared to nanocomposites with 0.6 and 1.0 vol.% Ni content.

Under the load of 25 N, adhesive wear is also seen in addition to delamination. And at the highest load of 30 N, more amount of material transfer from pin surface to disc due to frictional heating suggested adhesive wear as operative under this sliding condition. Once again, the nanocomposite with 1.0 vol.% Ni showed better wear resistance of about 30% when compared to nanocomposite with 0.3 vol.% Ni. Thus, the mechanism of reinforcing with nickel up to 1.0 vol.% in Mg/Y_2O_3 nanocomposite is beneficial in improving the wear resistance.

5.3 Mg/(0.7Y_2O_3 + (0.3-1.0Cu) Nanocomposites

5.3.1 Wear Rate for Mg/(0.7Y_2O_3 + (0.3-1.0Cu) Hybrid Nanocomposites

The results of the present study revealed that the addition of 1.0 vol.% copper as reinforcements in Mg/ 0.7Y_2O_3 led to slight improvement in the wear resistance compared to nanocomposite with 0.3 vol.% Cu. This could be attributed to increase in hardness of the materials with increasing content of copper as reinforcement. However, no improvement is seen in the nanocomposite with change in reinforcement from 0.3 to 0.6 vol.% of copper except under 20 and 25 N. Meanwhile, gradual increase in wear rates are seen in all the materials with increase in applied loads from 5 to 30 N at a constant sliding speed of 1 m/s. This behavior may be attributed to change in wear mechanisms with different values of applied load and also due to increase in real contact area between the pin and disc during sliding.

5.3.2 Wear Rate for Mg/(0.7Y_2O_3 + (0.3-1.0Cu) Hybrid Nanocomposites

At low load of 5 N, abrasion is found to be the dominant wear mechanism in all the materials. And the presence of oxide particles suggested oxidation wear as operative in addition to abrasion under this sliding condition. Moreover, abrasive wear appeared to be less severe in case of nanocomposite with 1.0 vol.% Cu due to its improved hardness. The Mg/Y_2O_3 nanocomposite with 1.0 vol.% Cu being the best performer showed an improvement of 9% in the wear resistance under lower load of 5 N. However, no improvement is seen in the wear resistance of nanocomposite with 0.6 vol.% Cu due to its lower strength.

As the load is increased to 10 N, presence of delamination is observed in addition to abrasion in Mg/Y_2O_3 nanocomposite with 1.0 vol.% Cu which reduced the improvement in wear resistance to 2%. At much higher load values of 15-20 N, abrasion, adhesion and slight delamination coexists on the pin surface. Adhesion is seen to be increasing with increase in load due to frictional heating which led to softening of the pin surface. Although, presence of delamination is seen in the form of cracks and shallow craters due to crack propagation, the severity of it is very less when compared to other mechanisms. Moreover, the nanocomposite with 1 vol. % showed about 8-13% improvement in wear resistance when compared to the nanocomposite with 0.3 vol.%. This could be attributed to increase in hardness of the material with increase in reinforcement content to 1.0 vol.% Cu. The present observation is in accordance with Archad's proposal which states that hardness is inversely proportional to wear rate of a material.

Under the highest load of 30 N, increase in frictional heating led to softening of the pin surface resulting in extensive material transfer between the pin and disc in all the nanocomposites. However, less adhesion is observed in case of Mg/Y_2O_3 with 1.0 vol.% Cu due to its increased hardness. But the presence of delamination as a result of high porosity lead to additional wear rate in the nanocomposite with 1.0 vol.% Cu under this sliding condition. Thus, no improvement is seen in the nanocomposite with 1.0 vol.% Cu under this sliding condition due to its poor mechanical properties (see table 3.1).

5.4 Comparison between Mg/(0.7Y_2O_3 + (0.3-1.0Ni) and Mg/(0.7Y_2O_3 + (0.3-1.0Cu) Hybrid Nanocomposites

At lower load of 5 N, both Mg/(Y_2O_3+Ni) and Mg/(Y_2O_3+Cu) nanocomposites showed nearly similar wear rates. Oxidation and abrasion were observed to be the dominant wear mechanisms under this sliding condition. The reason for no improvement in wear performance is attributed to near similarity in their hardness values (see table 3.1).

As the load is increased to 15 and 30 N, negligible difference in wear rates are seen in both hybrid nanocomposites with 0.3 vol.% of reinforcement. Almost, similar wear mechanisms were seen in both the materials with 0.3 vol.% of reinforcement due to their similar mechanical properties (see table 3.1). However, the nanocomposites with 0.6 and 1.0 vol.% Ni as reinforcement showed better wear resistance when compared to the nanocomposite with similar compositions of Cu reinforcement. This could be due to the improvement in mechanical properties of Mg/(Y_2O_3+Ni) nanocomposites with increase in Ni reinforcement which was not evident in case of Mg/(Y_2O_3+Cu). The improvement in 0.6 vol.% Ni nanocomposite was about 13 to 21% when compared to 0.6 vol.% Cu, while in case of 1.0 vol.% Ni nanocomposite an improvement of about 8 to 17% were observed when compared with 1.0 vol.% Cu. Abrasion, delamination and adhesion were observed as the dominant wear mechanisms in both Mg/(Y_2O_3+Ni) and Mg/(Y_2O_3+Cu) nanocomposites under these sliding conditions. However, adhesion appeared to be more severe in Mg/(Y_2O_3+Cu) nanocomposites because of its higher ductility with increase in reinforcement. Furthermore, an increase in wear rates of Mg/(Y_2O_3+Cu) nanocomposites can be attributed to decrease in mechanical properties of the nanocomposites with

increasing amount of ‘Cu’ content. In contrast, an increase in wear resistance of Mg/(Y_2O_3+Ni) nanocomposites was clearly evident due to increase in mechanical properties of the nanocomposites with increasing amount of ‘Ni’ content. Thus, Mg/(Y_2O_3+Ni) hybrid nanocomposites appear to be more beneficial when compared to Mg/(Y_2O_3+Cu) hybrid nanocomposites under most sliding conditions and are recommended for an application where light weight and better wear resistance is an important criterion.

CHAPTER 6

CONCLUSION AND RECOMMENDATIONS

Magnesium alloy (AZ31) and its nanocomposites AZ31-alumina (AZ31/Al_2O_3), AZ31-Carbon Nanotubes (AZ31/CNT) and two different group of hybrid nanocomposite materials namely: Mg-yttria + copper (Mg/Y_2O_3 + (0.3-1.0) vol.% Cu) and Mg-yttria + nickel (Mg/Y_2O_3 + (0.3-1.0) vol.% Ni) were tested using pin-on-disk wear tester under dry sliding conditions. The conclusions made in the each material are presented individually as follows:

- The addition of 1.5 vol.% of nano-sized alumina particles and 1 vol.% of carbon nanotubes increased the wear rates of AZ31 magnesium alloy when tested under applied loads of 5-20 N and at sliding speeds of 1, 2 and 5 m/s for a sliding distance of 2500 m. Five different wear mechanism were observed under these conditions. They are: abrasion, delamination, adhesion, oxidation and thermal softening. The nanocomposites displayed high wear rates under lower loads (5 and 10 N) due to additional abrasive wear caused by the presence of hard alumina particles at the interface during sliding. And at higher loads and speeds, the

presence of delamination and severe adhesion due to higher ductility, mismatch of coefficient of thermal expansion and high porosity lead to high wear rates in the nanocomposites.

- The reinforcement of varying amounts of nickel from 0.3-1.0 vol.% improved the wear resistance of Mg/Y_2O_3 nanocomposite when tested under applied loads of 5-30 N at a constant sliding speed of 0.5 m/s. Four different wear mechanisms were observed under these conditions. They are: abrasion, oxidation, delamination and adhesion. The nanocomposites displayed improved wear rates with increasing amount of Ni under all sliding conditions due to increase in hardness of the material. Under lower loads of 5 and 10 N, abrasion and oxidation were the dominant wear mechanism while at higher loads of 15-30 N, mild abrasion, delamination and adhesion were observed.
- The addition of varying amounts of copper from 0.3-1.0 vol.% slightly improved the wear resistance of Mg/Y_2O_3 nanocomposite when tested under applied loads of 5-30 N at a constant sliding speed of 1 m/s. Four different wear mechanisms were observed under these conditions. They are: abrasion, oxidation, delamination and adhesion. The Mg/Y_2O_3 nanocomposite with 1.0 vol.% Cu showed slight improvement in the wear resistance compared to nanocomposite with 0.3 vol.% Cu under all sliding conditions. However, no improvement is seen in the nanocomposite with 0.3 vol.% Cu except at 20 and 25 N. Under lower loads of 5 and 10 N, abrasion and oxidation were the dominant wear mechanisms. And at higher loads of 15-20 N, abrasion, adhesion and mild delamination were observed.

6.1 Recommendations for Future Work

- Coefficient of friction and temperature at the interfaces should be measured to get better understanding about the wear behaviour of nanocomposites.
- Wear tests for newly developed AZ31/CNT nanocomposite, should be conducted at lower sliding speeds, to understand the wear behaviour under lower speeds.
- Wear tests should be carried out under lubricated conditions by using suitable lubricant, to understand the effect of lubricant on the wear behaviour of nanocomposites.
- Wear tests for hybrid nanocomposites could be conducted at constant load and varying sliding speeds, to understand the wear behaviour of hybrid nanocomposites with variation of speed.

REFERENCES

1. M. Huda, M. Hashmi, and M. El-Baradie, "MMCs: materials, manufacturing and mechanical properties," Key Engineering Materials, vol. 104, pp. 37-64, 1995.
2. F. H. Froes, D. Eliezer, and E. Aghion, "The science, technology, and applications of magnesium," Journal of Minerals, vol. 50, pp. 30-34, 1998.
3. H. Ye and X. Liu, "Review of recent studies in magnesium matrix composites," Journal of Materials Science, vol. 39, pp. 6153-6171, 2004.
4. K. K. Chawla and N. Chawla, Metal Matrix Composites: Wiley Online Library, 2004.
5. M. Gupta and N. M. L. Sharon, Magnesium, Magnesium Alloys, and Magnesium Composites: A Guide: Wiley, 2011.
6. T. Clyne and P. Withers, An introduction to metal matrix composites: Cambridge University Press, 1995.
7. K. U. Kainer, Metal matrix composites: Wiley-Vch, 2006.
8. P. Rohatgi, Y. Liu, and S. Ray, "Friction and wear of metal-matrix composites," ASM Handbook, vol. 18, pp. 801-811, 1992.
9. Z. F. Zhang, L. C. Zhang, and Y. W. Mai, "Wear of ceramic particle-reinforced metal-matrix composites," Journal of Materials Science, vol. 30, pp. 1967-1971, 1995.
10. S. Prasad and R. Asthana, "Aluminum metal-matrix composites for automotive applications: tribological considerations," Tribology Letters, vol. 17, pp. 445-453, 2004.

11. A. Al-Qutub, I. Allam, and T. Qureshi, "Wear properties of 10% sub-micron Al sub 2 O sub 3/6061 aluminum alloy composite," International Journal of Applied Mechanics and Engineering, vol. 7, pp. 329-334, 2002.
12. S. F. Hassan and M. Gupta, "Development of high performance magnesium nanocomposites using solidification processing route," Materials Science and Technology, vol. 20, pp. 1383-1388, 2004.
13. S. Hassan and M. Gupta, "Effect of different types of nano-size oxide particulates on microstructural and mechanical properties of elemental Mg," Journal of Materials Science, vol. 41, pp. 2229-2236, 2006.
14. S. Hassan and M. Gupta, "Enhancing physical and mechanical properties of Mg using nanosized Al_2O_3 particulates as reinforcement," Metallurgical and Materials Transactions A, vol. 36, pp. 2253-2258, 2005.
15. M. Schwartz, Composite materials handbook: McGraw-Hill, 1992.
16. M. K. Surappa, "Aluminium matrix composites: Challenges and opportunities," Sadhana, vol. 28, pp. 319-334, 2003/02/01 2003.
17. S. Suresh, A. Mortensen, and A. Needleman, "Fundamentals of metal-matrix composites," Butterworth-Heinneman(UK), 1993, p. 400, 1993.
18. D. J. Lloyd, "Particle reinforced aluminium and magnesium matrix composites," International Materials Reviews, vol. 39, pp. 1-23, 1994.
19. V. K. Lindroos and M. J. Talvitie, "Recent advances in metal matrix composites," Journal of Materials Processing Technology, vol. 53, pp. 273-284, 1995.

20. I. A. Ibrahim, F. A. Mohamed, and E. J. Lavernia, "Particulate reinforced metal matrix composites — a review," Journal of Materials Science, vol. 26, pp. 1137-1156, 1991/01/01 1991.
21. W. D. Callister and D. G. Rethwisch, Materials science and engineering: an introduction vol. 7: Wiley New York, 2007.
22. P. Ajayan, "Bulk metal and ceramics nanocomposites," Nanocomposite Science and Technology, Wiley-VCH Verlag, 2004.
23. P. H. C. Camargo, K. G. Satyanarayana, and F. Wypych, "Nanocomposites: synthesis, structure, properties and new application opportunities," Materials Research, vol. 12, pp. 1-39, 2009.
24. B. Bhushan, Modern Tribology Handbook, Two Volume Set vol. 1: CRC, 2000.
25. M. J. Neale, Tribology handbook: Butterworth-Heinemann, 1996.
26. ASTM Handbook, "Volume 18," Friction, Lubrication and Wear Technology, 1992.
27. A. P. Sannino and H. J. Rack, "Dry sliding wear of discontinuously reinforced aluminum composites: review and discussion," Wear, vol. 189, pp. 1-19, 1995.
28. R. L. Deuis, C. Subramanian, and J. M. Yellup, "Dry sliding wear of aluminium composites—A review," Composites Science and Technology, vol. 57, pp. 415-435, 1997.
29. C.Y.H. Lim, S.C. Lim, and M. Gupta, "Wear behaviour of SiC_p-reinforced magnesium matrix composites," Wear, vol. 255, pp. 629-637, 2003.

30. P. Abachi, A. Masoudi, and K. Purazrang, "Dry sliding wear behavior of SiCP/QE22 magnesium alloy matrix composites," Materials Science and Engineering: A, vol. 435–436, pp. 653-657, 2006.
31. S.-J. Huang, Y.-R. Jeng, V. I. Semenov, and Y.-Z. Dai, "Particle Size Effects of Silicon Carbide on Wear Behavior of SiC.sub.p-Reinforced Magnesium Matrix Composites," Tribology Letters, vol. 42, p. 79, 2011.
32. S. K. Jo, W. J. Lee, Y. H. Park, and I. M. Park, "Effect of SiC Particle Size on Wear Properties of [Al.sub.2]O.sub.3SiO.sub.2/SiC/Mg Hybrid Metal Matrix Composites," Tribology Letters, vol. 45, p. 101, 2012.
33. C.Y.H. Lim, D.K. Leo, J.J.S. Ang, and M. Gupta, "Wear of magnesium composites reinforced with nano-sized alumina particulates," Wear, vol. 259, pp. 620-625, 2005.
34. M. Habibnejad-Korayem, R. Mahmudi, H.M. Ghasemi, and W.J. Poole, "Tribological behavior of pure Mg and AZ31 magnesium alloy strengthened by Al_2O_3 nano-particles," Wear, vol. 268, pp. 405-412, 2010.
35. M. Shanthi, Q.B. Nguyen, and M. Gupta, "Sliding wear behaviour of calcium containing AZ31B/Al_2O_3 nanocomposites," Wear, vol. 269, pp. 473-479, 2010.
36. M. Srinivasan, C. Loganathan, M. Kamaraj, Q. B. Nguyen, M. Gupta, and R. Narayanasamy, "Sliding wear behaviour of AZ31B magnesium alloy and nano-composite," Transactions of Nonferrous Metals Society of China, vol. 22, pp. 60-65, 2012.

37. S.C. Sharma, B. Anand, and M. Krishna, "Evaluation of sliding wear behaviour of feldspar particle-reinforced magnesium alloy composites," Wear, vol. 241, pp. 33-40, 2000.
38. M. Aydin and F. Fehim, "Wear properties of magnesium matrix composites reinforced with SiO2 particles," Industrial Lubrication and Tribology, vol. 62, pp. 232-237, 2010.
39. K. Xiu, H. Y. Wang, H. L. Sui, Y. Wang, C. L. Xu, J. G. Wang, and Q. C. Jiang, "The sliding wear behavior of TiCp/AZ91 magnesium matrix composites," Journal of Materials Science, vol. 41, pp. 7052-7058, 2006/11/01 2006.
40. J. Yao, W. Li, L. Zhang, F. Wang, M. Xue, H. Jiang, and J. Lu, "Wear Mechanism for In Situ TiC Particle Reinforced AZ91 Magnesium Matrix Composites," Tribology Letters, vol. 38, pp. 253-257, 2010/06/01 2010.
41. J. Umeda, K. Kondoh, and H. Imai, "Friction and wear behavior of sintered magnesium composite reinforced with CNT-Mg2Si/MgO," Materials Science and Engineering: A, vol. 504, pp. 157-162, 2009.
42. J. Williams, Engineering tribology vol. 10: Cambridge University Press, 2005.
43. B. Bhushan, Introduction to tribology: Wiley, 2002.
44. K. Hokkirigawa and K. Kato, "An experimental and theoretical investigation of ploughing, cutting and wedge formation during abrasive wear," Tribology International, vol. 21, pp. 51-57, 1988.
45. Bharat Bhushan, "Adhesion and stiction: mechanisms, measurement techniques, and methods for reduction," Journal of Vacuum Science & Technology B: Microelectronics and Nanometer Structures 21.6 (2003): 2262-2296.

46. S. Jahanmir and N. P. Suh, "Mechanics of subsurface void nucleation in delamination wear," Wear, vol. 44, pp. 17-38, 1977.

47. G. W. Stachowiak and A. W. Batchelor, Engineering tribology: Butterworth-Heinemann, 2005.

48. M. Paramsothy, S.F. Hassan, N. Srikanth, and M. Gupta, "Enhancing tensile/compressive response of magnesium alloy AZ31 by integrating with Al_2O_3 nanoparticles," Materials Science and Engineering: A, vol. 527, pp. 162-168, 2009.

49. M. Paramsothy, S. F. Hassan, N. Srikanth, and M. Gupta, "Simultaneous Enhancement of Tensile/Compressive Strength and Ductility of Magnesium Alloy AZ31 Using Carbon Nanotubes," Journal of Nanoscience and Nanotechnology, vol. 10, pp. 956-964, 2010.

50. K. S. Tun, M. Gupta, and T. S. Srivatsan, "Investigating influence of hybrid (yttria + copper) nanoparticulate reinforcements on microstructural development and tensile response of magnesium," Materials Science and Technology, vol. 26, pp. 87-94, 2010.

51. K. S. Tun and M. Gupta, "Development of magnesium/(yttria + nickel) hybrid nanocomposites using hybrid microwave sintering: Microstructure and tensile properties," Journal of Alloys and Compounds, vol. 487, pp. 76-82, 2009.

52. H.W. Coleman, and W.G. Steele, "Experimentation, Validation, and Uncertainty Analysis for Engineers", John Wiley & Sons, Inc. 2009.

53. M.M.A. Baig, "Friction and wear of 20% volume fraction submicron $A1_2O_3$/6061 aluminum alloy composite for brake system application," MSc Thesis, Mechanical Engg. Dept., KFUPM, 2009, pp. 51-52.
54. P. Rohatgi, P. Menezes, T. Mazzei, and M. Lovell, "Tribological behavior of aluminum micro-and nano-Composites," International Journal of Aerospace Innovations, vol. 3, pp. 153-162, 2011.
55. H. Chen and A.T. Alpas, "Sliding wear map for the magnesium alloy Mg-9Al-0.9 Zn (AZ91)," Wear, vol. 246, pp. 106-116, 2000.
56. H. J. Choi, S. M. Lee, and D. H. Bae, "Wear characteristic of aluminum-based composites containing multi-walled carbon nanotubes," Wear, vol. 270, pp. 12-18, 2010.
57. J. Jin-long, W. Hai-zhong, Y. hua and X. Jin-cheng, "Fabrication and wear behavior of CNT/Al composites," Transactions of Nonferrous Metals Society of China, vol. 17, pp. s113-s116, 2007.
58. I. Y. Kim, J. H. Lee, G. S. Lee, S. H. Baik, Y. J. Kim, and Y. Z. Lee, "Friction and wear characteristics of the carbon nanotube–aluminum composites with different manufacturing conditions," Wear, vol. 267, pp. 593-598, 2009.
59. S. M. Zhou, X. B. Zhang, Z. P. Ding, C. Y. Min, G. L. Xu, and W. M. Zhu, "Fabrication and tribological properties of carbon nanotubes reinforced Al composites prepared by pressureless infiltration technique," Composites Part A: Applied Science and Manufacturing, vol. 38, pp. 301-306, 2007.
60. J. F. Archard, "Contact and Rubbing of Flat Surfaces," Journal of Applied Physics vol. 24(8), pp. 981-988, 1953.

61. A. Al-Qutub, I. Allam, and M. A. Abdul Samad, "Wear and friction of Al–Al_2O_3 composites at various sliding speeds," Journal of Materials Science, vol. 43, pp. 5797-5803, 2008/09/01 2008.
62. J. Zhang and A.T. Alpas, "Wear regimes and transitions in Al_2O_3 particulate-reinforced aluminum alloys," Materials Science and Engineering: A, vol. 161, pp. 273-284, 1993.
63. S. Kustov, S. Golyandin, K. Sapozhnikov, A. Vincent, E. Maire, and G. Lormand, "Structural and transient internal friction due to thermal expansion mismatch between matrix and reinforcement in Al–SiC particulate composite," Materials Science and Engineering: A, vol. 313, pp. 218-226, 2001.
64. M. Narayan, M.K. Surappa, and B.N. PramilaBai, "Dry sliding wear of Al alloy 2024-Al_20_3 particle metal matrix composites," Wear, vol. 181–183, Part 2, pp. 563-570, 1995.
65. Q. B. Nguyen, M. Gupta, and T. S. Srivatsan, "On the role of nano-alumina particulate reinforcements in enhancing the oxidation resistance of magnesium alloy AZ31B," Materials Science and Engineering: A, vol. 500, pp. 233-237, 2009.
66. R. Morrell, "Handbook of properties of technical and engineering ceramics, Part I: An introduction for the engineer and designer," H.M. Stationary Office, 1985.
67. E.A. Brandes, G.B. Brook, "Smithells Light Metal Handbook," Reed Educational and Professional Publishing Ltd, Massachusetts (USA), 1998.

68. C.F. Deng, Y.X. Ma, P. Zhang, X.X. Zhang, and D.Z. Wang, "Thermal expansion behaviors of aluminum composite reinforced with carbon nanotubes," Materials Letters, vol. 62, pp. 2301-2303, 2008.
69. E.M. Sharifi and F. Karimzadeh, "Wear behavior of aluminum matrix hybrid nanocomposites fabricated by powder metallurgy," Wear, vol. 271, pp. 1072-1079, 2011.
70. K. Umanath, S.T. Selvamani & K. Palanikumar (2011). "Friction and Wear behavior of Al6061 alloy (SiC_p + Al_2O_3) hybrid composites," International Journal of Engineering Science and Technology, 3(7), 5441-5451.
71. S. Suresha and B. K. Sridhara, "Wear characteristics of hybrid aluminium matrix composites reinforced with graphite and silicon carbide particulates," Composites Science and Technology, vol. 70, pp. 1652-1659, 2010.
72. H. Ahlatci, T. Koçer, E. Candan, and H. Çimenoglu, "Wear behaviour of Al/(Al_2O_3+SiC_p) hybrid composites," Tribology International, vol. 39, pp. 213-220, 2006.

VITAE

Name : Syed Zabiullah

Nationality : Indian

Date of Birth : 22/05/1988

E-mail : zabiullah6008@gmail.com

Address : H.No:18-12-418/C/18/A, Hafeez Baba Nagar, Hyderabad, A.P, India, Pin 500005.

Telephone : 0091-9866032641 (India)

: 0534167543 (Saudi)

Academic Background: Received Bachelor of Engineering degree in Mechanical Engineering from Muffakham Jah College of Engineering & Technology, Affiliated to Osmania University, Hyderabad, India in 2009. Joined Mechanical Engineering Department of King Fahd University of Petroleum and Minerals, Dhahran as Research Assistant in March 2010-December 2012.